Ionic dynamics of stemflow on oak trees during a growing season in South Wales, UK.

Jack Houghton

Swansea University

Submitted to Swansea University in fulfilment of the requirements for the Degree of Master of science in Environmental Dynamics

September 2023

The ionic composition of stemflow over the course of early spring to summer (March to June) offers an insight into the movement of ions throughout this small area of the hydrological cycle and its development over the course of a single season. The water is collected from the six selected common oak trees (*Quercus Robur*) using stemflow collars, with the characteristics of the storm being taken from nearby weather stations to the study site in Clyne Valley, Swansea. This data is complimented by laboratory work to uncover how water behaves with bark as a medium to flow over as these porous medium reveals droplet characteristics to show how stemflow acts on a smaller spatial scale than it is usually discussed. Furthermore, how the bark reacts through its hygroscopic abilities to the ambient moisture content is studied using a climatically controlled chamber to attempt to understand fluctuations in barks moisture. The processing of both storm rainwater and stemflow samples was done by ion chromatography to determine its ionic composition. The quantities of ions then showed clear correlations within the acquired dataset to length of prior dry period, with various ions showing preference to at least one of the rainfall characteristics. Meanwhile, stemflow volume was primarily attributable to the storm depth. Many of the salt-based ions were correlated to one another, whereas movement dynamics of droplets largely disagreed with the few studies that came before one's own. These results lead to conclusions showing a disparity between the fluid solvent medium and the ionic content within it.

Key words: stemflow , Ions, Meteorology, Hygroscopicity, Climate change, Droplet Movement

I wish to thank my primary supervisor Dr Emilia Urbanek for her help in producing this piece of work and for the continued support of Professor Rory Walsh who acted as my secondary supervisor. I would further like to thank Rhodri Griffiths and Graham Walters for their help in the laboratory section of this thesis and for processing the samples through the ion chromatograph. A further thanks to Swansea council for granting the permissions to use the study site within Clyne Country Park.

Declarations

This work has not previously been accepted in substance for any degree and is not being concurrently submitted in candidature for any degree.

Signed……Jack Houghton…….

Date.....30/9/23.....……

This thesis is the result of my own investigations, except where otherwise stated. Other sources are acknowledged by footnotes giving explicit references. A bibliography is appended.

Signed……Jack Houghton……

Date.....30/9/23.....……

I hereby give consent for my thesis, if accepted, to be available for electronic sharing

Signed……Jack Houghton……

Date.....30/9/23.....……

The University's ethical procedures have been followed and, where appropriate, that ethical approval has been granted.

Signed……Jack Houghton……

Date.....30/9/23.....……

Table of Contents

List of Figures

List of Tables

1. Introduction

1.1 Opening remarks

Stemflow ’s ionic composition is the result of dynamic interaction between living foliage and the wider hydrological cycle (Figure 1), where matter (therefore energy) is dissolved and transported, enabling chemical and physiological reactions that sustain life and connect ostensibly separate ecozones. Stemflow specifically refers to intercepted rainwater that flows down the stem (or trunk) of a plant (Koichiro *et al.,* 2001) via preferential flow paths (PFP) (Germer, 2013), with the tributaries of branchflow feeding in from the various branches. As rainwater flows down stems, the medium on which it flows, evolves, dependent on tree species (Konopka *et al.,* 2022). This evolution further impacts barks interactions as the more multifaceted structure allows for further potential obstacles. Stemflow (alongside throughfall) further contributes to soil moisture and nutrient content (Figure 1), representing where the individual tree’s spatiality impacts soil chemistry, below the annual leaf senesce and the eventual decomposition of fallen trees. Furthermore, one can visually differentiate the exclusive and partial throughfall generating regions of the trees' architecture by looking for droplets of water on branches after a storm. The droplets either reveal a location where a branch goes beneath the horizontal plane, which would be exclusively throughfall generating, or an obstacle blocking a PFP, which would be either partially throughfall or stemflow generating dependent on the branch angle. Stemflow’s ionic fluctuations are attributable to sensitive discrepancies in weather phenomena that produce overall fluctuations (Levia and Frost, 2003). Therefore, the ionic compositions evolution along the storm-to-storm fluctuation as the tree transforms from dormancy to photosynthesising should garner academic interest as the evolution of ions will be demonstrated in a quantitative form. Current academic literature is lacking on how stemflow changes as a solvent throughout the seasons, with most of the study being done on rivers. This topic has wider implications as it deepens the understanding of ion movement within the hydrological cycle, with natural fluxes in weather (wind speed, temperature) and external sources influencing these oscillations. The stemflow process also shows how water further demonstrates its larger role as a solvent alongside its main role as a fluid. Stemflow as a process has only garnered adequate attention within the last 2 decades, with many elements remaining unknown to academia especially the movement of ions through the process, which remains remarkably understudied (Levia and Frost, 2003). The physical flow of stemflow is a variant of Wenzel and Carrie-Baxter flow (Mohammadrezaei *et al*., 2022), where the flow is partially on and within the medium. This occurs

because a single drop cannot form a full PFP from interception to trunk, and instead, successive drops extend the path generated by its predecessor.

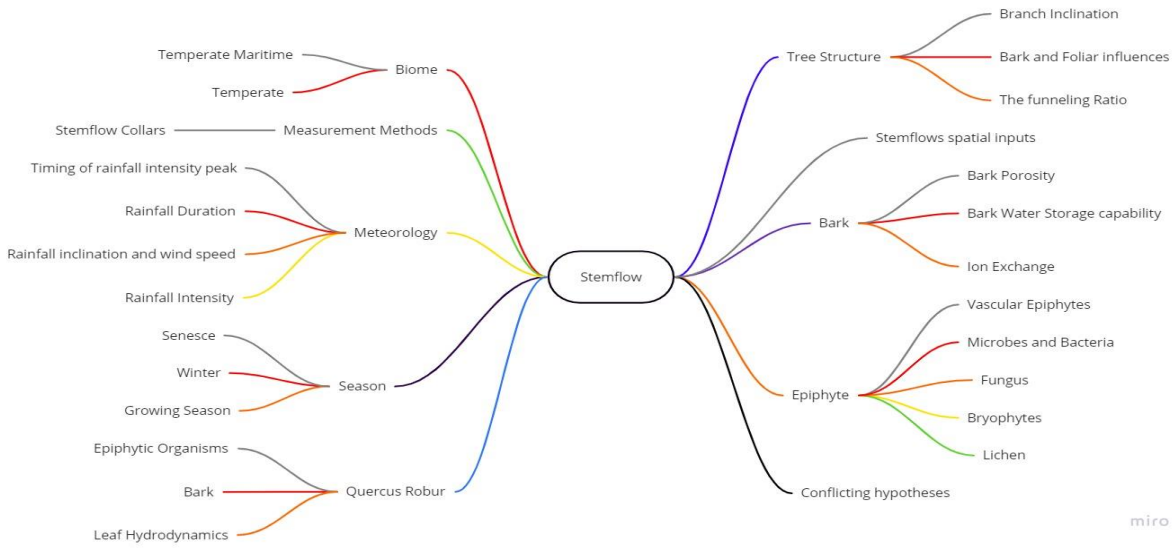

Figure 1: A mind map of the variables impacting stemflow volume and its ionic composition. The colour of the line represents the ranking in terms of quantity of academic papers that can be obtained through the Web of Knowledge database until 9/2/22. Grey indicates the most papers; red second most; orange third most; yellow fourth most; and green fifth most.

The physical flow of stemflow is a variant of Wenzel and Carrie-Baxter flow (Mohammadrezaei *et al*., 2022), where the flow is partially on and partially within the medium. This occurs because a single drop cannot form a full PFP from interception to trunk, instead, successive drops extend the path generated by its predecessor.

Stemflow, like all water flows, is primarily gravitationally induced, overcoming various resisting forces as it travels on a surface (Figure 2a). Stemflow encounters various epiphytes and levels of hydrophobicity attributable to the flow paths existing micro-nature and sensitive discrepancies in bark moisture content (Figure 2b). Consecutive stemflow drops generate a PFP enabling accelerated stemflow, which takes advantage of the thin film of water left behind, providing a smoother channel of travel (Germer, 2013). Accelerated stemflow constitutes the volumetric majority of the process. The movement of water on the barks surface was also measured to determine behavioural and velocity characteristics of the flowing droplets, along with recurring characteristics of path generation as this will provide a new approach to studying stemflow as it physically moves across a barks surface.

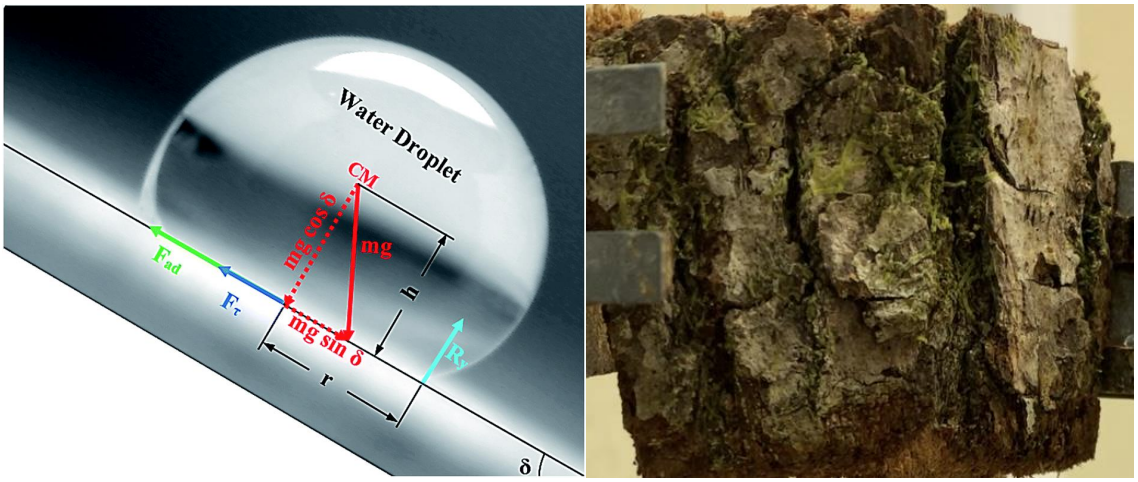

Figure 2a&b: The basic physics of water movement on an incline, with the biology of the incline in question photographed to the right.

The following section will review the state of current academic knowledge on stemflow and its ionic composition, with additional sections for wet and dry deposition for the understanding of ion movement before being recorded within stemflow. Chapter 2 will detail the field and laboratory methods used in generating the dataset, with details on the trees used within the study. The methods of which will address holes identified within the previous chapter. These methods and the results of which will be demonstrated in chapter 3 and discussed in chapter 4. The conclusions from this thesis alongside suggestions for developing this work further will be stated within chapter 5.

1.2 The current literature on stemflow and its ions

1.2.1 Definitions and introduction to stemflow process

Stemflow is the hydrological process where a tree or other plant body intercepts precipitation, which is directed to the soil around the base of the trunk through PFP on the plants woody surface (Levia and Frost, 2003; Carlyle-Moses et al., 2018; Lida et al., 2021; Levia and Germer, 2015). Stemflow can either be expressed as a percentage ($SF_{\%}$), which denotes the percentage of total precipitation from within the crown of the tree that has become stemflow; or cumulative stemflow (SFc), which denotes overall stemflow volume, usually in millilitres. Stemflow percentages can be in the range of 0.6-45% (Levia and Frost, 2003), dependent on a wide variety of plant-specific and meteorological factors, with this method being primarily used in comparing tree species abilities to produce stemflow but can also be used to compare the efficiency of producing stemflow within an individual tree. For example, a smooth-barked beech tree will likely produce a higher SF% than a rough-barked oak tree. Cumulative stemflow is often associated with the overall size of a tree and its funnelling ratio (FR), which is expressed as follows:

FR = V/(BG) (Levia and Frost, 2003)

Where: **FR** = Funnelling ratio; **V** = stemflow volume (Expressed in ml); **B** = Trunk Basal Area (cm^2); **G** = Incident Gross Precipitation (cm).

Academic literature states that stemflow's volume and its ionic signature are derived from the influences of biome (Levia and Frost, 2003; Eaton et al., 1973), meteorology (Crockford et al., 1996), season (Neary and Gizyn, 1994), bark (Levia and Herwitz, 2005; Oka et al., 2021), epiphyte presence and composition (van Stan and Pypker, 2015), tree architecture (Herwitz, 1985; Levia and Herwitz, 2002), and the spatiality around the trunk of stemflow's input (Gonzalez-Ollauri, 2020). Like rivers, the quantities of ions will increase with branch complexity, implying that trees could be differentiated based on their degree of complexity concerning their stemflow chemical content. For example, when two first degree tributaries of a river meet, they become a second-degree tributary, and when that meets another second degree, it becomes a third-degree and so on. Therefore, a similar method could be applied to trees. For example, the Mississippi River is an 11th-degree river, while the diagram of a tree on the left would be a 5th-degree tree.

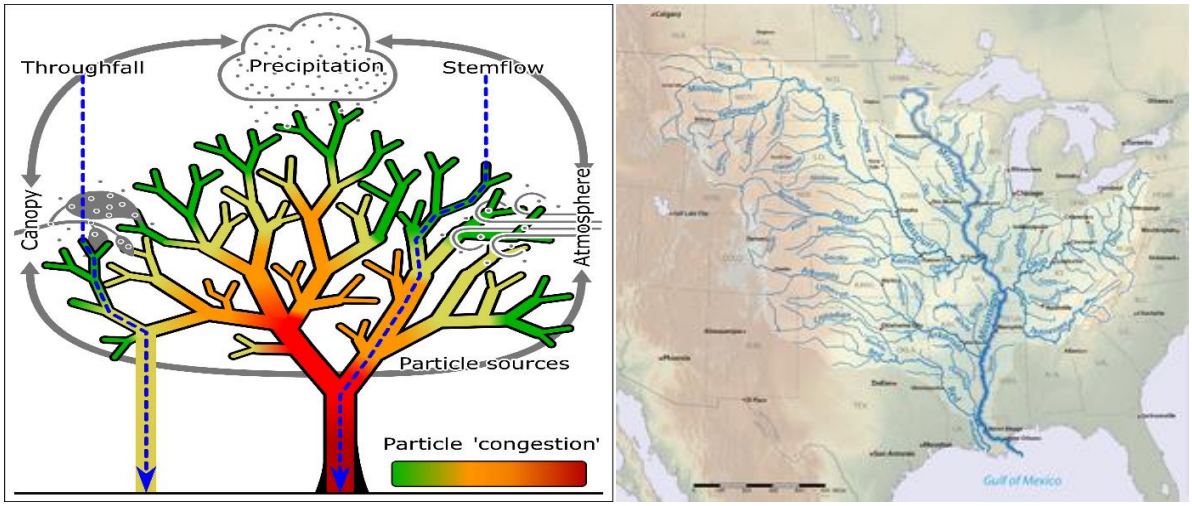

Figure 3: The particle congestion of stemflow within a singular tree. Source - Van Stan et al., (2021).

Stemflow commonly constitutes roughly 2% of gross precipitation in temperate regions (Oka et al., 2021). This comparably low percentage compared with throughfall, or evapotranspiration has meant that stemflow was formally overlooked in terms of its importance within the hydrological cycle (Levia and Germer, 2015). Levia and Frost (2003) reviewed stemflow to be the most isotopically dense input for precipitation into the soil and subsurface flows. However, Van Stan and Gordon (2018) found that stemflow's irregularities often lead soils located directly around trunks to be classed arid or semi-arid while residing in tropical regions. Furthermore, similar to arid regions, when the water did arrive in the form of stemflow, it often contained extremely high ionic contents, causing an overload within the small area of soil, therefore, making the soils less healthy than those that received a steady supply of throughfall water as many of the lifeforms would be starved of nutrients until these occasions . However, most studies note that tropical trees produce very little because of the density of the canopy and absence of an evolutionary adaption to scavenge all available water (Levia and Frost, 2003). There is evidence that artificially consistent rainfall intensities increase $SF_{\%}$ (Dunkerley, 2014), the extreme values demonstrate that their real-world applicability is greatly diminished. Furthermore, a study by Ford and Deans (1978) found $SF_{\%}$ values of 27% in a Sitka Spruce Plantation in Scotland, indicating that very dense canopies can increase stemflow percentages within certain species. However, the results provide a sharp contrast to the considerably low $SF_{\%}$ values found in dense tropical forests, indicating an influence of leaf size to this variable. Nevertheless, these extreme values for laboratory-based and adulterated "natural" environments within stemflow research are common and indicate the importance of natural sensitive fluctuations and spatial characteristics in regulating hydrological processes.

The Common Oak (*Quercus Robur*) is commonly used in stemflow studies. While a complete picture of the ionic dynamics is lacking attributable to academia's previous disregarding stemflow's role within the hydrological cycle (Levia and Frost, 2003), Quercus Robur has one of the deeper understandings. This comprehension includes research on its bark (Van Stan et al., 2016), epiphytic populations (Leith et al., 2008), and the hydrodynamics of their leaves (Klamerus-Iwan and Witek, 2018). In addition, the responses to meteorological influences are discussed throughout the literature review chapter in various sections.

1.2.2 The temperate maritime biome affecting stemflow

Stemflow varies significantly based on its inhabiting biome. Generally, foliage that receives consistent rainfall will have lower $SF_{\%}$ than plants where rainfall is a rarity, such as arid climates (Yuan et al., 2016; Levia and Germer, 2015), whereas annual SFc will be relative to the annual rainfall. For example, plants in arid conditions generally exhibit greater stemflow percentages as it is evolutionarily advantageous for them to have high capturing and funnelling capabilities. In contrast, tropical plants tend to have lower $SF_{\%}$ as they do not need to scavenge or direct limited water availability to the trees base and roots (Van Stan and Gordon, 2018).

The specific biome in which this study resides in the temperate Oceanic Climate (Cfb). This area is classed as having cool summers, mild winters, with a narrow annual temperature range. Cloudy conditions and rainfall are frequent, with severe weather being rare. Similar areas on a global scale are denoted in figure 4. These areas likely have elevated sea salts in their rainfall such as sodium chloride or magnesium sulphate, with prevailing wind directions often originating from maritime regions (Munger and Eisenreich, 1983; Ward and Robinson, 2000). The quantitative difference can be as significant as 32.14Kg/ha for maritime compared to 1.5Kg/ha for terrestrial salts delivered on an annual timescale (Eaton et al., 1973). In addition, there are the different influences of nearby agricultural and industrial activities, which could involve trace heavy metals and various nitric oxides within the stemflow (Radzi Abas et al., 1992).

Within Wales, there is sparse research on stemflow, with a body of work coming from the small town of Beddgelert and the Plynlimon mountain range. Neal *et al.,* (2003) researched a few notable ions within region, with the main findings showing Nitrogen compounds are higher within rainfall and cloud water, whereas phosphorus and salt ions are higher within stemflow.

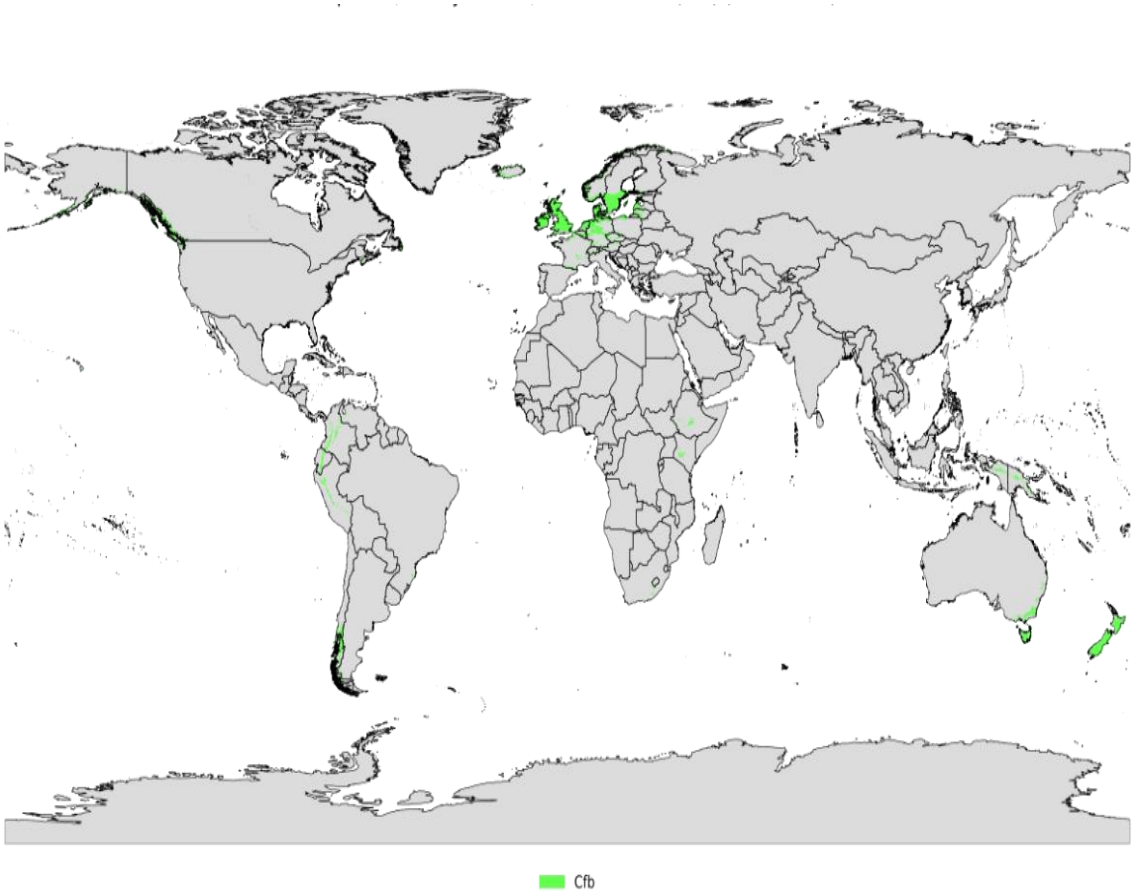

Figure 4: The scale of the Temperate Oceanic climate according to the Köppen-Geiger classification. Source - Beck et al., (2018)

1.2.3. Meteorological Influences on stemflow chemical composition

Precipitation is the primary input to stemflow and govern the general funnelling capability of plants. Each plant has a minimum capacity that must be breached before stemflow generation commences, which is a combination of tree specific characteristics such as bark texture, age, branch geometry and existing saturation on the plants surface, with each of these responding to rainfall inclination with its implied wind dynamics, duration and intensity (Levia and Frost, 2003).

1.2.3.1 Rainfall intensity

Rainfall intensity directly influences stemflow percentage with intense but short storms generating a low SF%, while light and long showers will generally produce a SF% (Muzylo *et al.,* 2012).

Storm characteristic	Tree State	
Intensity and Length	Leafed	No leaf
Low intensity - Short duration	0.30%	0.20%
Low intensity - Long duration	1.80%	3.80%
High Intensity - Short duration	1.65%	0.35%
High Intensity - Long duration	1.65%	4.80%

Table 1: Comparisons of SF% within the same tree for different tree states and rainfall characteristics. Threshold values dividing low/high intensity and short/long duration were 2m/hour and 5 hour respectively. Source – Muzylo et al (2012).

However, attributable to the shorter contact times, higher intensities have higher concentration gradients, leading to a kinetic solubility gradient. Furthermore, rainfall with multiple high-intensity peaks produced higher stemflow volumes than more uniform rainfall intensities (Cayvela *et al.,* 2018); however, this study also noted that funnelling capabilities only increased up to 20mm of rainfall or intensities of 1mm per minute. These findings are substantiated by Levia and Germer (2015), who found that funnelling ratio declined sharply with rainfall intensity, with smooth bark showing sharper declines. Zhang *et al.* (2021) further found linear decreases in stemflow production with increasing rainfall diameter, although this study experimented on arid shrubs, which are less likely to be evolutionarily adapted to handle high rainfall intensities. Overall, the academic literature states that stemflow increases with rainfall intensity but decreases attributable to overloading of the PFP after a critical threshold, variably dependent on tree specific factors, including bark morphology and funnelling capabilities.

1.2.3.2 Timing of rainfall intensity

The timing of the rainfall peak also influences stemflow, as high-intensity peaks at the onset of storms will likely produce more throughfall (Cayvela et al., 2018), while peaks at the end of storms allow for more PFP to be initiated, promoting stemflow generation. Furthermore, if the rainfall intensities remain under 1mm/min threshold, then the number of high-intensity peaks will increase the trees FR for that storm. However, Dunkerley (2014) found opposing results while experimenting with rainfall simulators, indicating that small, constant, and theoretically random minor fluctuations in rainfall intensity significantly influence real-world $SF_{\%}$. There is also an interesting coniferous versus deciduous comparison within this matter, as conifers will usually have lower rainfall synchronicity than deciduous (Cayvela et al., 2018); this is attributable to the higher interception losses found within conifers attributable to their general architecture. However, on an annual timescale, the variations in stemflow volumes and chemistry will be lower in conifer than deciduous trees because of the differing foliage cover on this timescale within deciduous trees.

1.2.3.3 Rainfall duration

Rainfall duration is partially a component of intensity and partially of air pressure. Table 1 displays higher SF% within storm length for comparable intensity characteristics (Muzylo et al., 2012). This generalisation is only disproven in the long storms in leafed conditions where the decrease is likely attributable to increased throughfall. Once stemflow generation commences, stemflow dynamics will closely match rainfall dynamics. This effect is most pronounced on smooth-barked deciduous, then rough-barked deciduous and lastly, conifer species. Increasing duration also increases the amount of ions as the bark is less likely to be overloaded with water, so it has more time to exchange ions (Levia and Frost, 2003; Zabret and Sraj, 2021). As the storm continues, the correlation of stemflow to rainfalls fluctuations decreases as water previously stored in activating flow paths becomes released with often large ion concentrations owing to the long residence times (Iida et al., 2017). These large ionic concentrations are because raindrops intercepted on an uninitiated PFP adhere well to the water film and the underlying adhesion to the bark, promoting branchflow while decreasing the probability of canopy drip (Herwitz, 1987).

1.2.3.4 Rainfall inclination and wind speed

The combined wind direction and strength produces the inclinatory rainfall vector, activating certain PFP's relative to the fluctuating incoming rainfall (Zwieback *et al.,* 2019). These PFP's will evolve parallel to the tree's growth, representing a dynamic component that constitutes a temporal sensitivity on a specific point within the tree's growth. Impacts from moss growing predominantly on the north side of trees or prevailing wind directions predominantly activating flow paths from specific angles also influence the overall stemflow volumes and chemistries recorded (Levia and Germer, 2015; Bates and Bell, 1991). The rainfall inclination is a factor that marries a point on the raindrop diameter and the wind velocity spectrums (Herwitz and Slye, 1995). For example, the raindrop diameter spectrum ranges from the microscopic mist, that near exactly follows the atmospheric wind turbulence, to theoretically 8.6mm in diameter, requiring increasingly significant wind speeds to deviate from the vertical. The following formulas can determine the raindrop inclination based on the droplet diameter and the average wind speed:

Uv = (3.378(in(D))) + 4.213

Tan P_{inc} = $\frac{Wwt5}{Uv}$

Where: ***Uv*** is the Droplet terminal velocity (m/s); ***D*** is the droplet diameter (mm); P_{inc} is the inclination of rainfall (°), and ***Wwt5*** is the weighted 5m average wind speed. A 5m interval is used because fluctuations throughout a storm can significantly impact the resulting stemflow chemistries and volumes; therefore, it must be considered at a reasonably small interval.

1.2.4 Seasonal effect on stemflow

Stemflow exhibits annual cycles within the dynamics of its ions that are attributable to the differences in precipitation type, and the trees annual growth cycle (Neary and Gizyn, 1994). These cycles are best highlighted within potassium's annual fluctuations in stemflow, which has an important regulatory role within photosynthesis, which results in it's a leaching cycle being somewhat correlated to the plants photosynthesis (Levia, 2003). Stemflow volumes and chemical concentrations are often higher in winter attributable to lower rates of wet canopy loss, lesser propensity to generate throughfall, and the higher scavenging efficiency of snow as it falls (Levia 2003; Levia and Frost, 2003). It is intuitive to study stemflow from the scope of the PFP during winter as one can discount to a larger degree the continuous growth of the tree, which could alter the PFP at any point. Whereas, for ionic values within stemflow, the higher scavenging ability and photosynthesising of spring into summer would be more dynamic (Levia and Frost, 2003). Moreover, one can further discount incorporating the point of growth the tree is at during the study, which allows more reliable meteorological implications to be made. A result of winter being the most prevalent time where temperatures fluctuate around freezing in heavily studied temperate regions means that winter stemflow studies also have interesting meteorological influences (Levia, 2004). However, these studies further prove the complexity of stemflow's relationship to meteorological conditions and show that more research is needed before a reliable model can be formed. The dynamics of stemflow alters during the growing season because of the growth of fresh leaves (Bialkowski and Buttle, 2015), which act as new points of interception and greatly complicate the trees structure. The nature of these leaves and the six month or so duration of their lifecycle is discussed within section 1.2.11.4. The increasing rate of photosynthesis during this period will cause fluctuations in the ions associated with it relative to the degree of photosynthesis, with alterations in the PFP of stemflow happening at any point, but somewhat predictable if prior research has been

undertaken, similar to the breach of a meander. Stemflow will alter parallel to the quantity at which the leaves fall, the rate at which they fall is proportional to the wind speeds and the weakened physiological connection to the branches (Niinemets and Tam, 2005). The timing of this fall further impacts the efficiency at which the senesced nutrients are re-absorbed by the tree (Del Arco *et al.,* 1991). Overall, therefore, there has been to date little research on changes in stemflow within single seasonal cycles. Thus further research on smaller timescales is needed to identify key features that differentiate stemflow between leafed and leafless seasons.

1.2.5 Bark

Bark influences stemflow volume and chemical composition through intercepted dry and wet deposition, leachates, exudates and decomposition products (Pallardy and Kozlowski, 2007). The variation between species is primarily through the bark's degree of porosity and its reaction to variations in meteorological conditions. The degree of porosity can be measured through the bark roughness scale (Levia and Herwitz, 2005). This scale counts the number of furrows at breast height and the mean furrow depth to produce a number between 0 and 3, where 0 is smooth-barked and three is rough-barked. For example, a trunk of an Oak tree would be a three, while a fresh branch may be a one, while the trunk of a Birch would be a one. A contributing factor in bark roughness is furrow orientation, which efficiently channels or inhibits stemflow yield (Levia and Germer, 2015), so this influence should be incorporated into the overall evaluation of a bark's roughness. Bark roughness is further known to decrease stemflow pH (Oka et al., 2021), affecting each ion species separately, depending on their relationship to acidity. The bark's overall acidity further influences the compositions of epiphytes growing upon it, which is ultimately a dynamic process that will change as the bark's pH alters temporally, alongside its largely static spatial dynamics.

Bark porosity could be determined as the ratio of free to occupied space within the differential between the innermost and outermost circumference, which would generate an evolution of free-space percentages with branch age. However, a different method could compare the actual and geometric surface areas (Shearman and Varner, 2021). This ratio could be related to its bark water storage capacity (BWSC discussed in 1.2.6.3). Ultimately, the literature is unsure what causes the bark to furrow (Sheridan et al., 2013).

1.2.5.1 The bark of *Quercus Robur*

The Common Oak has porous bark and deep furrows that provide pathways for stemflow travelling down their trunks. The larger furrow amplitudes and slopes inhibit effective drainage in larger storms, with intermediate storms being ideal for stemflow generation (Van Stan et al., 2016), with these furrows protecting entrained water from intra-storm wet canopy loss. However, this could also result in the water being absorbed by the tree (Jensen et al., 2020), which is statistically more common during the night in response to lower levels of transpiration. Furthermore, a slight influence comes from the soil moisture level, as higher soil moisture levels usually result in lower absorption levels, similar to the compensation point found within some atmospheric ions (Behera et al., 2013); however, this was not statistically significant. The bark water storage capacity (BWSC) does not differ greatly from a porous barked oak to the smooth-barked beech (Figure 6), which highlights that it is the ridges and furrows on a barks surface that ultimately control the quantities of stemflow with its respective FR.

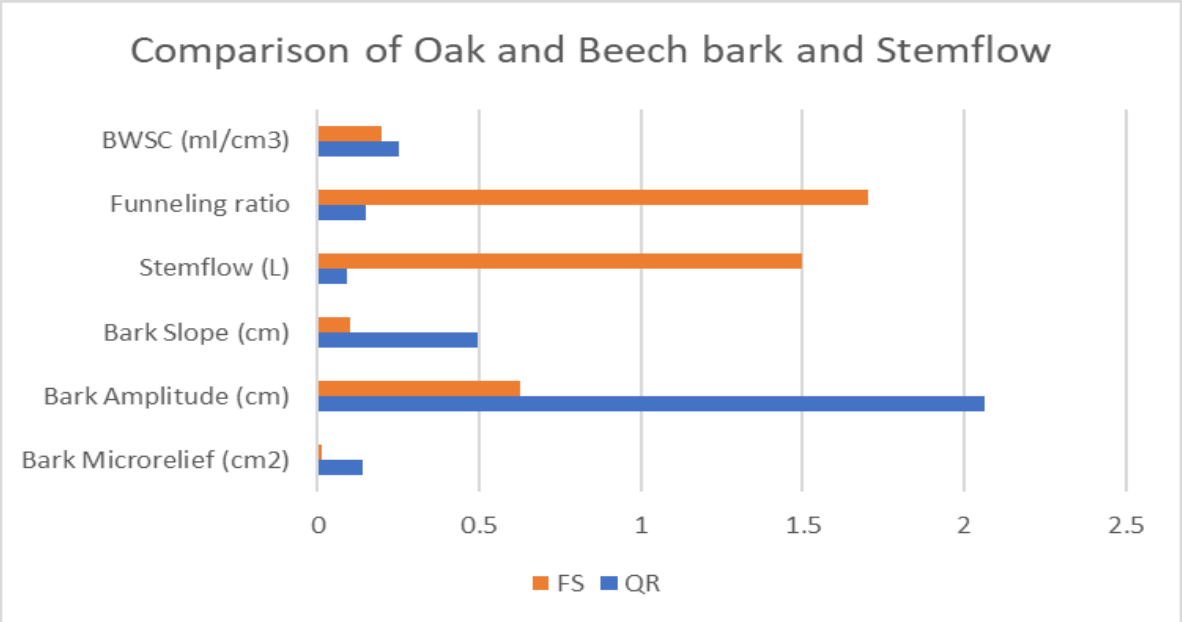

Figure 5: A comparison of Common Oak(Quercus Robur – QR) and Beech bark (Fagus Sylvatica – FS) and their resulting stemflow and FR's. Source: Van Stan et al., (2016).

Oak bark is heterogeneous over the scale of a tree attributable to the age differences related to its growth. The coefficient of this development was determined to be on average 1.45 (Ilek and Kucza, 2014). It should be noted that this describes the evolution of the interception surface; however, one

could argue that the evolution of the overall porosity is more important for the retention and generation of stemflow, as the ability to intercept is less important than the capacity to retain.

1.2.5.2 Bark wettability

The wettability of bark comprises the laboratory portion of some stemflow studies, providing various moisture parameters used to estimate the bark's real-world conditions at any given point (Tonello et al., 2021). For example, moist bark will produce stemflow closer to the storm onset than dry bark, with the speed at which bark moistens being dependent on its porosity (Ilek *et al*., 2017). The alternative is to simulate rain of fluctuating dynamics for varying durations of time. The before and after sample weights are then compared to determine the additional or diminished quantities of water (Blow, 1985). The hygroscopic nature of the bark can be determined similarly after placing the sample in varying levels of humidity to measure the weight change and is the active part of bark wettability.

1.2.5.3 Bark Water Storage Capacity (BWSC)

The bark roughness is the primary inhibitor to stemflow's initial generation. Therefore, bark's overall storage capacity should be discussed on the cm^3 or tree scale. Herwitz (1985) found a range of tropical bark storage capacities between 0.51-0.97 ml/cm3, with whole tree storage ranging from 81-297 L. The cm^3 descriptor is preferred attributable to its increased scientific rigour in comprehending the factor of rainfall inclination, which circumvents the full storage capacity of a tree being used in any singular storm, perhaps except extreme wind and wildly deviating wind directions. However, in no possible conditions will this activate the full storage capacity of the bark.

Furthermore, moisture absorbed from the atmosphere during dry periods can constitute 10-30% of the total bark storage capacity, with percentages of 60% achievable within maximal humidity conditions (Ilek et al., 2021). However, this is primarily done by the outermost bark layers, indicating that detailed knowledge of bark morphologies is required to determine the hygroscopicity. Therefore, the degree of hygroscopicity along the bark porosity spectrum should be evaluated to

fully understand water retention and absorption between storms and the degree to which bark is saturated at any given point in time and on its surface.

1.2.5.4 Bark porosity

Porous bark is bark that has a porous nature, is rough to touch, and is thick from the external layer to the outer sapwood. The degree of porosity of the tree's bark influences the lag time experienced before stemflow generation, meaning smooth-barked trees (e.g. of tree) will produce stemflow faster from the storm's onset than porous barked trees (oak, pine) (Levia and Frost, 2003). This effect is repeated at the other temporal end, with porous bark recording stemflow 48 hours after the storms offset (Levia and Germer, 2015), further indicating considerable windows for overlap for chemical enrichment of precipitation emanating from different storms through the stemflow process. However, if the furrows comprising this porosity are vertical, they will promote efficient stemflow (Carlyle-Moses and Schooling, 2015). Evaporation will remain a constant and annually cyclic process, with Holder (2013) stating a rate of 0.1-0.5mm/h.

Once the interception storage capacity is reached for trees, stemflow temporal dynamics match the incoming rainfall (Levia and Frost, 2003). This effect is more pronounced in hot and windy conditions with intense rainfall as the larger drop sizes reduce the chance of evaporation and relative amount of evaporation compared to smaller drop sizes. However, once this passes a threshold, relative to the degree of bark porosity and existing saturation of the bark, the PFP of the bark can be overloaded with water, causing excess stemflow to be partitioned to become throughfall (Crockford and Richardson, 2000).

The degree of porosity has a profound impact on stemflow when considering the snow and related types of precipitation (sleet, hail), with fluctuations around waters freezing point, attributable to waters expansion, infiltrates more effectively into porous barked trees. Longwave radiation or latent heat released through rainfall fusion causes significant leaching and very efficient washing of dry deposition, leading to high stemflow nutrient concentrations (Levia and Herwitz, 2002). There are different influences of increased kinematic viscosity and surface tension of stemflow. There is also an expectation of depletion of heavy stable water isotopes attributable to higher water condensation in colder air masses (Beria et al., 2018). Comparing snow-to-rain events, where rainfall melts during its descent and an exclusive rain event depicts snow's disproportionate impact on

stemflows ions. The differences in K highlight the increased leaching rate within snow-to-rain events (Table 2).

	Snow-to-Rain	Rain
Rainfall Total (mm)	20.1	21.8
Rainfall duration (hours)	28	10
Rainfall intensity (mm/h)	0.7	2.2
K (mg/L)	11	3.9
K (mg)	9.2	4.3
Mg (mg/L)	1.8	0.47
Mg (mg)	1.9	0.47
Na (mg/L)	1.5	1.3
Na (mg)	1.4	1.2

Table 2: A comparison of stemflow chemistries from comparable storms dominated by snow or rain , but with differing precipitation characteristics.

The inclination of the snowfall will create a more obvious rain shadow, but it will further impact the percentage of snow cover and uncovered, which will impact the trees albedo (Levia and Underwood, 2004). As longwave radiation controls the melt, this will happen more in the upper part of the canopy.

1.2.5.5 The exchange of ions between bark and stemflow

The exchange and selection of ions, where stemflow gains solutes were found to be inconsistent when considering dry deposition nutrients. At the same time, new flow path initiations, which was largely dependent on the current and former rainfall inclinations, intensities, and durations, made the input of ions and nutrients through leaching heavily random (Levia and Germer, 2015). This is while water flows in general are rather predictable on different size scales, so models of how stemflow moves could make the transport of ions more predictable, or provide insight as to why the different spatial scales have different levels of predictability. The dry deposition and canopy structure processes are inherently random, with canopy structure being a rigorous temporal dynamic that will constantly evolve, implying any theories about nutrient or ion throughfall hotspots are temporally sensitive. Dry deposition is equal to both the forces expelling the particle and the constantly changing wind making its path of travel a complicated parabola which are partially calculable through models such as the HYSPLIT_4 (Hybrid single particle lagrangian integrated trajectory) (Draxier and Hess, 1998). Where leaching occurs, rates of Mg2+ and Ca2+ were largely controlled by rhytidome and periderm thickness as this influences the distance between the living cells. Leaching rates of K+ were influenced by the presence of cellular structures linked to resource storage, such as parenchyma, sieve cells, sclereids, and cortex thickness (Oka et al., 2021b).

Further research on K+ within bark is required because it is an important factor in processes such as photosynthesis (Oka et al., 2021b). Specifically, potassium influences the osmotic adjustment in plants, and the formation of sclereids, therefore, the relationship between K+ and bark formation processes could indicate physiological activity of the tree's crown, or we could more accurately predict the orientation of tree growth, which would alleviate the impact of new flow path initiations and greatly improve our understanding of stemflow. Potassium Lidar and electrochemical methods have been used to detect potassium in the atmosphere (Papen et al., 1995) and on a graphene surface (Liu et al., 2018). However, these techniques have not been applied to a long-term stemflow study.

1.2.6 Epiphyte presence

Epiphytes grow on another plant for structural support but are not parasitic (Van Stan and Pypker, 2015) and can further be broken down into bryophytes, lichens, fungi, bacteria, and various sizes of vascular plants. Epiphytes are known to have a profound impact on the nutrient cycling within forests through extremely large water interception and storage capabilities (Pypker et al., 2006), carbon decomposition, nitrogen fixation (Ponette-Gonzalez, 2021), while nutrients leached from intracellular stores of K+, Mg2+, and Ca2+ show seasonal variations, which, in the case of K+ show a general quantitative decline after the senescing of leaves, with an increase in early summer, substantiating that K+ plays an important role in photosynthesis (Bates and Bell, 1991). Furthermore, epiphytes cause dynamic alterations to stemflow PFP dynamics by diverting water, producing throughfall or close throughfall gaps through large-leafed vascular epiphytes. The lower winter stemflow values are also partially attributable to epiphyte presence (Van Stan and Pypker, 2015) as the efficiency at which epiphytes intercept water decreases with increasing rainfall; however, this further depends on the antecedent conditions attributable to epiphytes being able to hold 250-1000% of their dry body weight in water.

1.2.6.1 Vascular epiphytes

Vascular epiphytes are most commonly found in tropical environments (Zotz, 2001); however, they can exist in vines in temperate environments. Chen et al. (2019) found that the overall size of the epiphyte was the most important factor in how vascular epiphytes influenced stemflow, followed by whether or not the epiphyte was substrate-forming. However, their analysis shows no pattern if one separates the ions by species. Vascular epiphytes can also alter the spatial dynamics of stemflow's infiltration area while increasing the overall canopy storage capacity (Fleischbein et al., 2005); however, this pattern of increase is not equal among different epiphyte classes. Vascular epiphytes will have a separate set of stemflow dynamics, as their growth is sometimes similar to a stemflow collar, but alongside their alterations to spatiality of stemflow inputs, some species are evergreen, which promotes greater interception of close-to-trunk rainfall or dislodged throughfall. No study to date has documented the ionic differences between primary trunk and temperate vascular epiphyte stemflow.

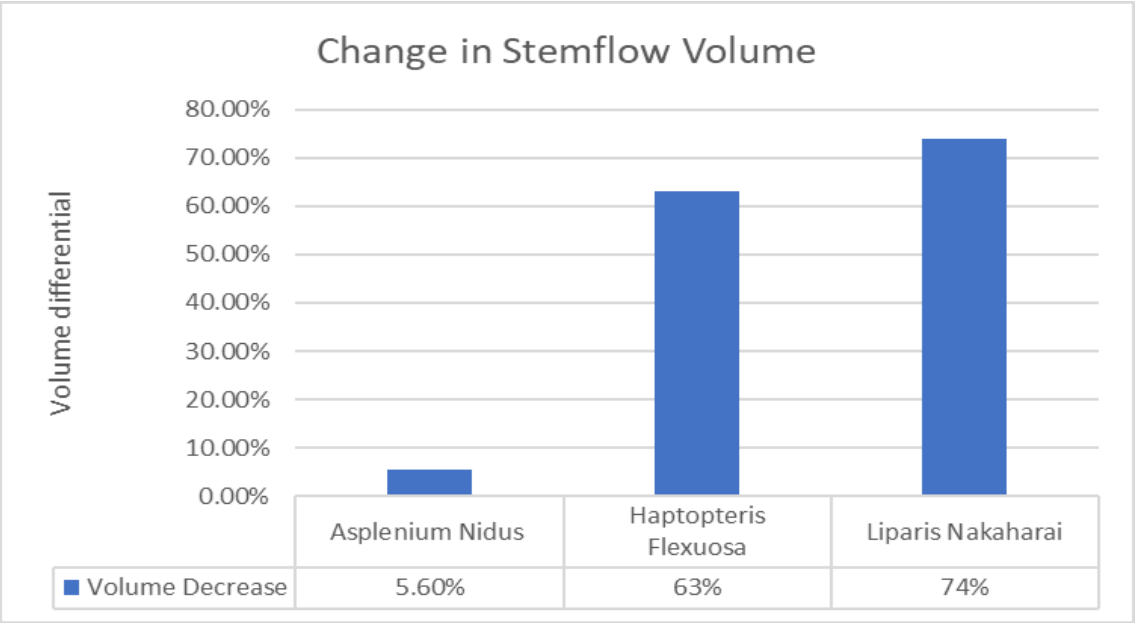

	Largest	Middle	Smallest
	Asplenium Nidus	Haptopteris Flexuosa	Liparis Nakaharai
Conductivity	-7.96	0.531	17.2
H+	14.96	-14.3	-1.38
Na+	-3	3.79	-2.45
NH4+	0.22	-0.79	-2.38
K+	-36.9	0.33	60.1
Mg2+	-11.1	1.32	2.48
Ca2+	-11.2	35.9	21.5
Cl-	-8.31	2.45	7.69
NO3-	4.67	2.76	29.4
SO42-	0.34	1.05	1.24
PO43-	-3.39	-1.66	22.9
pH	4.94 to 4.58	4.45 to 4.68	5.54 to 5.81

Figure 6a and b: Bar graph showing the stark differences in stemflow volume alterations with their matching ionic alterations in the table below, showing that substrate-producing epiphytes are far more efficient at retaining ions.Data from (Fleischbein et al., 2005).

1.2.6.2 Bryophytes

Bryophytes living on tree bark comprise liverworts, hornworts, and mosses (Budke et al., 2018), which, attributable to their porous nature, can capture and retain significant amounts of stemflow (Pypker et al., 2006), often increasing in biomass parallel to a tree's growth (Fritz et al., 2009). The main influences for bryophyte growth from the occupied phorophyte are the barks pH and tree vitality (Fritz *et al*., 2009). Bryophytes are commonly linked to nitrogen absorption in forests (Chuyong et al., 2004), with significant leaching of Ca2+, Mg2+, K+, and moderate to low leaching of SO24-, PO43- found in bryophyte and vascular/lichen assemblages. Upper canopy bryophytes are also known to release sugars during storms, possibly as a by-product of consuming decomposed organic nitrogen, which they do by using 15N-Labelled glutamic acid (Van Stan and Pypker, 2015). Deposition of nitrogen directly affects the pH of the bark, which is the influence that bryophytes directly respond to through the facilitation of spore germination. The pH of the bark is also attributable to soil nutrient content, and sulphuric deposition (Mitchell et al., 2005), which is a response to phorophytes spatiality, through the tree either being inland versus coastal or protected versus exposed will further affect bryophyte community quantities and compositions attributable to their poikilohydric nature. McGee et al. (2019) substantiate the full impact of bryophytes poikilohydric nature as they found that increased moisture, nutrient availability, either through

stemflow or throughfall and the hygroscopicity of the bark increases the percentage bryophyte cover and species diversity of the community. In addition, there is a disproportionate quantity of moss growing on the northern sides of trees attributable to the increased shade from the suns inherent angle in our hemisphere, meaning the bark is less likely to dry out, again highlighting bryophytes poikilohydric nature. However, no study could link this effect to alterations in stemflow volume, or PFP highlighted the scant attention that stemflow's spatiality has received compared to other aspects of the process.

1.2.6.3 The epiphytic and metazoan coverage of *Quercus Robur*

The bark of the Common Oak provides a moderately healthy environment for many epiphytic organisms to thrive. The long duration of the remaining saturated provides the perfect habitat for bryophytes, with lichens similarly responding to the abundant ions with its stemflow (Leith et al., 2008). However, the more acidic stemflow does prohibit some species from proliferating. Bryophytes absorb stemflow, which primarily determines their tissue N concentration, which is predominantly in the form of ammonium. Many studies use moss as a metric of atmospheric N deposition (Chuyong et al., 2004). However, Leith et al. (2008) found that the tissue N concentration was primarily influenced by the total number of nitrogen ions that pass over the bryophyte. Furthermore, bryophytes growing under the influence of a Common Oak tree were found to contain higher amounts of N, Mg, P, S, K, Ca, Mn, Ni, Cu, Pb, and H than those growing in more open conditions (Samecka-Cymerman et al., 2010), highlighting both the positive and potentially harmful effects of bryophytes spatiality nearby or inhabitation of a phorophyte.

Lichens can be found on Quercus Robur; however, Larsen and Rasmussen (2017) found that a lower bark pH and dense ion concentrations provided a strong inhibitory effect on corticolous lichen spore germination. Nevertheless, lichens that are more adapted to lower pH values could still survive on the bark of Quercus Robur, as corticolous lichen need a pH greater than 5.1 to germinate, with the oak bark samples being 4.7 and 4.9 at 15.5m and 5.5m from the surface respectively. In addition, fruticose lichen spotted on oak trees within the Clyne Country Park contained Fruticose lichen, which can germinate in pH conditions of 4.3-5.5 (Ponmurugan et al., 2016).

The furrowed bark of Quercus Robur allows firstly for plentiful amounts of bryophytes, bacteria, and some forms of lichen, which in turn, attract metazoans including nematodes, rotifers, tardigrades,

mites, and collembolans, however, in lower quantities than beech or maple trees (Ptatscheck et al., 2018). The moss, lichens and bacteria on oaks provide food for these metazoans. However, the lower pH is known to negatively affect nematodes, with possible negative effects on tardigrades and rotifers (Letham et al., 1982). The pH of the bark has also been shown to affect nematodes through its effect on tannins, providing a headache for both nematode movement and survival on oaks (Kraus et al., 2003).

1.2.6.4 Lichen

Lichens are a composite organism of algae or cyanobacteria living among filaments of fungi often living on tree bark. The mutualism of singular fungi and photosynthesising bacteria form body plans that resemble neither individually but together are known as lichen (Spribille et al., 2016). The difference in a fungus that partners with algae is that they cannot perform nitrogen-fixation, while lichen partnered with cyanobacteria often can (Henskens et al., 2012). The species composition of lichen on any given tree is a function of primarily age, secondly, the bark porosity, and thirdly, the percentage of moss cover. Lichens store most Ca^{2+} and Mg^{2+} in the inter and intracellular exchangeable tissue location, while they store K^{+} intracellularly (Van Stan and Pypker, 2015).For this reason, lichens living on tree bark are unlikely to leach significant quantities of these nutrients unless the lichen is damaged prior to stemflow generation. As part of their N-fixation, lichens readily uptake NH_4^{+}, but not NO_3^{-}because lichen contains plentiful apoplastic cation exchange sites containing carboxylic and hydroxylic moieties (Huack, 2010). They then promptly break this down into organic compounds because NH_4^{+} is cytotoxic. Mg^{2+} is another toxic element to lichen (Levia and Germer, 2015), so lichens are often less abundant on Holm Oak (Quercus Ilex), with some trees translocating Mg"+ to their bark to avoid having toxic concentrations in their leaves (Ponette-Gonzalez, 2021), which would cause reductions in lichen populations with the consequences felt within stemflow. Low stemflow pH can also reduce lichen populations through H^{+} toxicity to algal photobionts (Fritz et al., 2009); this is part of the reason why lichen populations are affected by tree age because bark pH decreases with tree age affecting stemflow pH, therefore lichen populations (Mcgee et al., 2019).

1.2.6.5 Fungus

The relationship between trees and fungus is a component of stemflow as this provides the main mode of transport for dendronatant fungi (Magyar et al., 2021). The relationships are primarily driven by bark physico-chemical properties, tree spatiality, and the spatial diversity of in-canopy microenvironments. In addition, the degree of bark porosity further delays stemflow, which prevents the scouring of fungal spores from the bark surface, further substantiating that porous bark is more suitable for fungi communities (Sansalone and Cristina, 2004).

1.2.6.6 Microbes and bacteria

Microbial communities within bark play important roles in the cycling of nitrogen and carbon in forests (Ponette-Gonzalez, 2021), often through fixation of nitrogen or through decomposition of complex carbon structures by heterotrophic bacteria and fungi. These communities can also consume methane through methane oxidising bacteria (Jeffrey et al., 2021). Some trees are known to have formed symbiotic relationships with N-fixing bacteria in exchange for nodulation; stemflow containing allelopathic compounds can therefore affect this modulation (Rosier et al., 2015). The effect can be detrimental in dry deposition sea salts, which affect root hair curling, or positive when Fe, B, Mn, and Mo are found within stemflow. The elements Fe and Mo are especially important attributable to their representation in the Nitrogenase enzyme FeMoCo, which catalyses the conversion of atmospheric nitrogen into ammonia.

1.2.7 Tree structural characteristics

Tree geometry is categorised into branch inclinations (Herwitz, 1985; Yuan et al., 2016), which controls the initial interception of rainwater (Levia and Frost, 2003). Then branch number and diameter, with the complexity and number of overlapping branches also important as quantitative influences on stemflow interception and tree FR. These influences evolve throughout a tree's lifespan, with certain trees having noticeable alterations in their FR (Levia and Germer, 2015), with the annual cycles of leaf growth and senesce adding routine complexity among deciduous trees (Levia et al., 2015).

1.2.7.1 Branch inclination

The angle of the branch's control is how likely a raindrop will be intercepted (Herwitz, 1985), with higher angles spreading the projected area of impact over a larger area, giving a higher chance of collection. The other impact of the foliar or woody surface and its size, as porous bark may circumvent the following formulas if a raindrop hits a deviation within a furrow, therefore collecting the drop at any angle. The following table is a branch inclination to stemflow quantity formulas from previous academic work.

Tropical Trees	Dry Branch	Y = 0.4 + 1.32x	Herwitz (1985)
	Saturated branch	Y = -14 + 24.02(in(x))	Herwitz (1985)
Xerophytic Shrubs	BD 5-10mm	Y = 4.23 * X – 4.61	Yuan et al. (2016)
	BD 10-15mm	Y = 12.74 * X – 21.57	Yuan et al. (2016)
	BD 15-20mm	Y = 24.11 * X – 50.55	Yuan et al. (2016)
	BD 20+mm	Y = 49.61 * X – 125.19	Yuan et al. (2016)

Table 3: The formulas between rainfall amount (X) and the amount that eventually becomes branch flow. Note that this does not mean that this branch flow will become stemflow. BD – Branch Diameter

These formulas require further modification when considering temperate environments, further impacting where the bark's spectrum of bark saturation lies; furthermore, variables such as incoming rainfall velocity, which is lowered through processes like canopy wash, will dramatically increase the percentage likelihood of interception by the branch.

The branch inclination will be relative to the results of the previous formulas with Levia and Herwitz (2002) studying the angles of 5°, 20°, and 38° on *Carya glabra* and *Quercus rubra* trees in a natural setting. An ideal of 20° was found as this angle allowed for reasonable residence times, with 5° having residence times long enough that it allowed for significant quantities to drain and drip from the underside of the branch. In contrast, angles of 38° promoted shorter residence times, therefore, lesser ion exchange, which is consistent in rank but no difference throughout the five studied ions. However, this considered artificial vertical rainfall, with altered rain shadows through real-life wind dynamics, will likely decrease this top-heavy preferability on a gradual scale with increasing angling from vertical. While larger branch inclinations relative to the horizontal will intercept a greater percentage of water, lower branch inclinations will produce more nutrient-rich branchflow.

Concentration (mg/L)	Angle of Branch		
Average +/- 1SD	5	20	38
K	3.4 +/- 0.4	8.3 +/- 1.1	5.9 +/-0.7
Ca	1.0 +/- 0.3	2.2 +/- 1.0	1.6 +/- 0.5
Mg	0.53 +/- 0.1	1.5 +/- 0.2	1.1 +/- 0.2
Na	0.85 +/- 0.1	1.1 +/- 0.1	0.89 +/- 0.1
Mn	0.06 +/- 0	0.12 +/- 0	0.08 +/- 0

Table 4: A table illustrating the quantitative differences in ions determined to be a function of the branches angle. Data from Levia and Herwitz, (2002).

1.2.7.2 Combined branch and leaf influence on Stemflow

Bark exhibits hygroscopic abilities, which is its ability to exchange moisture with the open atmosphere to achieve an equilibrium. As a branch's saturation is a dynamic variable that will vary rarely fall into a binary category, which in turn impacts stemflow's chemistry (Levia and Germer, 2015). The formulas (Table 3) imply that branchflow interception will increase with increasing branch inclination as the area and therefore, the impact of the raindrop is spread over a larger area; however, a threshold between the area of this force and the orthogonal projection of the branch will eventually decrease the overall quantity of stemflow (Levia and Frost, 2003). Similarly, a critical peak of stemflow productivity will be reached at a certain branch diameter, indicating that plants receive higher stemflow returns from several branches (Gotsch et al., 2018). For older trees, primary branches start to outweigh their rigidity and sag away from the trunk (Voigt, 1960), promoting greater throughfall generation. This observation partially explains why most stemflow is sourced in the upper half of the canopy (Bialkowski and Buttle, 2015), with the effects on a tree FR being somewhat comparable within species in comparable conditions, provided no damage had previously occurred.

Similarly, while there is more stemflow in winter due to the absence of leaves, they do increase the rate of interception and lower the force of impaction; therefore, a smaller number of leaves may increase stemflow for a short period during their growth (Levia et al., 2015); however, the hydrophilic nature of fresh oak leaves may prevent this to an extent (Klamerus-Iwan and Witek, 2018). Furthermore, one must consider the porous nature of oak bark, as this will provide micro dynamics of impact and splash portions of particular drops. The angles of the upper canopy are important as 98% of the water that becomes stemflow is intercepted in the upper half of the canopy (Hutchinson and Roberts, 1981). However, this could be a different influence of the less porous

young bark (Levia et al., 2015). If one further considers an oak, its bark can carry 0.25 ml/cm^3 (Van Stan et al., 2016); therefore, the number of branches could decrease stemflow amounts if there is significant absorption or evaporation (Herwitz, 1985).

1.2.7.3 The hydrodynamics of Quercus Robur's leaves

As the leaf of a Common Oak grows, exists, and senesces, its hydrodynamics fluctuates from hydrophobic when young to hydrophilic when old (Klamerus-Iwan and Witek, 2018). This water storage capacity (WSC) is determined by the spatiality of the tree, the age of the leave, the percentage cover of fungus such as mildew, and the angle of incoming rainfall. The most important factor is the leafage, as this controls the duration for which it has been susceptible to powdery mildew, with its spatiality controlling the level of pollutants in rainfall and the rainfall angle to an extent.

Throughout May to September, a leaf that remains free of mildew will increase in WSC from 0.89 to 11.21g/g in a natural forest and 0.915-15.86g/g in an urban forest, with increasing mildew coverage, the September value increases to 25.02g/g and 35.05g/g for natural and urban respectively. This disparity highlights the importance of mildew in increasing the surface roughness of the leaf (Klamerus-Iwan and Witek, 2018), presenting a positive relationship between mildew coverage and WSC (Klamerus-Iwan et al., 2017). The relationship between seasonality and WSC is partially a result of this; however, the increase in WSC does not require mildew but is improved by it (Aryal and Neuner, 2010). Furthermore, the spatiality of the tree is an independent variable, controlled by either wind dynamics or town planners, where urban trees will often receive consistently high temperatures, less wind protection, especially in many US cities because of the gridiron planform and higher levels of pollutants (Popek et al., 2012). These pollutants, in turn, alter the evolutionary dynamics of the leaves WSC.

1.2.7.4 The Funnelling ratio and evolution of it.

The combined geometry of branch angles, alongside their response to the meteorological variables during and prior to the storm, forms the FR, a tree's ability to funnel water. This metric should also

consider the percentage of the crown area from each inclination occupied by branches in winter and the ratio of woody to foliar surfaces in summer (Levia and Germer, 2015). This disparity does not apply to conifer trees. The funnelling ratio formulas are often simple representations that do not consider the percentage cover of epiphytes; however, the geometry of any given tree is a temporally dynamic influence that can dramatically change over its lifetime, with certain trees having noticeable age-related jumps in their FR (Levia and Germer, 2015). For example, Japanese Cypress trees average FR decreases from 81.3 at nine years to 30 at 12 years (Levia and Germer, 2015). In addition, there is an ecological influence on FR, as in a study considering the FR of desert shrubs, Garcia-Estringana (2010) found no sub-horizontal branches, with the lowest average branch angle being 50°, so one can theorise that desert shrubs forgo some chemical enrichment of the stemflow in order to increase stemflow.

1.2.8 Stemflow measurement methods

Stemflow is typically collected using stemflow collars (Herwitz, 1988), which are made of flexible tubing that is fixed to a tree and sealed to the tree surface using a silicone sealant, or any sealant that provides a waterproof seal. The first method is the spiral stemflow collar, where the tubing wraps around the tree (Levia and Herwitz, 2000); the second is the straight collar, where the tubing is wrapped around a single height on the trunk (Wang et al., 2011), usually at the lowest convenience. These methods could be modified to test other parameters; for example, multiple collection buckets for each quarter or half of the tree's circumference could test the impacts of epiphyte spatiality or precipitations incoming vector relative to the wind dynamics during the storm. However, the spiral collar is predominantly used in larger plants, whereas straight collars are predominantly used in arid foliage or in comparing branches of a single tree.

The collection bucket is where the volume of stemflow is collected. This can be modified to study time-related characteristics of stemflow, for example, the collection bucket could be connected to a datalogger, determining temporal dynamics throughout the storm (Durocher, 1990). These dynamics apply primarily for volume, as temporal stemflow chemistry analyses will require manual collector changes at chosen intervals to avoid contamination from the previous volumes; however, this can be somewhat circumvented if one is researching the chemistries development.

1.2.9 Conclusion on stemflow

To conclude, any single storm event can cause damage at any level to the tree stem, which will also generate new PFP, so a complex understanding of tree growth predictions alongside an accurate 3-D model of any given tree is required. The bark hygroscopicity, epiphyte population compositions and their evolution alongside bark pH and its roughness, with a full comprehension of the meteorological and external biotic influences, is also required to understand the dynamics of stemflow within any given tree comprehensively. Previous studies have often attempted to tackle each of the issues separately, often completely ignoring one of the primary contributors to stemflow's ionic composition. Therefore, an understanding of how the ionic composition of stemflow evolves from early spring to early summer could deepen the understand of stemflow and open new insights into waters role as a solvent. Further elements of bark moisture and stemflow droplet movement could help with the overall understanding of stemflow as a waterflow process.

1.3 Dry deposition of ions

Dry deposition (DD) removes airborne particles or gases from the atmosphere by gravitationally delivering mass to a surface (Mohan, 2016), which delivers some on the constituent ions to the overall stemflow ionic composition. This mechanism is an important part of the biogeochemical cycling of many elements and involves three motion categories and exchange dynamics: aerodynamic transport, boundary layer transport, and uptake by a receptor (Mohan, 2016). Within each of these, the dynamics of DD are influenced by meteorological factors, primarily wind speed and direction, with relative humidity and temperature being secondary influences (Levia *et al*., 2011). However, the independent size of the particle will determine its gravitational influence, therefore the weighting of primary over secondary influence. Moreover, the particles found within DD can either be primary aerosols, which are the results of direct emission, or secondary aerosols, which result from physical and chemical processes within the atmosphere (Morallis *et al*., 2016). As evaporated water is a gas, it removes all of the ions within the process (Rovelli *et al*., 2020), meaning that the biogeochemical cycling within the hydrological cycle effectively refreshes once it reaches this point. In addition, micro-scale physics influences the particles' kinetic energy, impacting the bark

or foliage morphology at the Spatio-temporal point of interception (Mohan, 2016), which is further complicated with functional relationships between epiphytic organisms and DD transported particles.

1.3.1 Influence of particle size

Airborne Particles can theoretically be any size relative to the wind speed; however, the larger the particle size is, the quicker gravitational influences will take hold. Particles in the range of 0.1-1µm, which includes most nitrate, sulphate, and ammonium ions (Table 5), along with most ions from urbanised and industrialised sources, fall within this category. These particles are removed very slowly by DD, having some gravitational influences but small enough that travelling significant distances in the right conditions is still possible. There are often size disparities within each ion species, which can place them in the 1-10µm category, meaning these particles can be removed from the atmosphere by impaction onto leaves and other obstacles. Particles that fall beneath 0.1µm in diameter come under the influence of Brownian diffusion (Petroff et al., 2008). When particle sizes are above 10µm, they fall slowly by gravitational settlement (Mohan, 2016), where larger diameters fall faster. For example, particles with a 150µm diameter will have a settling velocity of 1m/s, meaning they remain airborne for very short periods. The settling velocity of any particle, which is the same as its terminal velocity, can be calculated through the Stokes equation:

$$v = \frac{g\left(\frac{p_1}{p}-1\right)d^2}{18v}$$ (Stokes, 1851)

Where: V is the settling velocity of the particle; g is the gravitational constant; P_1 is the mass density of the solid; P is the mass density of the fluid; d is the diameter of the solid; and v is the kinematic viscosity of the fluid.

Brownian diffusion affects particles under 0.1µm in diameter and is the characteristic random wiggling motion of the particles, which is the result of the continuous barrage from surrounding gas molecules (Lui, 2010), which disproportionately diffuse towards obstacles (Petroff *et al.,* 2008). The Brownian diffusion coefficient (D) can be calculated with the following formula:

$$D = \frac{kTCc}{3\pi\mu\, dp}$$ (Lui, 2010)

Where: K is Boltzmann's constant ($1.38x10^{-23}J/k^{-1}$); T is the temperature in Kelvin; C_c is the slip correction factor for small particles; μ is the dynamic viscosity of the air; and Dp is the diameter of the airborne particle.

1.3.2 Influence of Weather

Dry Deposition responds in some way to all weather dynamics, with the primary influence coming from the wind speed and direction, as this provides the mode of travel for airborne particles (Mohan, 2016). Therefore the predominant direction of travel for airborne particles at any given point is dependent on the areas of high and low air pressure within the larger atmosphere. The secondary influences are through relative humidity, which increases particle size, increasing the rate of deposition (Mohan, 2016). Therefore the wind and humidity variables work in tangent to determine the ultimate parabola of travel of each particle.

Dry deposition's relationship to temperature is complicated as various factors appear to contradict each other (Mohan, 2016). Meteorology states that higher air temperatures increase atmospheric mixing, which should decrease DD, however temperature will also increase particle velocity, which increases DD for particles more influenced by gravity, so the relationship between DD and temperature is primarily dependent on particle diameter. Therefore a spectrum likely exists where the correlation between temperature and DD dips to a minimum, however the exact diameter is not yet known.

1.3.3 Boundary layer dynamics and uptake by the bark

As the ion approaches the obstacle, in this instance, the bark of an oak tree, the dynamics of the particles velocity along with the eventual exact position of its impact will generate different dynamics dependent on the micro-scale morphology of the bark (Petroff *et al.,* 2008). The eventual fates of the particle are either interception, impaction, sedimentation or rebound, each of which are dependent on the particles velocity vector and the force of their impact, which is a result of their size or diameter.

Interception occurs when a particle of small inertia travels within half of its diameter in proximity to the obstacle, therefore this process is partially particle size and wind speed dependent. The wind speed is more influential as this governs the overall inertia of the particle and whether the particle can eventually follow the flow deviation caused by the obstacle (Petroff *et al*., 2008). Impaction follows and involves the morphology of the surface (Petroff *et al*., 2008).

1.3.4 Sources and behaviours of different ions

There are ultimately three categories in which the ions can fall when considering coastal environments with a marine originating prevailing wind, that is atmospheric ions, which constitute a combination of nitrogen and oxygen compounds (O_3, SO_2, NO, NO_2, NO_3-, NH_3, NH_4, NHO_3) (Wesely and Hicks, 2000), or sea salt ions (Ca^{2+}, Mg^{2+}, Cl, Na^+, SO_4^{2-}, K^+) (Andreas *et al.,* 2016), which originate from the spray of seawater. There are also heavy metals and miscellaneous ions (Al, Fe, F^-, Mn etc.), which are either trace metals or pollutants that have become airborne through various means (Liu *et al*., 2019). Each of these ions have varying effects of plant life if they are deposited on a plant surface, dependent on both the concentration of deposition and the species of plant.

The atmospheric ions are primarily emitted through industrial and agricultural means, originally as NO and NO_2 (Bjorkman *et al.,* 2012), with the abundant amounts of nitrogen and oxygen in the atmosphere allowing for plentiful reactions into the more complex compounds, including NO_3-, and HNO_3. The degree of atmospheric reactions is assumed through large NO emissions but close to negligible DD of the compound, an example of this are soil emissions of NO reacting with O_3 to form NO_2. NO_3^- can be formed in the atmosphere or it can be found in the form of Nitratine, which was a source of nitrogen in fertilizers (Ellis, 1999). HNO_3 is less common but can be formed rapidly in large near-surface ammonia quantities (Wesely and Hicks, 2000). Ozone and sulphur dioxide are both results of fossil fuel combustion, so their prevalence is greater around urbanised areas with decreasing prevalence as proximity from these areas increases (Nowlan *et al.,* 2014). The uptake of these ions is primarily linked to the existing moisture on the plant surface, as increasing wetness will increase uptake substantially for both, however for O_3 there is some resistance to uptake by epiphytes inhabiting their phorophyte. Ammonia and Ammonium are combinations of Nitrogen and Hydrogen, which are emitted through the use of fertilizers, livestock, and various other exchanges (Behera *et al.,* 2013). The range of global emissions for NH_3 ranges considerably from 45-75 million tonnes per year (Schleninger *et al*., 1992; Dentener and Crutzen, 1994), and are increasing, with the

formula y = 621.6x + 26281 (r^2 = 0.95) detailing the relationship between year (X) and the global emission of NH_3-N in Gg. The emissions of NH_3 cannot travel large distances, with a 50% reduction 600m from source (Erisman *et al.,* 1987) and a 70% reduction 4km from the source (Asman *et al.,* 1989). NH_4^+ is produced when NH_3 chemically reacts with water to then be used as a source of nitrogen in plants. Plants can both emit and absorb NH_3 depending on whether the atmospheric quantity is above or below the compensation point, therefore, showing that plants regulate their own microclimate (Behera *et al.,* 2013).

The sea salt ions are sourced from the emitting of sea salts that become airborne through the dynamics of wind interacting with the sea surface (Andreas *et al.,* 2016). For this reason, the quantity that is emitted is a relationship between proximity to the coast and the fluctuating strengths of wind. The first instance in which this can happen is through the spray on the back of breaking waves. Owing to the circular motion of the waves there is a vertical component to the wind, which supports the dragging of spray droplets, allowing the ions to become airborne and follow the turbulence of the wind. The second part is the spray produced through the bursting of bubbles on a whitecap.

The proportions of sea salt vary on a global scale, so the actual amount of each ion that is emitted is inherently random. With a range of sizes between 0.05-10µm in diameter, meaning that they can fall within 3 DD categories, ranging from Brownian diffusion to removing through impaction on obstacles. This size disparity is further impacted by relative humidity attributable to the hygroscopic nature of sea salts (Levin and Cotton, 2009).

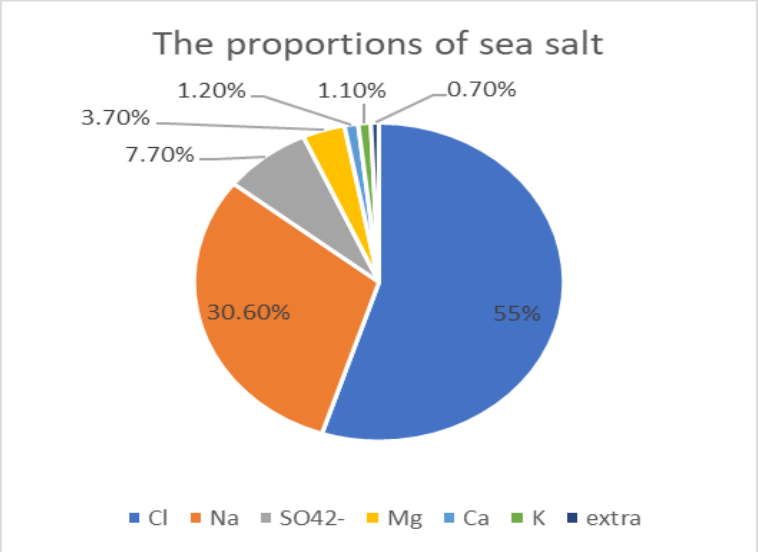

Figure 7: The average proportions of sea salinity, with the ion species identified by their period table and empirical formula in the case of sulphate

The third category of heavy metals is the smallest by mass; however these ions also have a very large impact of foliage they come into contact with (Dumat *et al.,* 2017). There are two further subcategories within the heavy metals, the ones that are essential micronutrients but toxic to foliage at higher concentrations (Mn, Zn, Cr, Cu, Fe, Ni) and those that are toxic at any concentration (Hg, Cd, As, Pb). These metals are overwhelmingly emitted through heavy industry, with many of the metals having to be applied in combination with others to provide toxic affects which varies dependent on the plant (Shahid *et al*., 2017). There is a further possibility of heavy metal speciation once the metal is absorbed, however this further depends on the metal as Pb is likely to speciate, while As will not. Plants can further regulate their heavy metal intake through methods such as avoidance, which simply reduces overall uptake; tolerance: where the metals are translocated to a sink within the plant; or binding where they can limit the toxic effects of some metals.

1.4 Wet Deposition of Ions

Wet deposition (WD) is the movement of airborne particles to the Earth's surface through precipitation, snow or any other moisture (Cheng et al., 2021). This movement implies a gravitationally induced vertical component, whereas the partial WD of mist and fog comprises a unique set of dynamics within this hydrological process (Trautner et al., 1991). The ions are emitted into the atmosphere through the processes discussed in section 1.3, meaning that WD is generally higher for industrially sourced ions in urban areas. However, WD involves the particles scavenged within or below clouds before they can be deposited. In-cloud scavenging involves particles acting as cloud nuclei, which affects climatic dynamics through the absorption and reflection of radiation while modifying in-cloud properties (Croft et al., 2009). Meanwhile, below-cloud scavenging involves particles intercepted by falling precipitation and absorbed within the droplet or flake (Xu et al., 2017). The underlying forces which control WD dynamics are the air temperature and humidity (Paramanov et al., 2011), the precipitation rate, the element dependent Scavenging ratio , which is the ratio of precipitation to atmospheric particles (Duce et al., 1991), with further influences of the solubility of the element, and the spatiality of the deposition.

1.4.1 Meteorological Influences

The meteorological influences on WD are rainfall, air temperature and humidity. The most influential is the precipitation flux, which ultimately controls the voluminous limit to WD (Cheng et al., 2021); however, dilution can be expected with dense cloud cover and precipitation as industrial emissions of each element are reasonably consistent in their annual fluctuations, with rainfall being less predictable. In addition, the positioning of high and low air pressure systems will ultimately determine the direction of cloud travel which will impact the proportions of elements scavenged, along with the cloud type, as higher-flying clouds will not be able to scavenge heavier elements through in-cloud scavenging. Therefore, a positive correlation between WD and precipitation rate exists until a threshold, where dilution reduces the average WD quantities. A further influence implements air pressure as higher air pressures are associated with clearer skies (Dempsey, 2018), therefore a higher rate of DD over WD.

The air temperature ultimately decides on the positioning on the ice to water spectrum the droplet falls into, modifying the surface area of the droplet/flake, which impacts its potential scavenging efficiency (Wania and Lei, 2004). The temperature will also impact the energy at which ions collide (Gabelica and Marklund, 2018), which is within the droplet's fluctuating viscosity, dependent on the temperature within a liquid phase. This efficiency increases with snowfall attributable to the larger surface areas and smaller falling velocities for an average factor of 3 for all common elements; however, for metals (Al, Cd, Cu, Fe, and Mn), this efficiency increased by over a factor of 4, while sea salts were slightly below average, with their hygroscopic nature boosting their scavenging ratio. Potassium was the only element with a larger scavenging ratio in the rain (Cheng et al., 2021). This scavenging ratio bodes well for deciduous trees as when metals are scavenged and deposited more easily; there is less foliage to absorb them, reducing the chance of phytotoxic effects (Gall et al., 2015). The further factor of precipitation pH is that forming bonds with hydrogen increases scavenging efficiency by roughly the same amount in both rain and snow (Wania and Lei, 2004). This efficiency is because of the H+ binding favouring absorption over dissolution in both rain and snow, which are comparable because of a small water film on snowflakes.

Humidity's influence depends on the element's hygroscopicity; therefore, humidity has a larger impact on marine WD as sea salts have a higher hygroscopicity. Sea-salts are also far more likely to be scavenged below the cloud; however, any increase in below-cloud scavenging will be partially

attributable to decreases in in-cloud scavenging (Croft et al., 2009). Carbonaceous and sulphate particles are the least likely to incorporate in-cloud scavenging or below-cloud scavenging within their cycles; this is partially attributable to their insolubility which inhibits them from acting as cloud nuclei.

1.4.2 Elemental influences

The individual elemental influences are primarily attributable to their solubility and solubilities response to the parameters of temperature, pH, emission source, particle size, and atmospheric reactions causing chemical forms of the element and concentrations of each element. Therefore, the ability to dissolve and be incorporated within a cloud, raindrop or snowflake allows a particle to be measured as WD (Cheng et al., 2021). However, elements can be categorised into gaseous and non-gaseous, where the non-gaseous have what is known as a sedimentary cycle (Likens and Bormann, 1995). The difference is that the hydrologic input and outputs are very evenly weighted for gaseous elements. However, there is a large disparity between the input through deposition and hydrological output for sedimentary cycles because of the high input rates through weathering. Examples of the sedimentary nutrient cycles are the sea-salts calcium, Magnesium and Potassium (Obum, 1959), whereas the gaseous cycles involve carbon, nitrogen and sulphur.

There are additional influences on solubility from the particle matter the element is bonded to, as coarser material will always have lower solubility than finer matter, with the concentration of elements in ambient air being inversely correlated with their solubility. The notable exception of zinc has a wide range of solubility depending on the source of its emission (Oakes et al., 2016), with more soluble zinc being industrially sourced and less soluble being sources from sources traffic emissions.

1.4.3 Fog and mist deposition

Mist and fog form when hot and cold air masses interact; in the case of fog, it condenses suspended liquid water, while mist occurs when a warmer air mass encounters the cooler surface of the land (Ahrens, 1994). This difference causes spatial discrepancy, as the fog is more common at higher altitudes (Zimmerman et al., 2003), while mist commonly happens at the bottom of valleys. A further discrepancy is that fog has often travelled to its destination, while the mist is a sort of suspended evaporation, meaning the potential for in-cloud scavenging is far greater in fog. This discrepancy

results in fog having greater ionic densities, up to a factor of twenty-five over WD. However, this further depends on the altitude and slope exposition. Meanwhile, the mist will often only have the potential to scavenge the particles directly above it.

Fog deposition has been associated with elevated SO_4^{2-}, F-, and NOx inputs (Krupa, 2002; Bytnerowicz and Fenn, 1995), which attributable to the high levels of moisture, also provide suitable conditions for atmospheric chemical reactions and a mode of transport for microorganisms (Polymenakou, 2012). These chemical reactions are known to make fog water, on average, more acidic through the production of H_2SO_2 and HNO_3, where evapotranspiration from the bark or foliage surface can leave heavily acidic solutions on the tree's surface (Frevert and Klemm, 1984). However, the branch density and leave prevalence will control the efficiency of scavenging fog from the atmosphere. Because of this, coniferous trees are annually more efficient at scavenging fog deposition (Ponette-Gonzalez et al., 2010), with each tree scavenging ability getting better with age and density of architecture (Zimmerman et al., 2003). The degree of bark hygroscopicity further complicates the matter, as more hygroscopic bark will inevitably take in more atmospheric moisture. Further research could incorporate an in-depth look into trees degree of complexity, degree of bark porosity as it relates to the age of the branch and how these factors relate to the scavenging efficiency of fog, with the effects of the ionic dynamics.

The coverage of epiphytes on the bark often correlates to fog deposition rarely becoming stemflow (Nadkarni, 1984). This phenomenon is attributable to their large water holding potential (250-1000% of dry body weight), inhibiting stemflow from occurring attributable to fog. However, epiphytes most interesting relationship with fog is that they use it to travel. Epiphytic spores, bacteria and viruses are known to use atmospheric turbulence to travel; however, fog may provide a more suitable mode attributable to the prevalent moisture, preventing dehydration before deposition. In addition, they can be incorporated into both particles and water droplets within the fog, with plentiful amounts of nitrogen available.

1.4.4 Wet Deposition studies in Wales, United Kingdom

Wet Deposition of ions within Wales is primarily a matter of maritime originating ions, with some agricultural influence inland (Munger and Eisenreich, 1983). This involves many salts such as NaCl, $MgSO_4$, Ca, and K, with sea salt originating ions being roughly 78% (Reynolds *et al*., 2004). However, the origins of these salts are not all maritime. Roughly 66% of sulphate is non-marine, though, the input of non-marine sulphate is decreasing (0.53mg/l in 1984 to 0.24mg/l in 2000) because of

changes in trans-Atlantic shipping to reduce pollution (Reynolds *et al*., 2004). Some ions have been noted to have cyclical natures on the scale of a few years, while depositions of chloride are highly episodic. The same study did not specify whether sodium has this same episodic nature but did say quantities are often correlated. Smaller salt ions such as bromide are often highly correlated with chloride (Neal *et al.,* 2007), with their elevated stemflow quantities indicating a large amount within dry deposition. Nitrogen compounds, mainly NH_4+ and NO_{3-} show similar decadal patterns that are potentially related to the North Atlantic Oscillation (Neal *et al*., 2001; Neal *et al*., 2003), whereas on smaller timescales, the concentrations of NH_4+ and NO_{3-} tend to be higher with the summer months. Phosphorus is higher within cloud and gets released by foliage which increases the quantities 6x (Brown and Iles, 1991; Neal *et al*., 2003) within stemflow, whereas bromide could have quantities an order of magnitude higher (Neal *et al*., 2007). This body of work helps one identify some pertinent research gaps, as one's own study will add to the studies mainly focused on ions within rainfall and could indicate some modern updates to the trend of decreasing sulphate for example.

1.5 Aims and Objectives of the following study

Aim 1: To gain a better understanding of how and why the stemflow of the *Quercus Robur* trees changes within the spring season.

Aim 2: To gain a better understanding of stemflow ionic composition **of the *Quercus Robur* trees within the spring season.**

Aim 3: To explore the nature of bark storage and stemflow movement on sampled oak bark using laboratory approaches.

Objective 1: To establish what meteorological conditions influence stemflow's volume within the study site and where these overall meteorological conditions sit within a historical average to contextualise the results within the viewpoint of contemporary climate change.

Objective 2: To determine, to what extent, does the hygroscopic nature and moisture content of oak bark impacts the creation of stemflow and therefore, the eventual volume of stemflow.

Objective 3: To establish for each of the chosen ions (Cl, Na, Mg, SO_4^{2-}, K, Ca, Br, F, NO_{3-}, NO_{2-} NH_4^+, PO_4^{3-}), what meteorological conditions impact the quantities within stemflow and compare this with the meteorological conditions influencing stemflow volume. These ions were chosen to represent a

strong array of potential salt compounds, nitrogen compounds, and common pollutants to gain a comprehensive picture of stemflows ionic composition.

Objective 4: To evaluate the relationships between the quantities of these ions to theorise about the movement of salt compound and other inputs into stemflow's ionic signature.

Objective 5: To theorise about the movement of stemflow as a fluid flow along a porous bark medium.

2. Methodology

2.1 Research Design

In response to the research gaps identified within sections 1.2-1.4 and to address the aims and objectives in section 1.5, the following approach (Figure 7) was taken to generate relevant datasets. Stemflow was collected from 6 Common Oak trees during 10 storm events in spring 2021 to determine the evolution of stemflow's ionic composition using an ion chromatograph. The concentration of ions in the stemflow was compared with the collected rainfall to determine the directions of ionic transfer (deposition or leaching).

To complement the fieldwork stemflow analyses (Figure 8) additional laboratory experiments were conducted on pieces of bark cut out from the same tree species (different trees). Laboratory analysis (Figure 7) focused on studying how the bark interacts with water. Firstly, the behaviours of water on the bark's surface, and the degree of active or passive absorption or discharge of water, otherwise

known as hygroscopicity. Furthermore, the characteristics of the PFP generation alongside the eventual velocity of droplet travel were recorded for further droplet movement discussions.

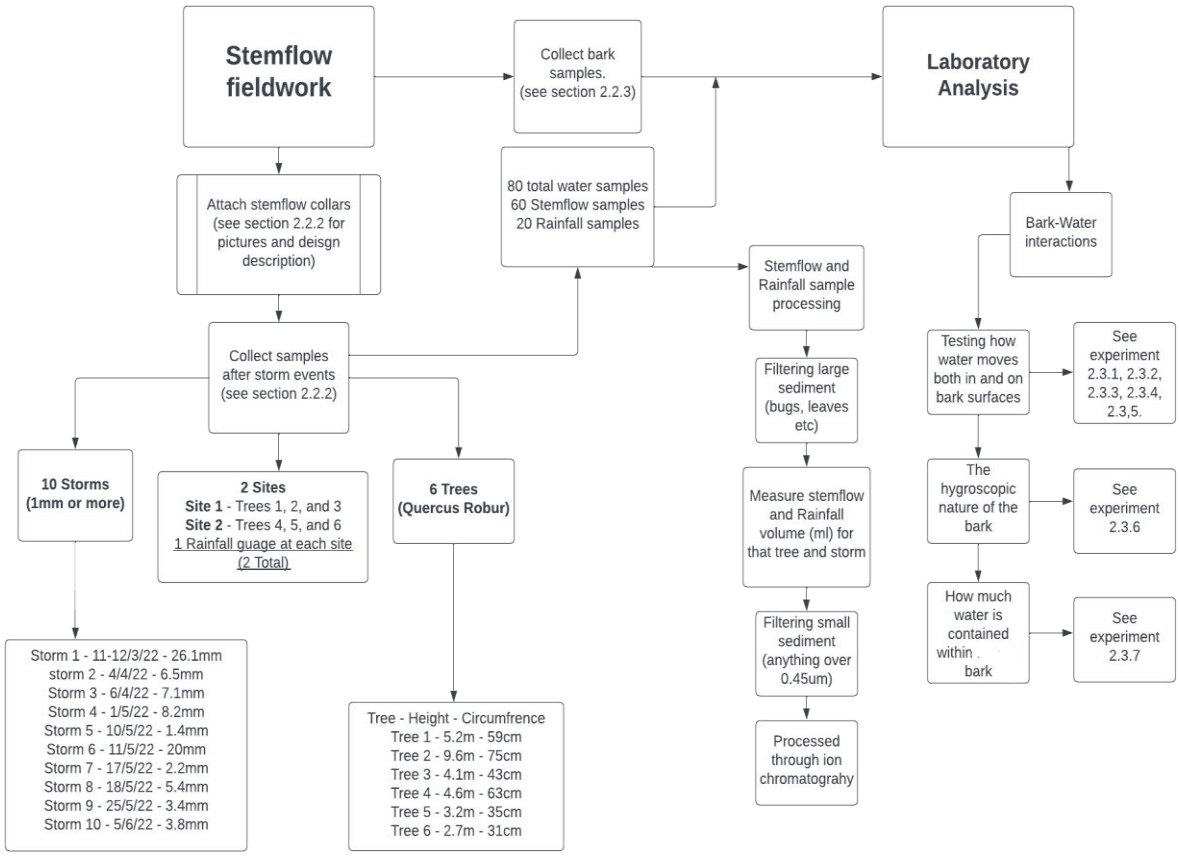

Figure 8: A flow chart of the methods described within the remainder of this chapter

2.2 Fieldwork

2.2.1 Study site

The study site located in Clyne Country Park, Swansea, UK (Figure 9) was chosen because of easy access to a semi-natural environment. The 700-acre park is a mixed stand of Oak, Birch and Beech, while this study is focuses on the population of young Common Oaks (*Quercus Robur*). The area has a long mining and industrial history, including arsenic and copper between 1837-1860; brickworks from 1875-1975; and coal mining as early as the 14th century. The soils are seasonally wet acid, clayey and loamy soils in the South Wales lower coal measures. The parent material is mudstone, siltstone, and sandstone formed during the Carboniferous (Appendix 8 - BGS geology map). There is

also potential contemporary industrial contamination from the Port Talbot Steelworks (10km) across Swansea Bay and the nearby recycling centre (0.5km).

As this thesis focuses on the stemflow process, a prerequisite is that the trees crown area should be independent of other trees, meaning that this study exists in two clearings within this forest, with three trees being studied at each site. The differences of the two sites will also allow for more robust results as results will demonstrate how the ions behave in two separate clearings within the forest characterised by factors such as received rainfall, rainfall inclination, and surrounding forest use. The areas do not appear to have been purposely deforested in the past, with site 1 having heath, fern, and various fruit trees while site 2 has tall grass, with some recently planted trees scattered around. All six trees lie close to an unpaved path which fractures off from the main and mapped paved paths that circulate the forests and partially follow old train lines.

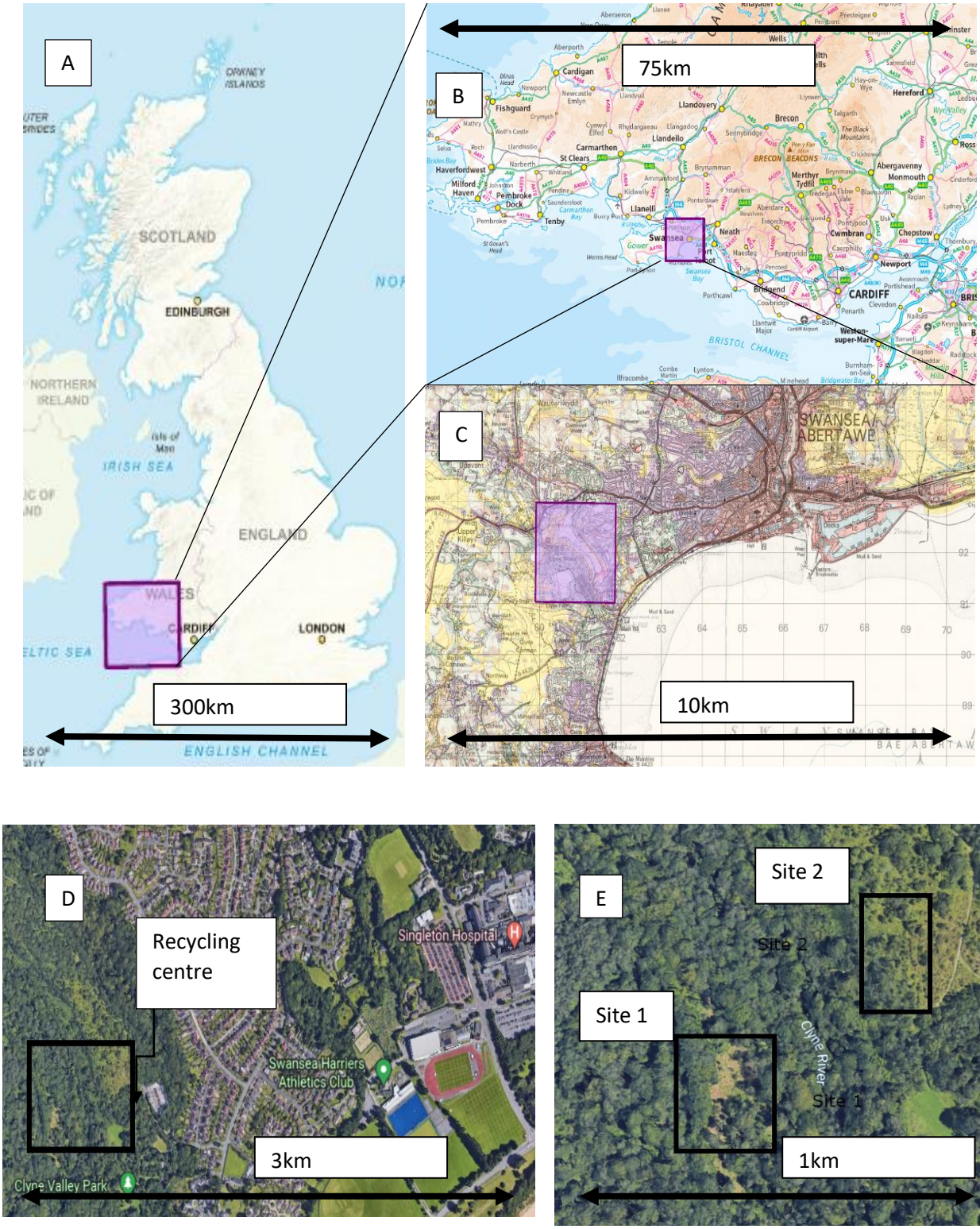

Figure 9: The location of the fieldwork site within the Greater Swansea area ©, and its location within South Wales (B) and then the UK (A). Maps sourced from Google Maps.

2.2.2 Studied trees

The studied trees are 6 oak trees (*Quercus Robur*) of approximate age between 12 to 31 years (Figures 9-14). The trees have a range of shapes, ranging from fairly round to levelled with distinct branches being more apparent. They were consistently taller than wider. The heights of the trees range from 2.7-9.6m tall which was estimated using the formula:

$$H = x + d\,tan\,y$$

Where H is the height of the tree in metres; x is the height of the measurer in metres; y is the angle from the eye to the top of the tree; and d is the distance to the tree.

The girth ranging from 30-78cm at breast height and was measured using a tape measure. Most have some evidence of epiphytic life, which will be adjoined to the pictures of the full tree. The height was calculated using a clinometer and tape, while the age was calculated by dividing the girth by 2.5. The 2.5 was determined by a government document by Newport Council (https://www.newport.gov.uk/documents/Leisure-and-Tourism/Countryside/Measuring-Trees.pdf)

Trees	Girth beneath lowest branch (cm)	Estimated height (m)	Estimated age (years)	Present Epiphytes
Tree 1	58	5.5	30.9	*Erysiphe Alphitoides Thiudium Tamariscinum Physcia Adscendens*
Tree 2	78	9	41.5	*Erysiphe Alphitoides Thiudium Tamariscinum Physcia Adscendens Usnea Subfloridana*
Tree 3	44	4.5	23.4	*Erysiphe Alphitoides Hedera Helix Hylocomium Splendens*
Tree 4	52	5	27.7	*Erysiphe Alphitoides*
Tree 5	35	3.5	18.6	*Erysiphe Alphitoides Thiudium Tamariscinum Hylocomium Splendens*
Tree 6	30	3	16.0	*Erysiphe Alphitoides Thiudium Tamariscinum Physcia Adscendens Hylocomium Splendens*

Table 5: A summary table of each of the studied trees. Source of tree measurements methods - https://www.newport.gov.uk/documents/Leisure-and-Tourism/Countryside/Measuring-Trees.pdf.

Tree 1 (Figure 10) is approximately 5.5m tall, with its first significant branch at 2m in height. The angle of branches increases from the horizontal ones near the bottom of the crown, too steep at the top of the crown. The length of some of the lower branches the branch causes much of it to be beneath the horizontal plane, while it originally connects to the trunk at a 50° angle. There is a strong moss population growing on tree's bark throughout the tree's height, with a stronger lichen population within the higher branches of the tree. There is also evidence of oak mildew which are fungi colonies (*Erysiphe Alphitoides)* growing as white spots on the bark's surface. The moss appears to be of the Tamarisk species (*Thiudium Tamariscinum),* while the lichen is a foliose lichen (*Physcia Adscendens).* There is some sheltering to the south-west by the birch tree in the background of the image.

Figure 10: Photograph of a tree 1 (Height 5.2m, crown area 13.1m^2) with a close up of its bark and resident epiphytes.

Tree 2 (Figure 11) was the largest of the studied trees at at approximately 9m in height. There are only 3 branches in the first 2.5 m from the ground, two of which were broken, and the third was similarly drooped by its weight. Past 2m in height, most branches are above the horizontal plane, however some of the larger ones dropped in the bottom half of the height. Tree 2 also has a high epiphyte coverage, with a lesser foliose lichen (*Physcia Adscendens)* (bottom-left) and a dense corticolous lichen (*Usnea Subfloridana)* population within the upper canopy (Top-Left), with some moss coverage (*Thiudium Tamariscinum)* noted on the lower branches and trunk . There is also similar evidence on oak mildew. There is some easterly shelter by neighbouring trees, meaning that tree 2 is protected from more horizontal rainfalls coming from an easterly

Figure 11: Photographs of tree 2 (Height 9.6m, crown area 24.1m^2), with further images showing moss and foliose lichen (bottom-left), oak mildew upon the white spots (bottom-right) and the dense corticolous lichen in the upper canopy (top-left) of the bark surface.

direction.

Figure 12: Photograph of tree 3 (Height 4.1m, crown area 11.9m^2) with a picture of the vascular epiphyte (bottom-left) and oak mildew and moss (bottom right).

Tree 3 (Figure 12) is roughly 4.5m in height, with a separated shape in its crown because of a noticeable split near the top. The branches in the first 2.5m of height are all no more than 15° above horizontal. The higher branches are less steep do not become too steep than for trees 1 and 2, they tend to fall beneath the horizontal towards their ends. They also tend to possess leaves very far from the trunk. with some vascular epiphytes growing up its trunk. The vascular epiphyte appears to be English Ivy (*Hedera Helix)*, which grows within the furrows until about 1.5m in height (bottom-left). There is evidence of oak mildew, with the moss species (*Hylocomium Splendens)* having small colonies scattered throughout the trunk and on some branch-trunk connections. Tree 3's location towards the edge of the clearing means that it is heavily sheltered by more mature oak and birch

trees to the west, while it is lightly sheltered to the southwest by a large gorse bush. Tree 4 (Figure

Figure 13: Tree 4 (Height 4.6m, crown area 5.0m^2) with a smaller image of the fungal growth on its barks surface.

13) is roughly 5m tall with major trunk splits where the trunk splits to a ratio of 13:9cm in circumference at 1.6m in height, with a similar split at 3m, which also coincides with the branches increasing their average angle above the horizontal plane. Below the trunk split at 1.6m, all but one branch lies below 10° above the horizontal. The singular branch separating out from the trunk at 55°. None of these branches are very large, with a circumference range between 5-13cm. Tree 4 has very little epiphyte coverage, with only sparse evidence of oak mildew. Unlike the three trees at site 1, tree 4 is completely exposed with no sheltering from surrounding trees and shrubs.

Figure 14: Tree 5 (Height 3.2m, crown area 5.6m^2), with further images of the different moss types both in the architecture (bottom-left) and at the base of the tree (bottom-right)

Tree 5 (Figure 14) is approximately 3.5m tall and has the main trunk dominant throughout the full height, with noticeable curves, which can be partially seen in the bottom-left image. The branch angles in the lowest 2m of the tree are all close to the horizontal plane but still pointing upwards, with the degrees of inclination away from the horizontal getting steadily larger further up the tree. Moss is similarly exclusive to these first 2m. There is a strong westerly sheltering from larger plants on the opposite side of the footpath. There is evidence on epiphytic moss, being Common Tamarisk (*Thuidium Tamariscinum)* towards the base and Glittering wood moss (*Hylocomium Splendens)* within the denser canopy of the tree.

Figure 15: Tree 6 (Height 2.7m, crown area 4.2m^2), with further images of the epiphytic lifeforms on its barks surface.

Tree 6 (Figure 16) is approximately 3m tall and was the smallest of the studied trees, and also had the lowest girth (30cm). The main trunk splits into 5 separate smaller trunks at height 1.3m (bottom-centre). It has the largest epiphyte population within the site 2 having larger and more plentiful

populations of Glittering wood moss (*Hylocomium Splendens),* with the similar Common Tamarisk *(Thuidium Tamariscinum)* towards the base of the trunk. There is also a substantial number of lichen colonies, which is a foliose lichen (*Physcia Adscendens),* the only lichen present within a site 2 tree. There is a north-westerly shelter and a weaker north-easterly shelter from nearby large plants.

2.2.3 Stemflow collection

The stemflow collection system comprise of stemflow collar spiralled around the tree trunk and a collection bucket (Figure 15). The collar was made of a duct coil (Black Twinwall Duct 40mm x 50m Coil PM398) cut through the centre to create an opening for the stemflow, forming a gutter, with appropriate lengths for each of the 6 trees determined by 1.3x the circumference at breast height (Table 1). The collar was nailed to the tree (McJannet *et al*., 2007) and a silicone sealant applied to form a watertight barrier between the collar and the tree trunk. The collar was attached towards the base of the trunk to incorporate stemflow from lower down branches alongside the predominant upper tree branches. The collar is spiralled so that it includes water flowing down the entire trunk, which then channels any stemflow down into a collection bucket. The collars were positioned in the first metre in trunk height from the ground for each of the 6 trees, while being as discrete as possible to avoid vandalism, but also in a way that is most effective to collect stemflow.

Figure 16: An example of the stemflow collar as attached to tree 2.

The stemflow was collected after each major storm of at least 1 mm of total rainfall and duration of a minimum of two hours. After each storm where stemflow occurred and was sampled, the total volume of stemflow in each of the collectors was recorded to determine the total volume of the stemflow for each individual tree. The total rainfall at each study location was collected using manual rainfall gauges placed in a small pit. The opening for the rainfall collector was 18.85 cm^2. The volume of water in the rainfall gauges was recorded after each storm. These were made from the same containers used to collect the stemflow .

Field measurements were conducted between March and June 2022, with the stemflow collars fitted in the first week of March and the first selected storms for the analyses on 17/3/22 and the final storm on 5/6/22. In total 10 storms were sampled from a range of meteorological conditions throughout the 3 months, including various wind directions, storm depths and rainfall patterns, which constituted 62.5% of significant stemflow occurrences over that timeframe.

After measurements of stemflow, a 125ml subsample was retained and stored at 5°C for further analyses of the ionic composition, and if 125ml was not available, then the full sample was retained. The total stemflow collected from each tree was filtered by loosening the lid of the container to remove any plant or animal residues trapped within the collector before the volumetric sampling. This was done by weighing the samples and assuming that 1g=1ml. Stemflow generation was observed on several other dates outside of the recorded samples but due to insufficient volumes the stemflow was discarded and not used for any further analyses. The collectors were left out permanently in order to collect any random storm events after some storms in March were missed, this also allowed observation of any anomalies of stemflow production, for example, the minimum storm duration, volume, and prior conditions. This further allowed observation of any stemflow attributable to hygroscopic abilities during droughts.

2.2.4 Bark Sampling

Bark samples were obtained from oak trees growing at the study site but not selected for stemflow measurements and analyses. Bark samples were collected to represent five different circumference categories 10-20cm; 20-30cm; 30-40cm; 40-50cm; 50+cm. Within each sample, if furrows were visible, then the bark sample size was cut enough to incorporate the full furrow width. Eight samples from each circumference class were taken with sample lengths ranging from 3.6 to 5.4cm long, with

the width increasing with tree circumference from 2.6 to 5.1cm. Circumferences were measured with a flexible tape. Therefore, for the rest of this thesis, the term “bark sample” denotes a group of five samples with a representative in each circumference class.

The bark samples 1-5 were collected on 7/3/22. They were all weighed upon arrival to the laboratory. Bark samples 1 and 2 were left exposed for 20 hours in a constant temperature room at a temperature of 21°C, with a relative humidity of 45% to remove excess moisture from prior storm events (Ilek et al., 2017). Bark samples 3 and 4 were sealed in plastic bags to prevent this moisture loss, and bark sample 5 was placed in the oven at 105°C. Further bark samples were collected when field moisture samples were required.

Figure 17: An image of the bark samples, with all the circumference sizes represented.

The bark was sampled using a hammer and chisel after the initial outline of the sample was marked and then extracted from the tree (adopted from Boura and Franceschi, 2008). The 3 larger sample categories were taken from the main trunks of three separate trees (to avoid significant damage of a single tree), while the 2 smaller were taken from a primary branch from the same tree as the 50+cm

samples were taken. The depth of the sample depended on the thickness of the inner and outer bark layer, with most samples having traces of the outer sapwood. Bark samples were cut vertically from the same tree to avoid girdling the tree, this also means that the bark samples were as similar to each other as possible as they inhabited adjacent parts of the tree. The moss coverage on the bark was noted for each sample as contextual evidence for potential differences in water flow behaviour attributable to the difference in furrow volume, the depth of the bark sampling represents this.

2.2.5 Meteorological data collection

Meteorological data including hourly rainfall (mm/H), relative humidity (%), temperature (°C), wind speed (m/s) and wind direction were collected from the Cwm level car park monitoring station in Landore, Swansea, situated 3km away from the study site. Differences between Cwm and the two rainfall gauges at the study were minimal so the rainfall data was kept. All data was in an hourly format, allowing ease of comparison and processing, with the exception of wind which fluctuates at a very high temporal rate that was averaged over the hour. Mumbles head weather station located closer to the study site (2km) was originally used in March, however, due to their rainfall data being halted in early April because of technical problems, the station at Cwm level car park in Landore was used from the 7th of April onwards.

2.3 Laboratory Experimentation

2.3.1 Ion Chromatography

A total 80 samples, including 20 rainfall and 60 stemflow were taken from the field, and their ionic compositions were derived using ion chromatography (Huang *et al.,* 2021). A volume of 10 ml from each sample was required for determination of both the anions and cations. The 20ml amount was filtered at 0.45µm to remove any sediment. This method works by passing the sample through a pressurized column. An ion extractant liquid (eluent) was run through the column, with the retention time of the ion determining the species. The ion chromatograph used was a Metrohm Eco IC with a Metrohm compact autosampler 863, in which the anion column is a Metrosep A supp 5

with an eluent consisting of Sodium hydrogen carbonate: 1.0 mmol/L; 168 mg/2 L, Sodium carbonate: 3.2 mmol/L; 678 mg/2 L. The cation column is a Metrosep C4, 150/4mm with an eluent consisting of Nitric acid (c = 1 mol/L): 1.7 mmol/L; 3.4 mL/2 L, Dipicolinic acid: 0.7 mmol/L; 234 mg/2 L, 250/4mm. The results of the ion chromatograph are in mg/L for each of the ions.

2.3.2 Ionic composition of the stemflow

The stemflow ionic composition chosen to be studied included the following ions: Chloride (Cl^-), Sodium (Na^+), Potassium (K^+), Calcium (Ca^{2+}), Magnesium (Mg^{2+}), Sulphate (SO_4^{2-}), Bromide (Br^-), Fluoride (F^-), Ammonium (NH^{4+}), Nitrite (NO_2^-), Nitrate (NO_3^-), and Phosphate (PO_4^{3-}). The first seven of these were chosen because of their prominence within sea salts, common at field sites situated in close proximity to the sea (Dickson and Goyet, 1994). Therefore, based on the quantities and ratios between specific ions (from within relevant adjoining pairs – NaCl/MgSO4), it will be possible to indicate levels of certain salt compounds or if some mineral wash from a nearby deposit is possibly contained within the deposition. Fluoride serves as a bridge between the sea salts, mineral deposits, and a pollutant as elevated levels would indicate pollution or fluorspar deposition, whereas minimal amounts may indicate sea salt deposition amongst one of its known compounds (Dickson and Goyet, 1994). The Nitrogen compounds (NH^{4+}, NO_2^-, NO_3^-) represent the level of biotic activity upon the trees surface. Phosphate is likely to be representing fertilizers used on nearby farmland but could also originate from natural deposits or be released by the plant on impact (Brooker and Johnson, 1984; Neal *etal.,* 2003). Methods such as conductivity, pH, and other total dissolved solids (TDS) measurements were considered but not taken as they reveal little on the behaviours of specific ions and focus on the mass of ion species within a sample.

2.3.3 Water drop movement on dried and field moist bark samples

Movement of stemflow on the bark surface was simulated under constant laboratory conditions by applying a single water drop on the top of two bark samples from each circumference class and recording the time and the pathway of the flow with bark positioned at different angles (90°, 75°, 60°, 45°, and 30°) (adapted from Imai et al. (2022)). These measurements were done on one dried (Bark sample 2) and one field-moist bark sample (Bark sample 4) to compare the role of bark

moisture content. The dried bark sample was left exposed in the temperature-controlled room for 72 hours at approx. 21°C and 50% relative humidity prior to the experiment, while the field moist samples were placed in plastic bags adjacent to the five dried samples dried samples for the same duration. Each sample was weighed prior to the experiment starting to ensure that minimal weight was lost for the samples within bags or that the excess moisture had been removed for those not in bags. This weight also served as a rough starting point to ensure replicable conditions as the bark samples would undergo numerous experiments.

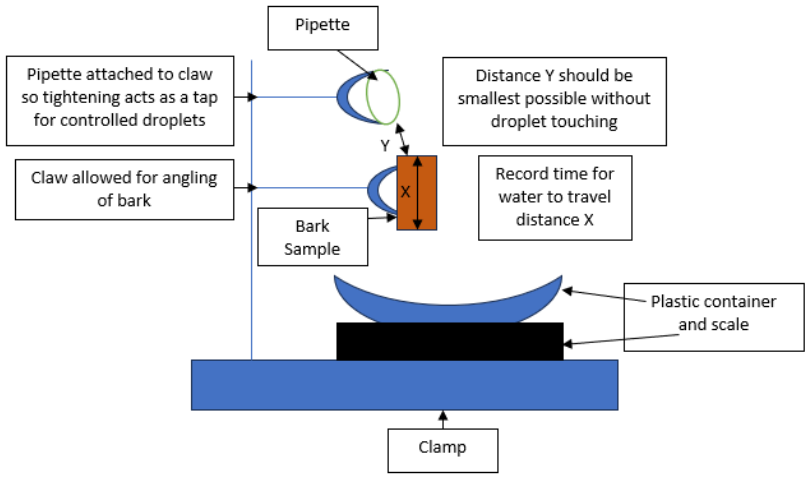

Figure 18: The design of the drop movement experiment.

The bark was fixed at a specific angle using a clamp at an angle between 30-90° at 15° intervals. The pipette was fixed using a clamp at a height of 1-2cm above the bark to avoid any unnecessary splash or unwanted drop-bark contact and to replicate field conditions of stemflow entering an area of bark more closely. This has the added consequence that the time between drops was more controllable as the screw that held the pipette in place acted as a tap. Five consecutive drops at the same location were administered, with the following drop either being administered after a drop had dislodged from the bottom of the sample, the previous drop appears motionless, or the drop has been absorbed either by epiphytes or the barks surface. The bark samples were then placed face down on a paper towel to speed up drying ahead of measurement at the next angle, where it was weighed until the weight had returned to its starting weight. This experiment was conducted a total of 3 times on two further days to generate some replications and to determine if any major discrepancies occur for any of the applications.

The flow path of the first drop was studied closely to determine any predominant preferential flow patterns or stemflow channels, the velocity of the flow and the reasons behind the chosen flow path in relation to the bark microstructure. The observation of the flow pattern of the subsequent drops was focused on understanding if subsequent drops followed the same stemflow channel as the first drop and changes in velocity. The velocity and the pathway of water drop movement were determined through videorecording and processing the results through a frame counter (Tour Temp Frame Counter Golf) with the accuracy of approx. 0.03s attributable to the 30fps filming.

2.3.4 Hygroscopicity of the bark

Bark air moisture absorbance (hygroscopicity) was tested in a climate-controlled chamber at a constant temperature of 20°C and 10% increments in relative humidity from 50 to 80%. Three bark samples, bark sample 7 which had been used in the oven drying experiments 3 days prior (see section 2.3.5), bark sample 8 which was sampled from the field the morning of the experiment, and bark sample 4 that was saturated in water from experiment 2.3.3 for 5 days prior the measurement, were placed in a climate-controlled chamber at a specific humidity until the stable weight of the sample was reached. The weights were recorded at every 2-hour interval, meaning there were 4 weighing for each day of the experiment. This experiment was repeated a second time under the same conditions as before.

The relative humidity was increased after all samples had reached a stable weight. A stable weight is defined as no change in weight accurate to a centigram either for three consecutive weighing (6 hours) or no change in weight overnight (16 hours). The samples changed for the second experiment to make it more replicable and to not overuse any sample. The field-moisture sample was the sample taken from the field (bark sample 10), and care was taken to match the samples weight and surface characteristics by taking them from the same trees. While the dried samples (Bark sample 9) had been left exposed in the constant temperature room for 72 hours prior to the experiment. There was no sample that had been oven dried as this was determined not to be field replicable.

2.3.5 Bark moisture content

In order to determine a 0% moisture weight for the samples, two freshly sourced field samples (bark samples 5, 6, and 7) from each circumference category were dried at 105°C in an oven for 72 hours

(Ilek *et al*., 2017). The first round of experiments was with bark sample 5, with bark sample 6 and 7 fixing errors that arose from taking the bark out too soon during the first round. The weight was then checked on the hour until a stable weight is achieved. A stable weight is identified as an identical weight to the centigram accuracy for 3 consecutive hours. The two samples, which were identical in weight to the second decimal of a gram were sampled simultaneously and juxtaposed so that the only moisture difference is attributable to the epiphytic population or sensitive differences in the sample structure.

2.4 Data analyses

2.4.1 Statistical data analyses

Possible relationships that occurred during the fieldwork campaign between meteorological and stemflow data were tested using correlation coefficients (M^{c}Carroll, 2016). This allows for comparisons as to what climatic variables influence influences each ion. Comparing results from the two fieldwork sites was done using the Mann-Whitney U test. Comparing the quantities of ions within stemflow throughout trees and storms was done using the Kruskal-Wallis test. This test was chosen as the sample sizes do not very between each tree or storm, and the null hypothesis is that they are identical throughout the trees and storms. The reasons the Mann-Whitney U test is used instead of the T-Test was because the data failed in the Shapiro-Wilk test of normaility within both sites.

2.4.2 Stemflow calculations

Several parameters defining the stemflow characteristics have been calculated in the current study. In addition to the stemflow volume (cm^3 or ml) produced in a particular rainstorm, the percentage of stemflow (stemflow %) to storm depth (mm) expected to fall on the tree crown area was calculated. The 2-D plane of the tree's crown cover (cm^2) was calculated first, which was an estimation from the length of several low-hanging branches. The average length was taken, with the area calculated using $A = \pi r^2$. This result was then multiplied by the depth of the storm in mm to generate the volume in cm^3 the volume of rainwater fallen of the specific tree within a storm was estimated and denoted in Litres.

Another metric of quantifying how effective a tree is at producing stemflow is the funnelling ratio (FR). The FR determines the input of the branches into the volume of stemflow by firstly calculating how much rainfall have fallen over the main trunk, where the cross-sectional area of the main trunk at breast height is used. The total volume of stemflow recorded is inputted over this value and the FR is the resulting fraction where values over 1 determine that the branches have had an input, with the higher the number showing the strength of the branches influence, while the opposite is true for values under 1.

3. Laboratory and Fieldwork Results and Analysis

3.1 Meteorological conditions during field measuring campaign

The field measuring campaign experienced various meteorological conditions, with diverse levels of dry periods, storm characteristics and relative humidity. The air temperature, on average, increased throughout the fieldwork campaign (Figure 18), while the growth of leaves started between S2 and S3, with the full growth being achieved around the time of S7. Storm 1 occurred on 11-12/03/2022, with storm 10 coming on 05/06/2022. These storms were the only ones sampled within their respective months, with two other storms (S2 and S3) sampled in early April and the remaining six (S4-9) sampled throughout May. There were dips in relative humidity that both came at the onset of the two longer dry periods towards the end of March and April, with higher relative humidity's coming alongside wetter times during the fieldwork campaign (Figure 18).

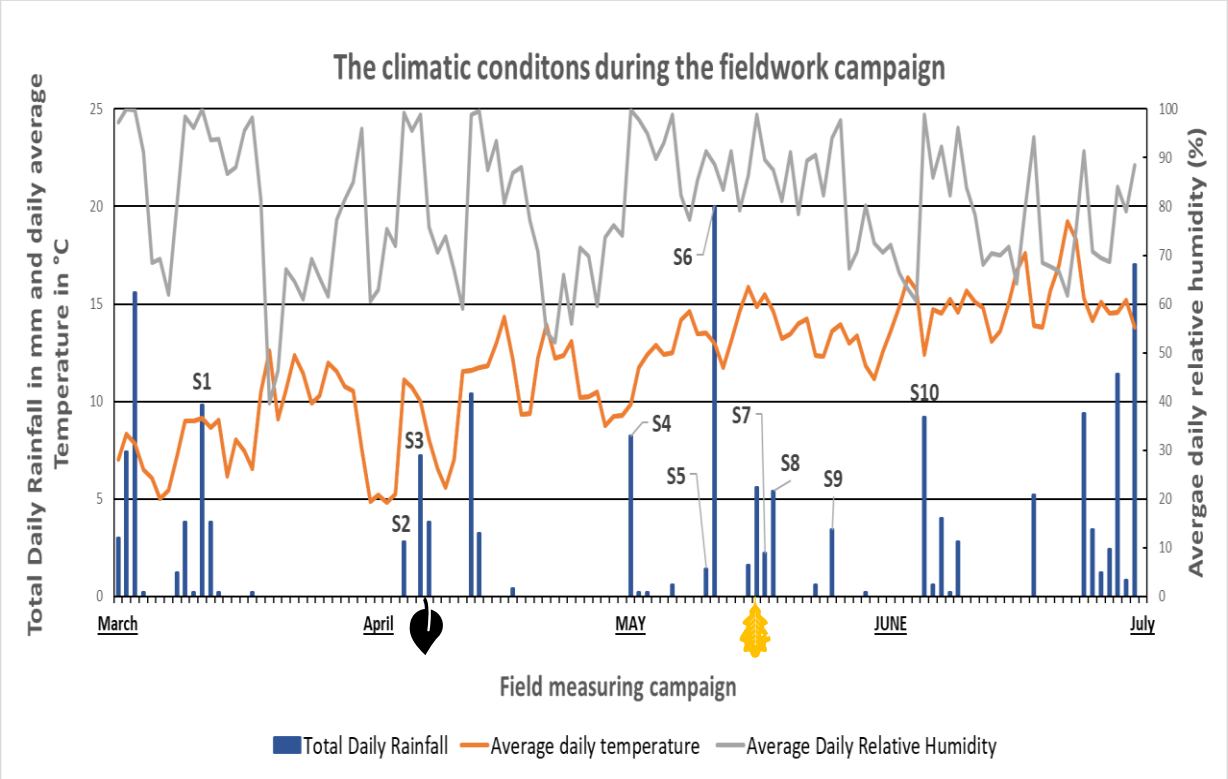

Figure 19: A combination line and bar graph showing the climatic conditions over the field measuring campaign. The black leaf indicates where leaf growth started, while the yellow leaf indicates where leaf growth appeared to hit its peak.

The average monthly temperature was hotter by between 1-2°C than the average between 1980-2016 in each of the four months (Figure 19) with the monthly total rainfall being below this average for March, April, and May and above average for June. Long dry periods were recorded during the measuring campaign which lasted 17 days before storm 2 and 13 days before storm 4 (Table 1). These dry periods highlight that while March experienced more rainy days than average, similar to rainfall daily preference (Figures 20a&b), these all occurred within the first half of the month, with a similar pattern happening in April. A similar pattern happened in May, with the end of the month being noticeably dryer than the start. Most storms over 5mm in depth were incorporated within the data aside one that occurred shortly after S3 (Figure 19).

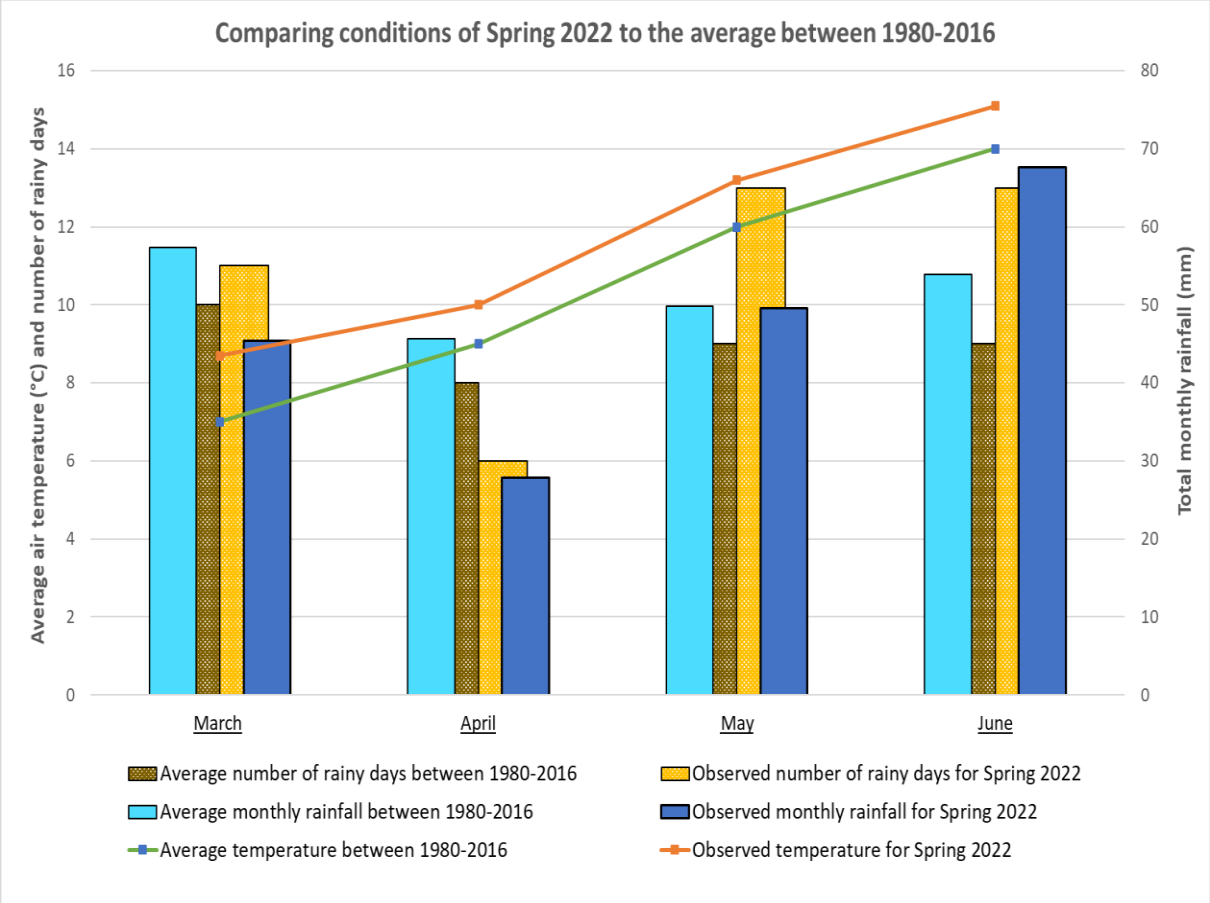

Figure 20: A combination of line and bar graph comparing the climatic conditions of spring 2022 with the average from between 1980-2016.

Each storm had relatively unique characteristics regarding its hourly fluctuations, with preference for morning rainfall (Figures 21a&b), as only storm 8 had an onset after midday. Furthermore, each storm tended to have its peak intensity in the first half, with only storm 7 having its peak in its second half. The largest storm had singular hours that experienced more rainfall than many individual storms (Table 8 - storm 6 6.8mm hour). Storm 6 is by far the largest storm, being nearly double the second largest storm (Storm 1); however, they differ from one another as storm 6 has a singular peak, while storm 1 has multiple peaks. The storm length and average storm intensity have large ranges, with storm length ranging from 2 to 23 hours (a 11.5x difference), while storm average intensity ranges from 0.31-2.5mm/H (8x difference).

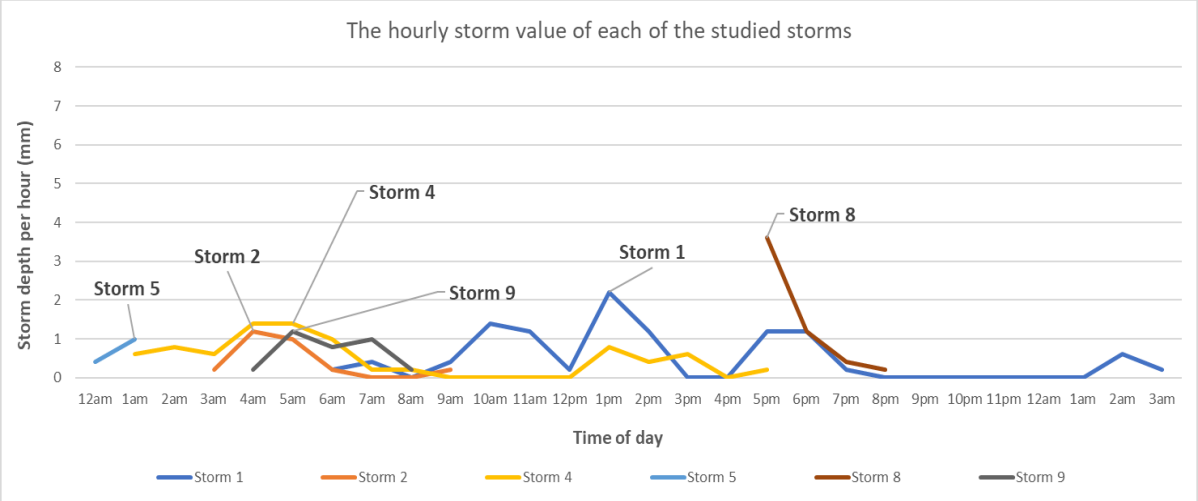

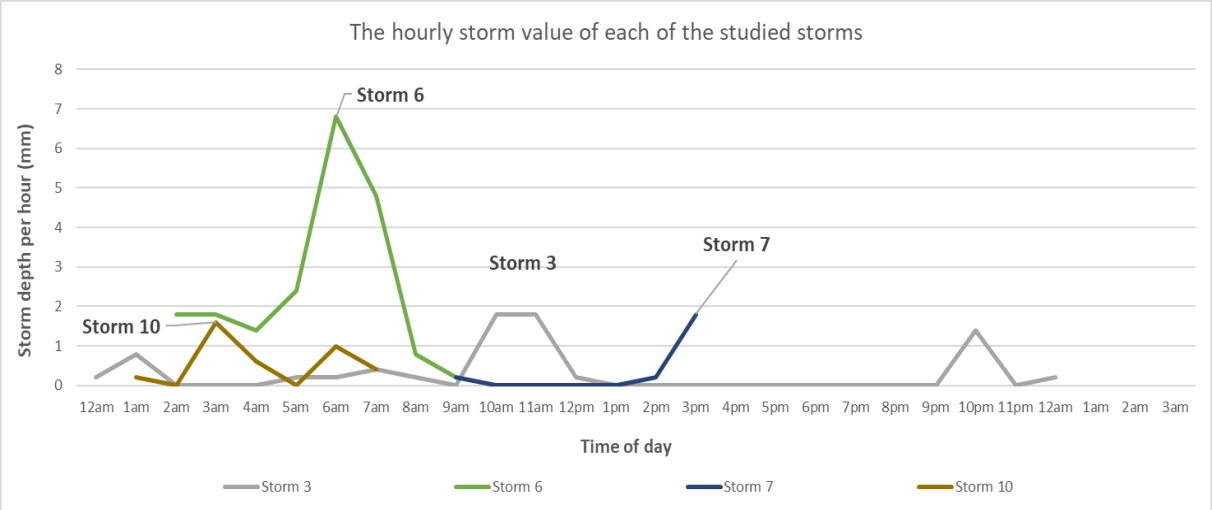

Figure 21a&b: A line graph denoting the hourly volumes of each of the 10 studied storms. The storms are separated to reduce the level of overlap as the morning had a large quantity of the rainstorms.

Storm Characteristics	Storm 1 11-12th March	Storm 2 4th April	Storm 3 6th April	Storm 4 1st May	Storm 5 10th May	Storm 6 11th May	Storm 7 17th May	Storm 8 18th May	Storm 9 25th May	Storm 10 5th June	Total	Average
Total Rainfall (mm) *1	10.9	2.8	7.2	8.2	1.4	20	2.2	5.4	3.4	3.8	65.3	6.53
Rainfall at Site 1/ Site 2 (mm) *2	10.6/ 13.0	3.2/ N/A	8.4/ 8.8	8.3/ 5.3	N/A/ 4.0	20.1/ N/A	3.3/ N/A	4.2/ 5.5	5.1/ 5.6	7.4/ 7.5	-	7.46
Storm length (Hours)	22	7	23	17	2	8	7	4	5	7	102	10.2
Avergae storm intensity (mm/H)	0.48	0.40	0.31	0.48	0.70	2.50	0.31	1.35	0.68	0.54	-	0.78
Prior dry period (Hours) *3	22	421	27	316	75	24	19	25	30	155	1114	111.4
Peak Hourly Intensity (mm)	2.2	1.2	1.8	1.4	1	6.8	1.8	3.6	1.2	1.6	-	2.3
Peak storm volume (% of total)	21	43	25	17	71	34	82	67	35	42	-	44
Hours to Peak Rainfall	7	1	11	3	1	4	6	0	1	2	-	3.6
Average wind orientation (°)	153 SE	271 NW	246 SW	193 SW	262 SW	216 SW	131 SE	156 SE	243 SW	80 NE	-	195 SW
Average wind strength (m/s)	6.6	3.0	3.4	1.4	4.1	3.3	3.4	2.8	3.3	2.0	-	3.3

*Table 6: The characteristics of each studied storm. *1 is the rainfall depth as found for the local meteorological station, while *2 is the comparative depths as calculated from the rainfall gauges and were situated close to trees 3 and 6. *3 is the length of the dry period from the last rainfall recorded on the meteorological data source.*

There was often a small difference in the recorded volumes of rainfall taken from each site's rainfall gauge after each storm, with 4 storms only having a single value (Table 1 - S2, S5, S6, S7), and one storm being nearly identical (Table 1 - S9). There was no occasion where a site matched the rainfall data from the Cwm level car park station, which was expected attributable to the distance from both fieldwork sites. There were 3 occasions where the amount was only off by 0.1mm (Table 1 – S4, S6, S8), with the amounts received at the fieldwork sites being more than expected for 13/16 occurrences, and under for 3/16.

The observed wind speeds and orientations range showed a heavy southern prevalence, with a smaller western prevalence (Table 1). Most storms were within one or two cardinal areas (NW, SE, SW, NE), with storm 6 having an orientation range of 147.49°, which covered three cardinal areas (SE, SW, NE). Storm 4 covered all four cardinal areas over 17 hours, covering the orientations because of a southward, low-pressure system. Storm 10 was the most prominent outlier, prevailing primarily from northerly winds, whereas every other storm had dominant south winds, besides a 50/50 split in the two-hour storm 5. Storms 3 and 8 came exclusively from the South-East, while Storm 9 was exclusively from the Southwest. The five storms from 2 cardinal areas were Storms 1 and 7, which both had southerly winds; Storms 2 and 5 with westerly winds; and storm 10 with Easterly winds, substantiating the strong southern and weaker western prevalence.

3.2 Stemflow volume

3.2.1 Funnelling ratio and stemflow percentages

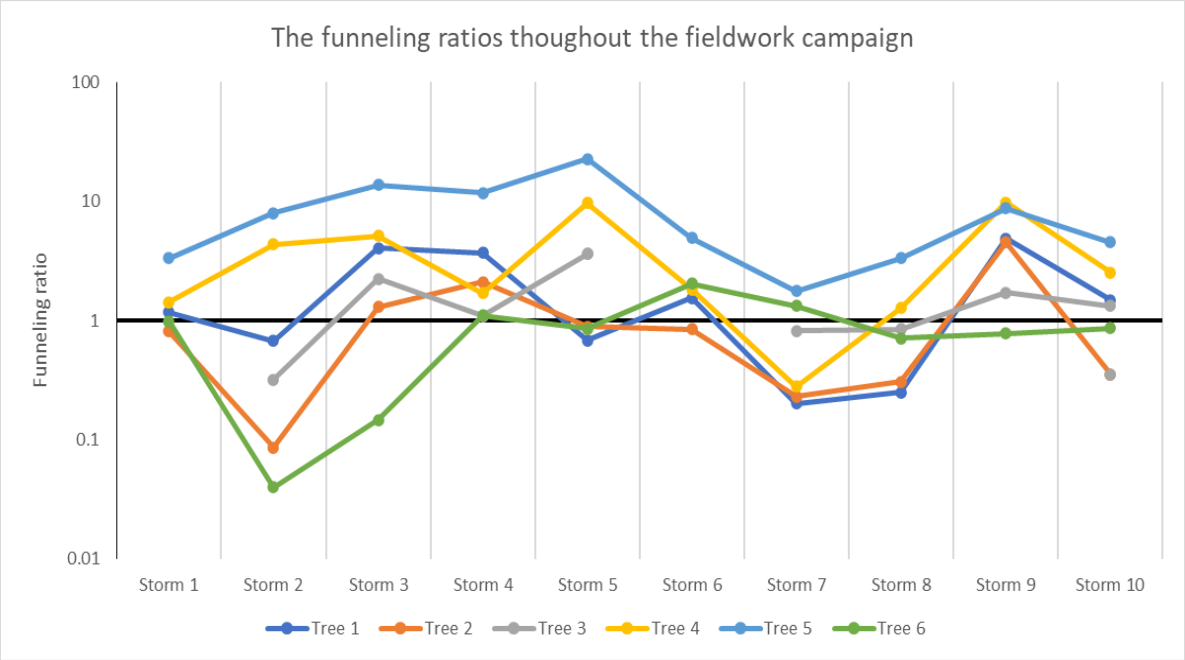

Figure 22: A Line graph showing the FR of each tree and storm, with the value 1 defined as this signifies any input other than the trunk.

There was only one tree that had FR exclusively higher than 1 (Figure 22), being tree 5, other trees' FR was variable depending on storm. Only storm 4 had consistent values above 1 for all trees. The full range of FR values were between 0.04 to 22.6, with the highest FR being found within storm 9 for trees 1, 2, and 4; while trees 3 and 5 had their highest FR in storm 5, with both of these storms being amongst the smallest by total rainfall. Tree 6 had its highest FR within storm 6, which is starkly different as this was the second greatest storm in terms of its total rainfall. The lowest FR were found in storm 2 for trees 2, 3, and 6; with storm 7 for trees 1, 4, and 5. Both of these storms had vastly different dry periods, but were both very low in intensity, with storm 7 having the lowest intensity and second lowest total rainfall, with storm 2 having moderate characteristics but with longest dry period prior to the storm (Table 1)

The following table denotes the stemflow percentage of each tree within each storm. This is the percentage of the rainwater that fell on the tree that eventually was recorded within the volume of stemflow . The results seen within table 9 show that oak has the vast majority (80%) of its SF% values under 1%, with trees 2, 3, and 6 being uniformly under, while tree 1 has 1 occurrence that comes out at 1%.

Storm	Tree 1	Tree 2	Tree 3	Tree 4	Tree 5	Tree 6
S6 - 20mm	0.317	0.17		0.762	0.846	0.35
S1 - 10.9mm	0.241	0.162		0.598	0.575	0.168
S4 - 8.2mm	0.757	0.422	0.14	0.71	2.034	0.189
S3 - 7.2mm	0.829	0.261	0.286	2.156	2.367	0.025
S8 - 5.4mm	0.051	0.062	0.109	0.532	0.573	0.122
S10 - 3.8mm	0.304	0.071	0.171	1.058	0.781	0.147
S9 - 3.4mm	1	0.908	0.22	4.108	1.501	0.133
S2 - 2.8mm	0.139	0.017	0.041	1.828	1.373	0.007
S7 - 2.2mm	0.041	0.046	0.105	0.117	0.305	0.226
S5 - 1.4mm	0.14	0.179	0.467	4.034	3.898	0.146

Table 7: The stemflow percentages (SF%) for each storm and tree, with the larger values showing green and the lower values showing red. Where values above 0.5 appear green, values between 0.25-0.5 appear pale; and values below 0.25 appear red.

Out of the single largest and smallest SF% values from each tree, 11 out of 12 of these were recorded in the four smallest storms (S5, S7, S2, and S9), with only the largest value from T6 coming from the S6. The second lowest values come from S7 & S8 for T1-5, with only T6 breaking the trend as its second lowest value came from S3. The second largest values came in S3-5 for T1-5, with T6 again breaking the trend with its second largest coming from S6.

3.2.2 Stemflow volume

A large range of overall volumes was recorded between 1.8 to 1022.6ml, with these values coming from the smallest and largest tree, respectively. Furthermore, the range seen within each tree was also large, which represents the large variation in storm depth (Figure 23).

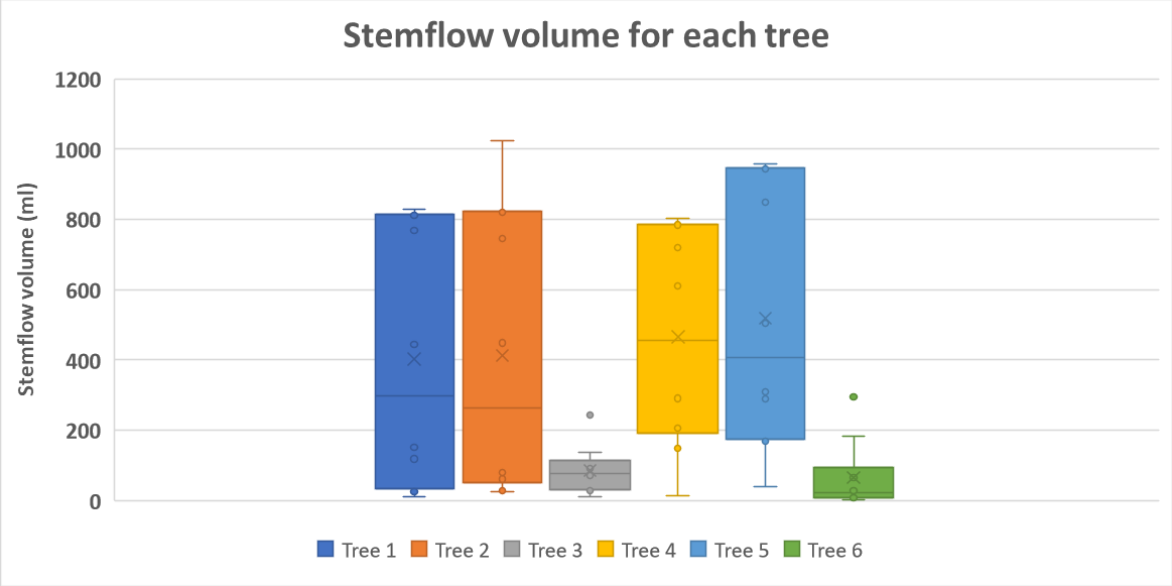

Figure 23: A box and whisker graph showing the range of stemflow volumes throughout the six studied trees over the ten selected storms. Where the dots are the data points; the box is the Interquartile range; the Whiskers are the range; the line across the box is the median; and the x is the median.

Figure 23 further shows a distinct difference in behaviour between trees 1, 2, 4, and 5, and trees 3 and 6. This is mainly expressed in an apparent variable restricting trees 3 and 6 recording volumes over 400ml in total stemflow even when their sizes and geographic location are very similar to the other studied trees. Tree 3 does have the similarity in that it had a lower interquartile range, not shared by T1, T4, or T5.

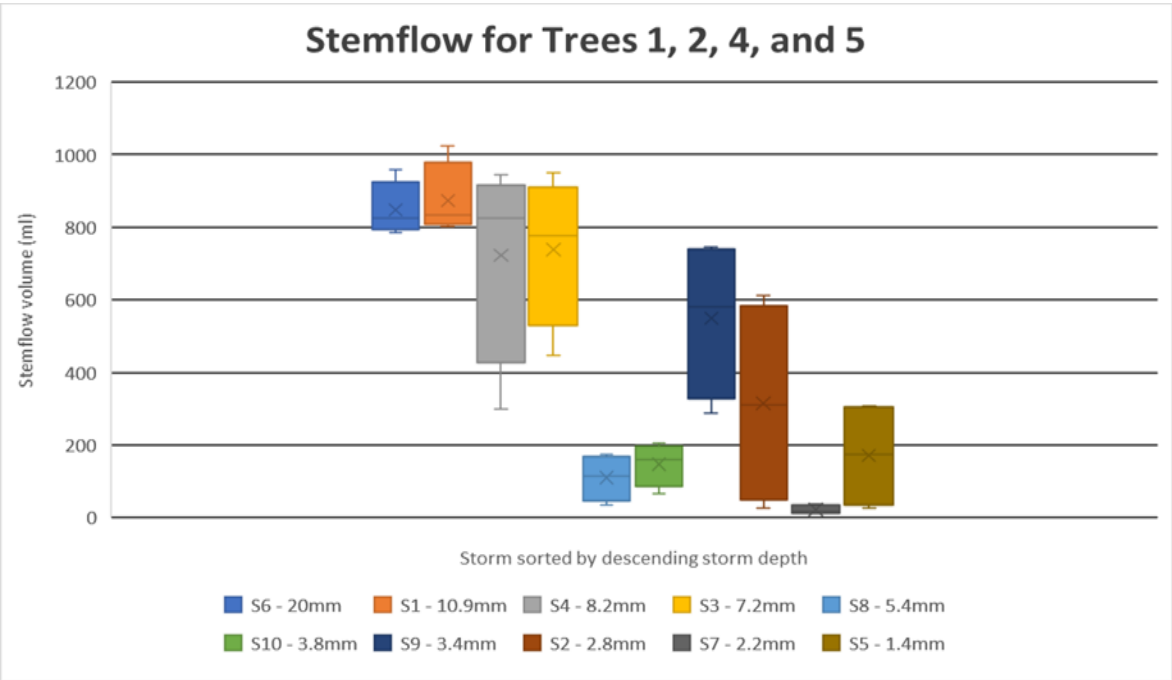

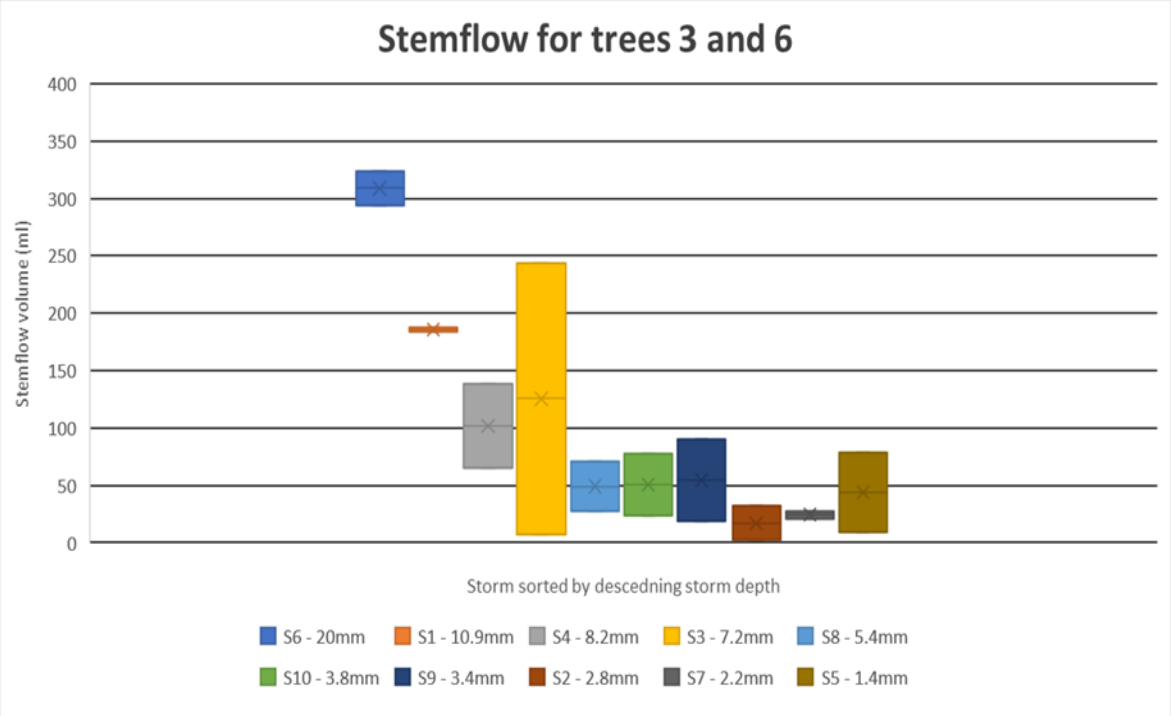

Figure 24a&b: A box and whisker graph showing the range of stemflow volumes throughout the six studied trees over the ten selected storms ranked largest to smallest.

Comparing the overall behaviour seems to show curves of an opposite nature, where trees 3 and 6 drop rapidly after the largest storm, whereas trees 1,2, 4, and 5 show a gentler gradient down to its lower values. Furthermore, while trees 3 and 6 seem to have a clear pattern of exponential decrease, trees 1, 2, 4, and 5 seem to show groupings where the two largest storms are consistently high, the 3rd and 4th largest storms have high potentials but also high ranges, followed by a large drop in volume for the 5th and 6th largest storms.

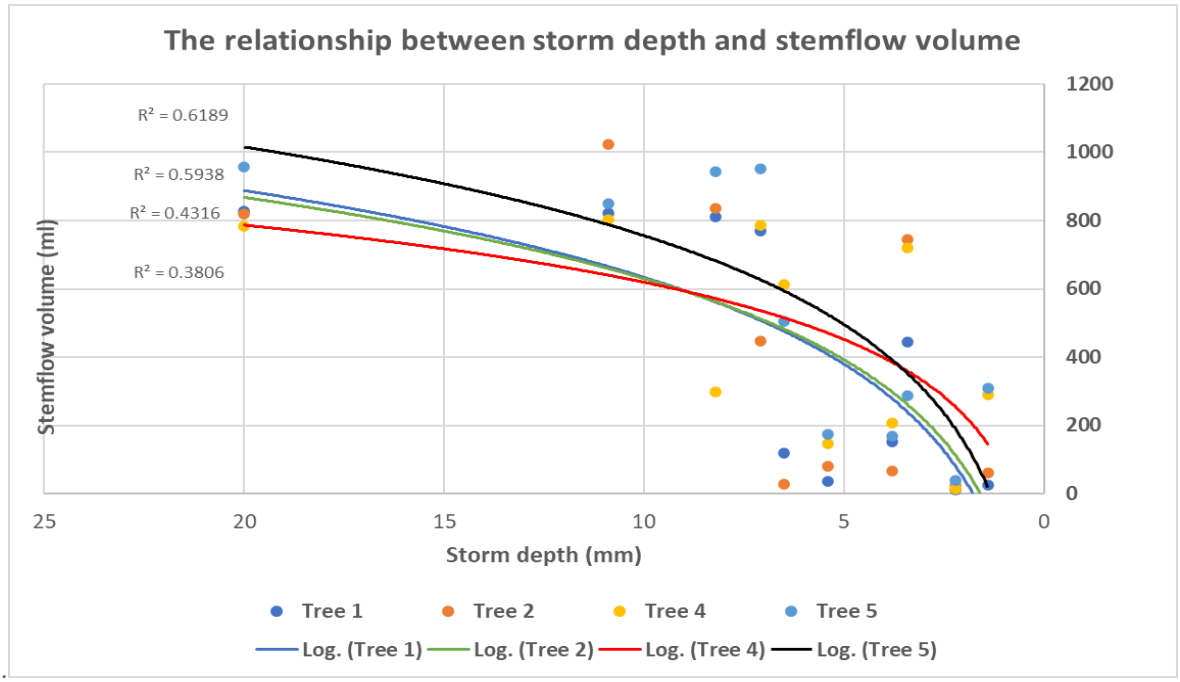

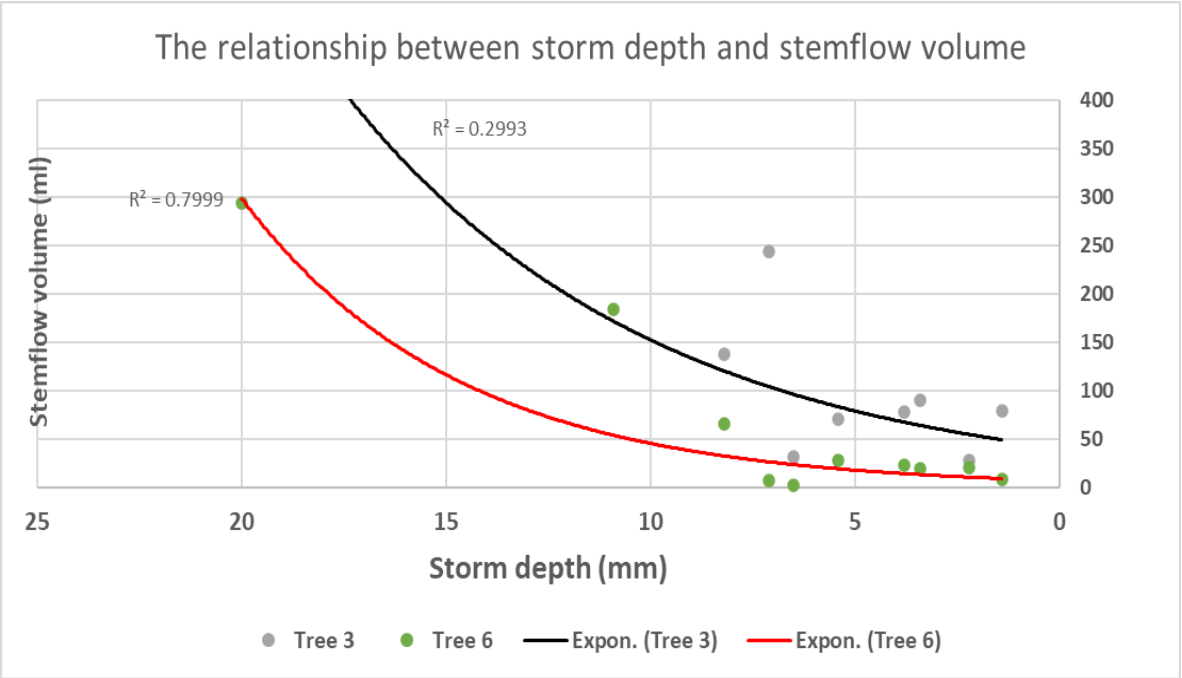

Figure 25a&b: The relationships between stemflow volumes (ml) and the total rainfall (mm). These are joined with the regression formula which demonstrated the highest R^2 value, half of which were linear (above) and half of which were logarithmic (below). The two larger storms had no tree 3 as the heavy rain dislodged the collection bucket, which voided any sample that happened to remain within.

The equations that showed the highest R^2 values were exponential equations in Trees 3 and 6, with logarithmic equations being the best fit in trees 1, 2, 4, and 5. Tree 1 appears to have a maximum

stemflow volume of around 800ml, achieved alongside storm volumes of 8.2, 20.0, and 26.1mm (S1, 4, and 6). Whereas its unusually low value in storm 7 was also the only storm to have its peak within the second half of the storm. The fluctuations under a total rainfall of 10mm appear to have more sensitive controls than sheer total rainfall as is seen in larger storms.

Tree 2's maximum stemflow is less obvious, with its largest value being the only one over a litre; however, this was 200ml more than its next highest. The values within the largest three volumes correlate with storm lengths in the respective storms (Table 1). This shows the potential of the largest tree producing the highest stemflow , with the maximum quantity required a truly magnificent storm to occur.

Tree 3 had sampling errors in storms 1 and 6, likely attributable to heavy rain knocking over the collection bucket. Tree 3 is far smaller than tree two but had greater stemflow volumes in 4/8 of its good recordings, which happened in 3 of the four smallest storms in terms of total rainfall, while the last occurred after the 17-day dry period, so the heavy epiphyte covering on tree 2 is likely the cause (See section 1.2.7).

Tree 4 had the 2nd highest average stemflow volume, with two occurrences of the greatest storm stemflow volume (S2 and 10), with a further four occurrences as the second greatest (3, 5, 8, and 9). Its maximum volume is roughly 800ml, achieved in the 20.0 and 26.1mm storms (S1 and 6), with prodigious stemflow values coming alongside northerly storms (S2 and 10). The lesser maximum stemflow volume meant tree 4 had the fourth highest stemflow volume in these storms. The two remaining storms (S4 and 7), where tree 4 had the fourth highest stemflow volumes had the 2 lowest rainfall intensities.

Tree 5 had the greatest stemflow in 6/10 storms and the highest average stemflow throughout the fieldwork campaign. It had the second greatest volume in three other storms while being the 4th greatest in storm 9. Its maximum value appears to be roughly 950ml, recorded in the 7.1, 8.2, and 20.0mm storms, with an 848ml reading in the 26.1mm storm. This shows that tree 5 produces more stemflow quicker than tree 1 as its limit is met with lesser storms.

Tree 6 recorded the lowest stemflow volume in 9/10 storms, with the 4th greatest in storm 7. Tree 6 had the highest correlation to total rainfall, rainfall intensity, peak storm intensity and prior dry

period, with the 2nd highest correlation to time to rainfall peak and rainfall inclination range. This likely results in tree 6 having the highest R^2 value for its linear equation (Figure 25b).

Comparing the volumes of stemflow each tree produces shows that tree 6 consistently produces the least stemflow , with nine occurrences being the lowest. Tree 1 had the lowest stemflow within storm 7. The greatest amounts of stemflow were observed by tree 5, which had the greatest stemflow volumes for 6/10 storms, with the larger tree 2 having the most 2/10 times and tree 4 the remaining two storms. Storms 2 and 10 had their greatest volumes in tree 4, with similar storm characteristics throughout the variables (Table 1), primarily the two northern storms. In contrast, the similarity between storms 1 and 9 are non-existent.

Correlation Table	Total storm depth	Storm length	Av Storm intensity	Dry period	Peak intensity	Time to peak
Tree 1	0.717	0.738	0.378	-0.099	0.525	0.478
Tree 2	0.737	0.698	0.388	-0.186	0.492	0.422
Tree 3	0.526	0.499	-0.079	-0.191	0.192	0.152
Tree 4	0.624	0.380	0.453	-0.095	0.510	0.249
Tree 5	0.683	0.690	0.409	0.122	0.524	0.401
Tree 6	0.869	0.407	0.848	-0.284	0.888	0.476
	0.693	**0.569**	**0.399**	**-0.122**	**0.522**	**0.363**

Table 8: A table showing the correlations between the trees volume (ml) and the storm characteristics (Table 1).

There were no instances of a significant correlation (0.95+) between any climatic variables and the volume of stemflow of any individual tree. The individual trees stemflow correlate to the total rainfall between 0.526-0.869 (Table 3), which was also the strongest average relationship. The variables of antecedent dry period and timing of rainfall peak were both exceptionally weak, with the weakest correlations being inter-storm temporal variables. This indicates that stemflow has a low temporal dependency and will respond to different climatic variables if and when they arrive during a storm. The correlations in table 10 shows that stemflow does not have a single significant variable. It is a combination of multiple variables that form the resulting volume, with variables like total rainfall having greater importance than the dry period. There was a statistically significant difference between the trees ($p = 0.001$) and storms ($p = 0.0025$). However, there was no statistically significant difference between sites 1 and 2 ($p = 0.5793$).

3.3 The ionic composition of stemflow and rainfall

3.3.1 Sodium

The values of sodium concentration in stemflow have been considered by storm number and specific tree. The highest average value and also the largest range have been observed in storm 2. The lowest values were of Na+ were recorded for storm 6. It can also be seen that larger trees (T1 and T2) show higher Na+ average values but also larger range of the values than smaller/younger trees (T4, T3, T5, T6).

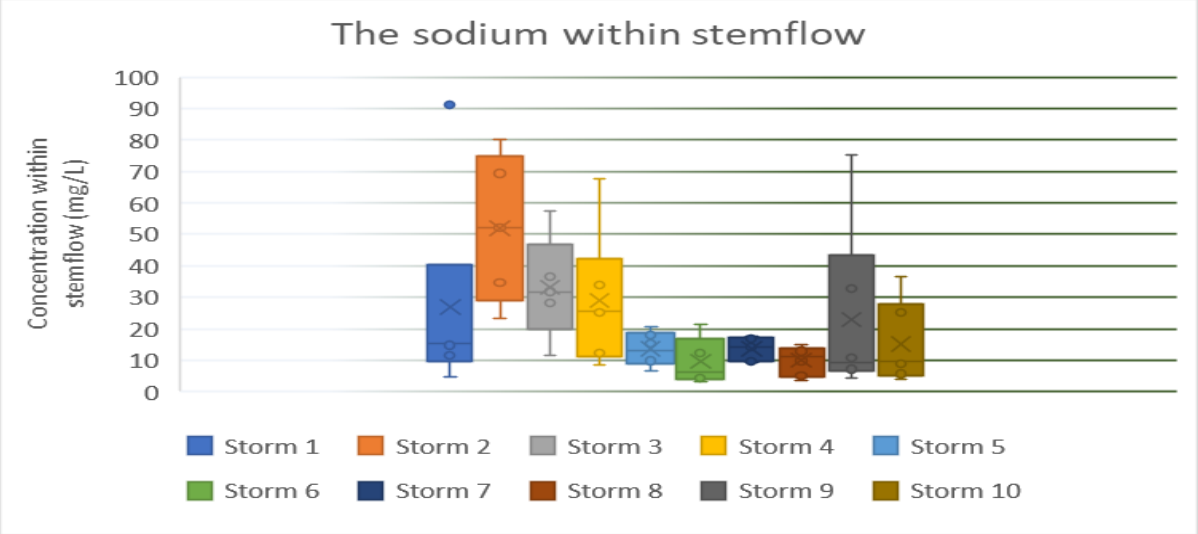

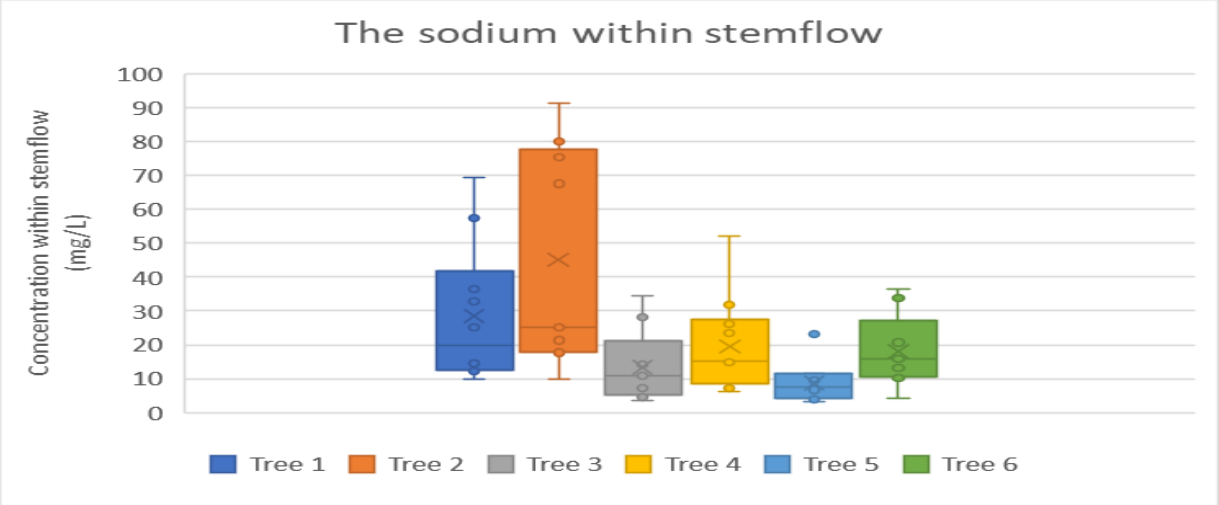

Figure 26a&b: A box and whisker graph showing the distributions of sodium concentrations both between storms (above) and between trees (below). An X represents the mean; the line through the box represents the median; the box in the interquartile range and the whiskers are the full range.

Sodium averages 22.03mg/L across all of its readings (Figures 26a&b), there does appear to be a small seasonal influence on the quantities of sodium with earlier storms having higher quantities and ranges, while S5-8 having values were consistently below the ions average (Figure 26a). These lower values were then followed by larger values once full bloom was achieved in late May. There is a single external outlier from S1, which is also the highest sodium value with 91.23mg/L. There are other values within 20% of this, however because of a higher average within those storms, these values are not deemed to be outliers, but instead contribute to the low interquartile skew seen in S4, S6, S9, and S10. A similar skew can be seen in T1, T3, and T4. Tree 2 produces the most sodium, with an average quantity higher than all but three readings from the other five trees. Tree five consistently has the lowest sodium values, with only one value above average, which is deemed an external outlier for this tree. Every other tree has an internal outlier which all contribute to the high ranges seen in S2-4.

3.3.2 Chloride

Chloride was the most abundant ion with an average of 36.5mg/L and shows a partial seasonal influence with exceptionally large values and ranges before leaf growth and a small increase after full bloom (Figure 26c).

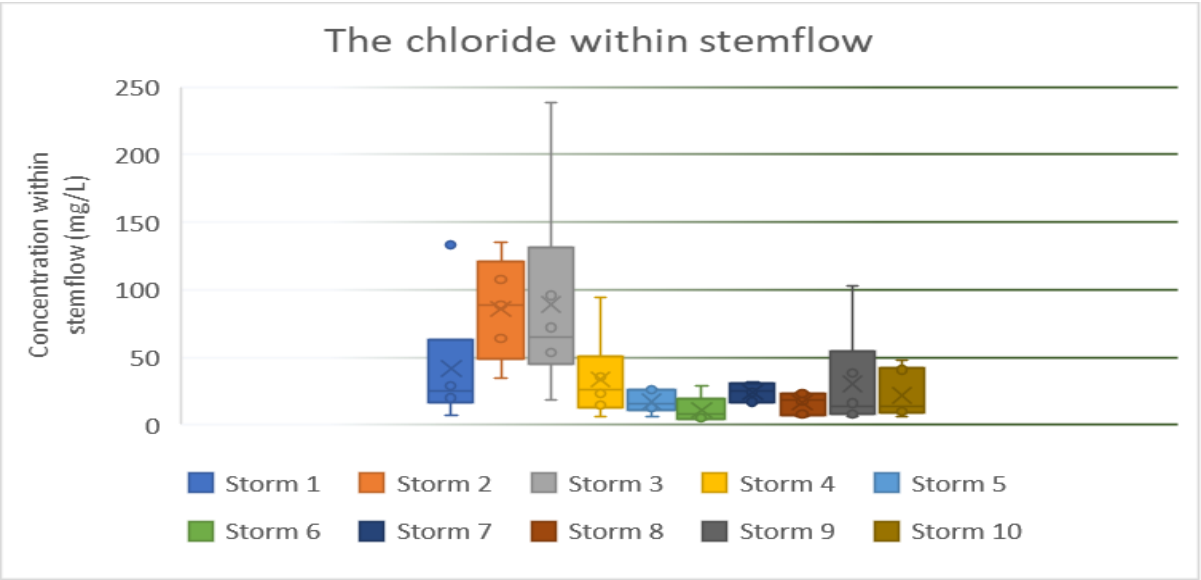

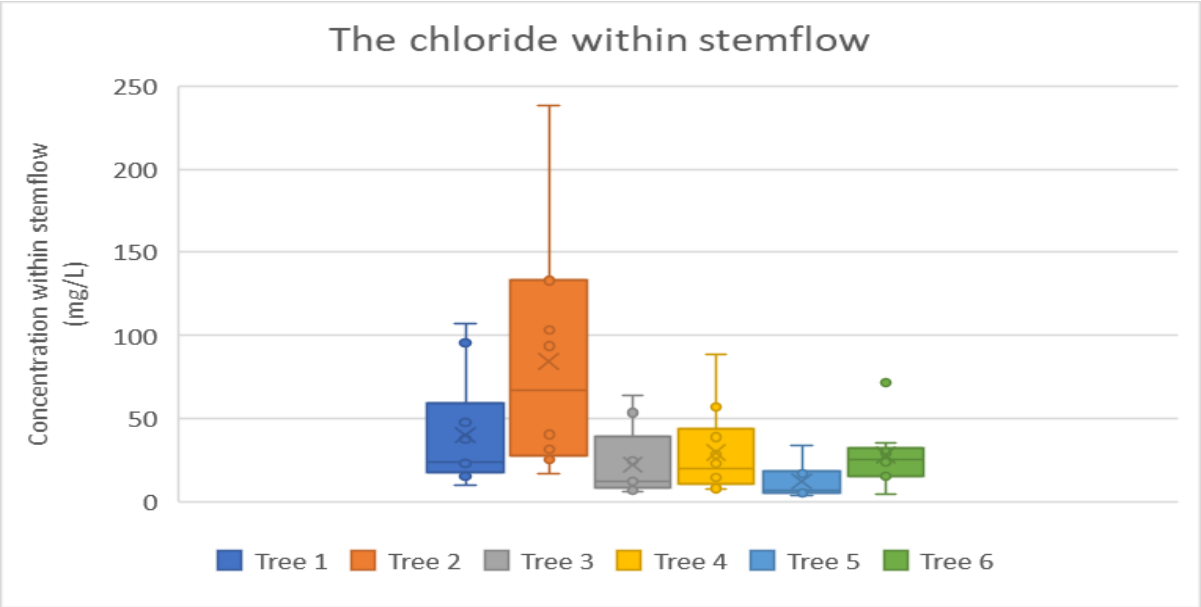

Figure 26c&d: A box and whisker graph showing the distributions of Chloride concentrations both between storms (above) and between trees (below). An X represents the mean; the line through the box represents the median; the box in the interquartile range and the whiskers are the full range.

The external outlier from S1 is from the same tree as Sodium (Figure 26a), which also caused a skew within potassium (Figure 26k). The low skews from S3, S4, S6, and S9 all come from T2, where similar skews (same tree and storm) can be found in all aforementioned ions with the exception of ammonium. Within the trees T1-5 show a similar low skew (Figure 26d), caused by either S2 or S3, where S3 also causes the external outlier for T6 and the internal outliers for T1, T3, and T4. Tree 6 shows a different pattern, having a higher skew for its interquartile range. Tree 2 commonly

produces the highest concentrations out of the trees, however it is within chloride that it shows the greatest dominance and likewise, where T5 often shows the lowest concentrations, it is the weakest within chloride.

3.3.3 Magnesium

Magnesium averages 3.26mg/L across all its readings and shows a partial seasonal influence with higher values and ranges which then decrease after leaf growth between S3&4 (figure 26e).

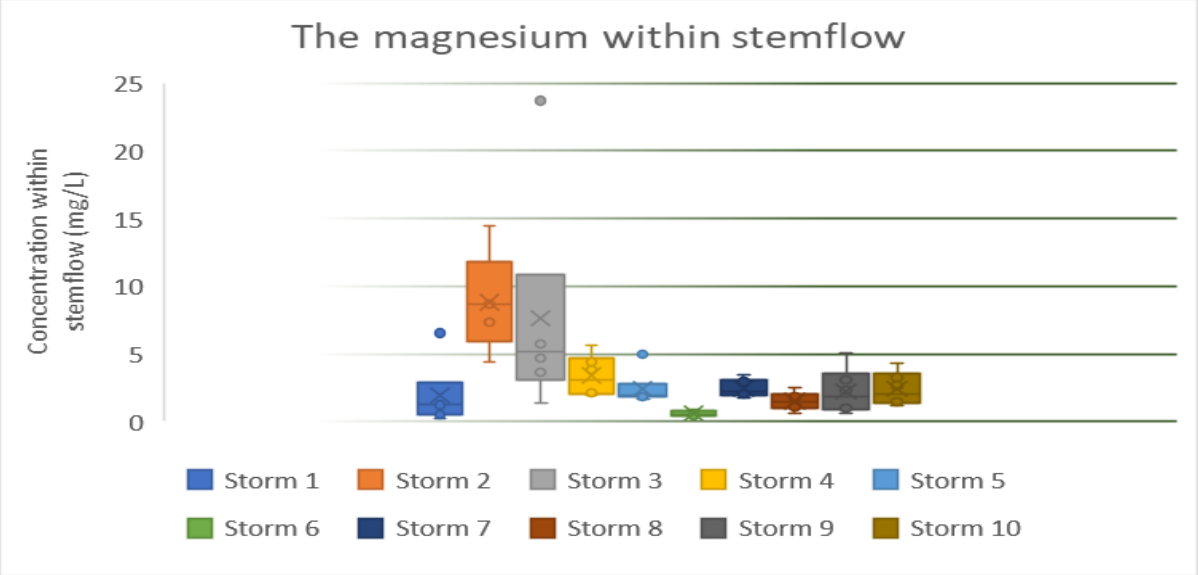

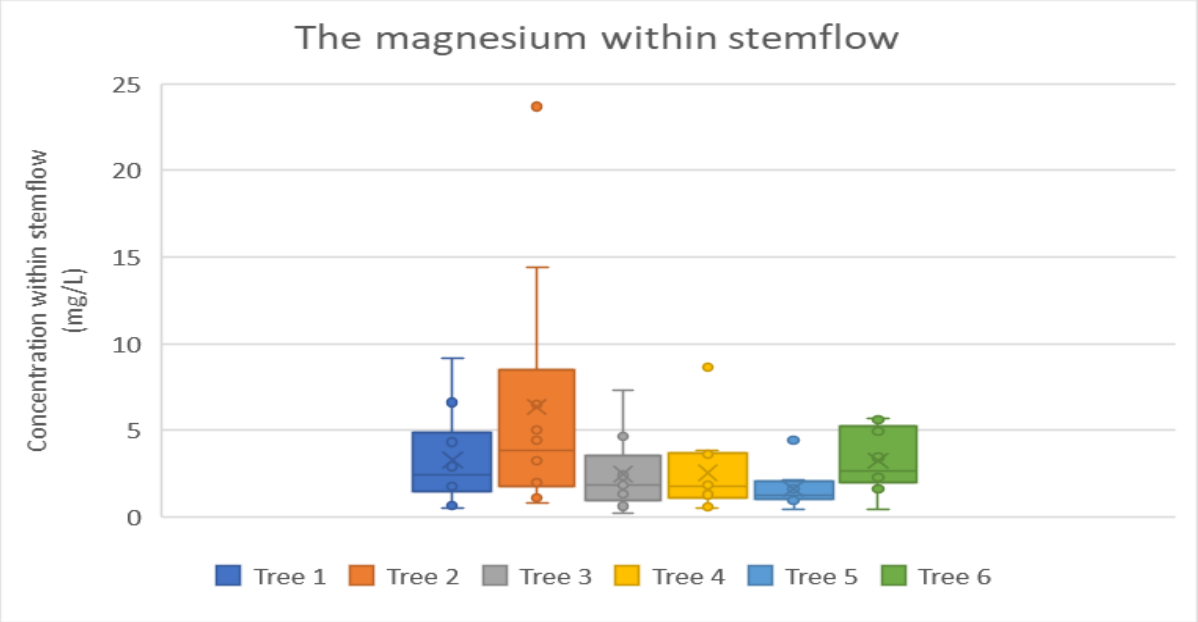

Figure 26e&f: A box and whisker graph showing the distributions of Magnesium concentrations both between storms (above) and between trees (below). An X represents the mean; the line through the box represents the median; the box in the interquartile range and the whiskers are the full range.

Magnesium shows the same trend as calcium and potassium with noticeably low ranges for S1 and S6. The external outliers from S1 and S5 are from the same trees as potassium (T6) and calcium (T2) respectively (Figures 26e, 26k, and 26i), while the external outlier from S3 (and T2) is also the highest value at 23.69mg/L (Figures 26i&j). The low skews seen in S4, S8-10 were partially consistent with other ions, as S9 and 10 received a similar skew from sodium, while S10 had similar skews in both calcium and potassium. There was a contrast between the sites as site 1 (T1-3) had a low skew for their interquartile ranges, while site 2 (T4-6) had high skews, there was a comparison in that each tree had an outlier on both sides of their interquartile ranges. The external outlier for T2 is already referenced while T4 and T5 actually causes the more even skew in S2 (Figure 26e).

3.3.4 Sulphate

Sulphate averages at 8.08mg/L over the fieldwork campaign with larger ranges and concentrations found within earlier storms that does not recover in S9-10 like in some other salt ions.

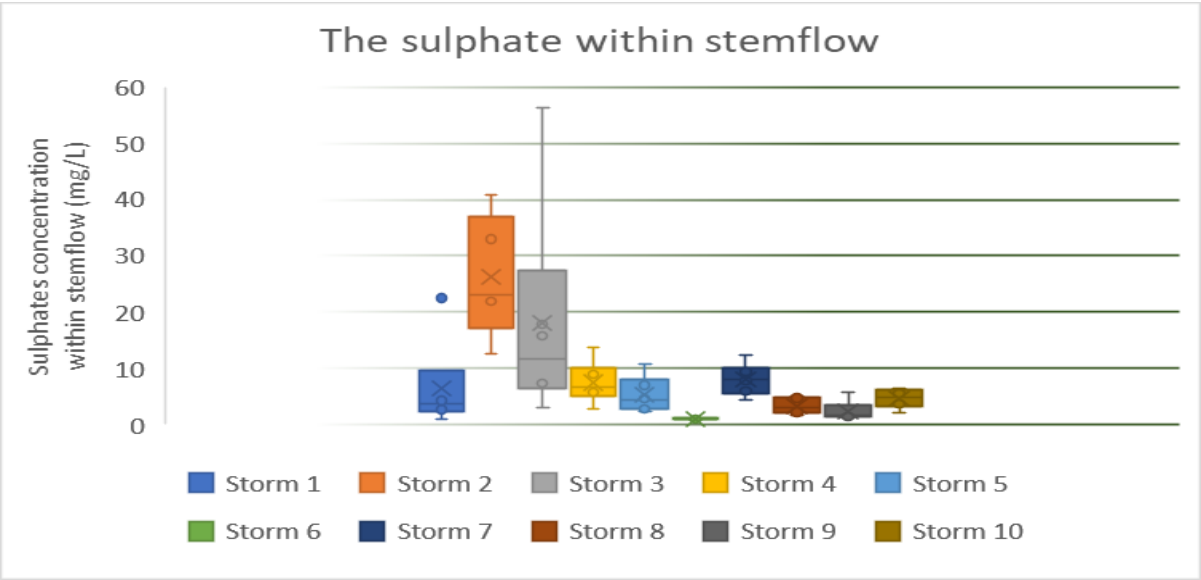

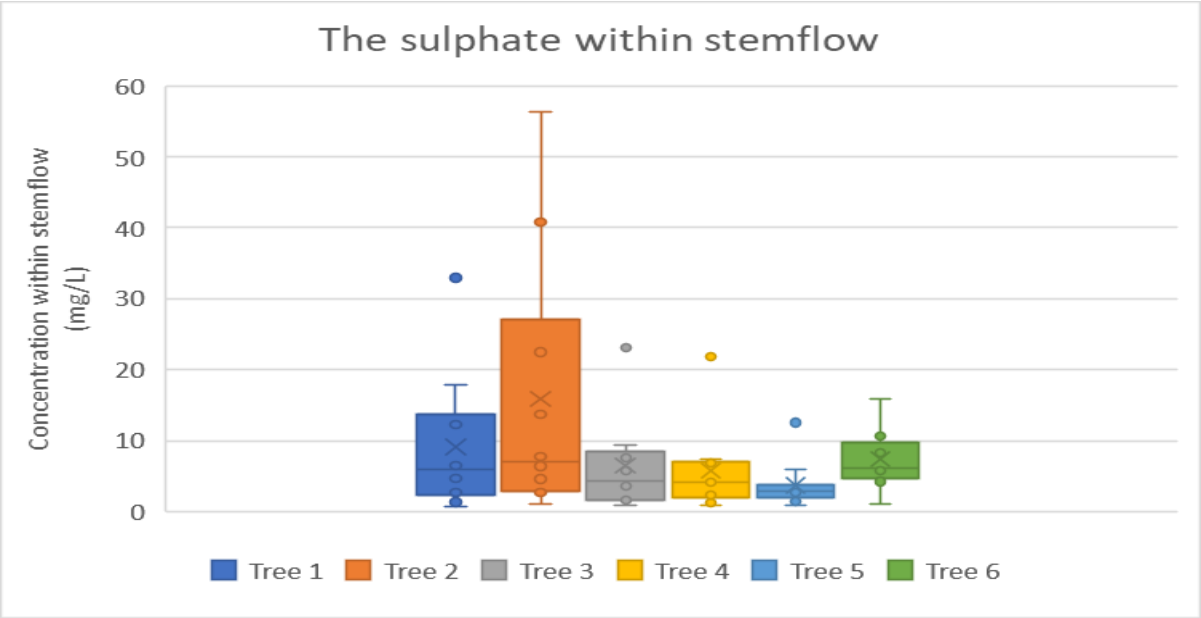

Figure 26g&h: A boxplot graph showing the distributions of Sulphate concentrations in stemflow separated by storm (above) and tree (below);. An X represents the mean; the line through the box represents the median; the box in the interquartile range and the whiskers are the full range.

The recurring outlier is found within S1 (Figure 26g), while S3 shows the same large low skew which provides a further similarity to the other major salt ions. Similar attributions for the Skews can be found within a range of ions with more salt ion similarities but some nitrogen and phosphate similarities too. Comparing the trees highlights a closer similarity to the salts (Figure 26h) as there is the characteristic large interquartile and normal range, with consistently small concentrations from

T5. More of the skews are lower aside from T4, where the external outlier is from the same storm as the outliers in T1-5.

3.3.5 Calcium

Calcium averages 6.15mg/L across all its readings, with larger ranges seen both before leaf growth started or after the trees were in full bloom (Figure 26i).

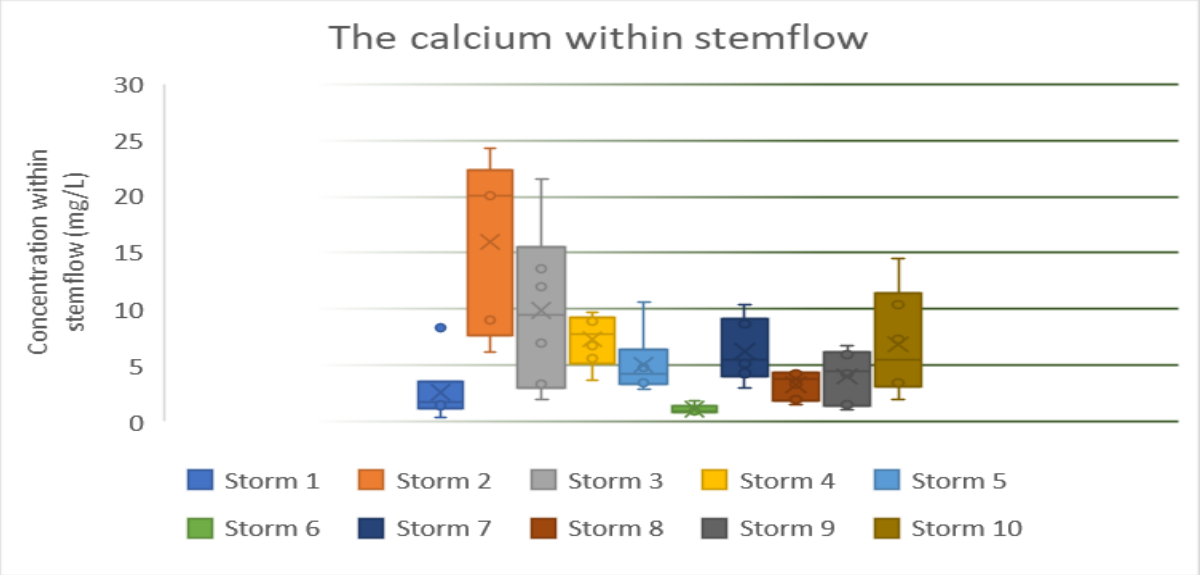

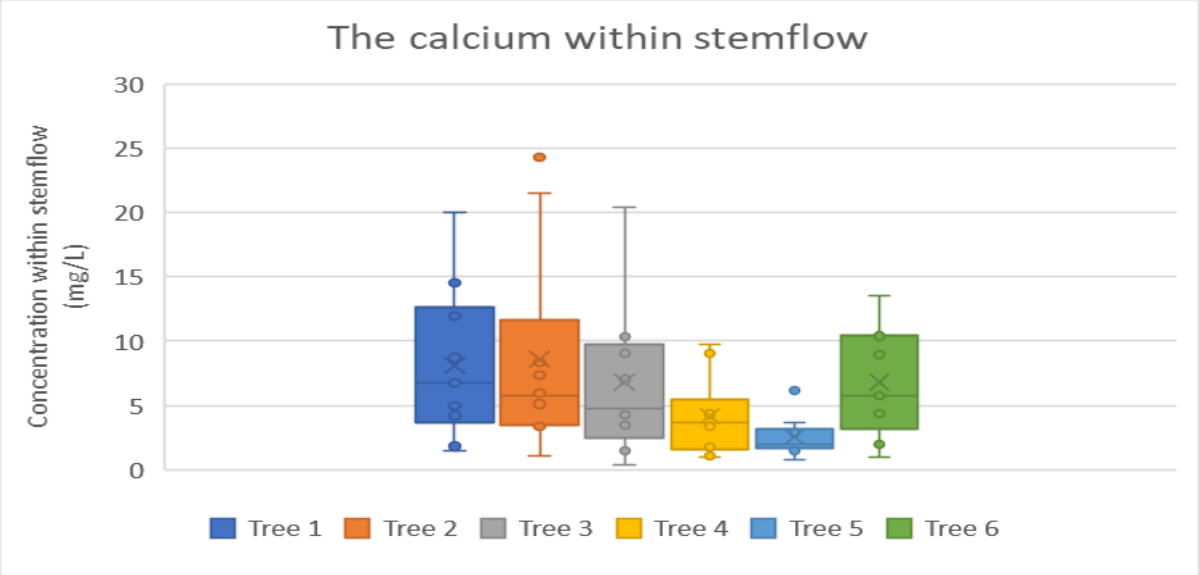

Figure 26i&j: A box and whisker graph showing the distributions of Calcium concentrations both between storms (above) and between trees (below). An X represents the mean; the line through the box represents the median; the box in the interquartile range and the whiskers are the full range.

There are two noticeably low storms (S1 and S6) where both the values and ranges were small, however there was an external outlier within S1 that differentiates calcium from potassium (Figure 26i). Outside of S1, most other storms have a low interquartile skew (S3, S5, S9, S10), which are often caused by the same trees as potassium. This low interquartile skew can also be seen in T1-4 (Figure 26j). The trees at site 1 appear to have similar behaviours in regard to calcium, with this being the only salt ion where T1 has a larger interquartile range than T2 and a low interquartile skew and outliers on both sides. Tree 2 has an external outlier, which is also the highest calcium value of 24.32mg/L, with T5's external outlier also being the lowest reading from its storm, highlighting T5 consistently low concentrations. In comparison, T6 maintains reasonably high concentrations like the previous ions.

3.3.6 Potassium

Potassium averages 9.94mg/L across all its readings, with no apparent seasonal influence.

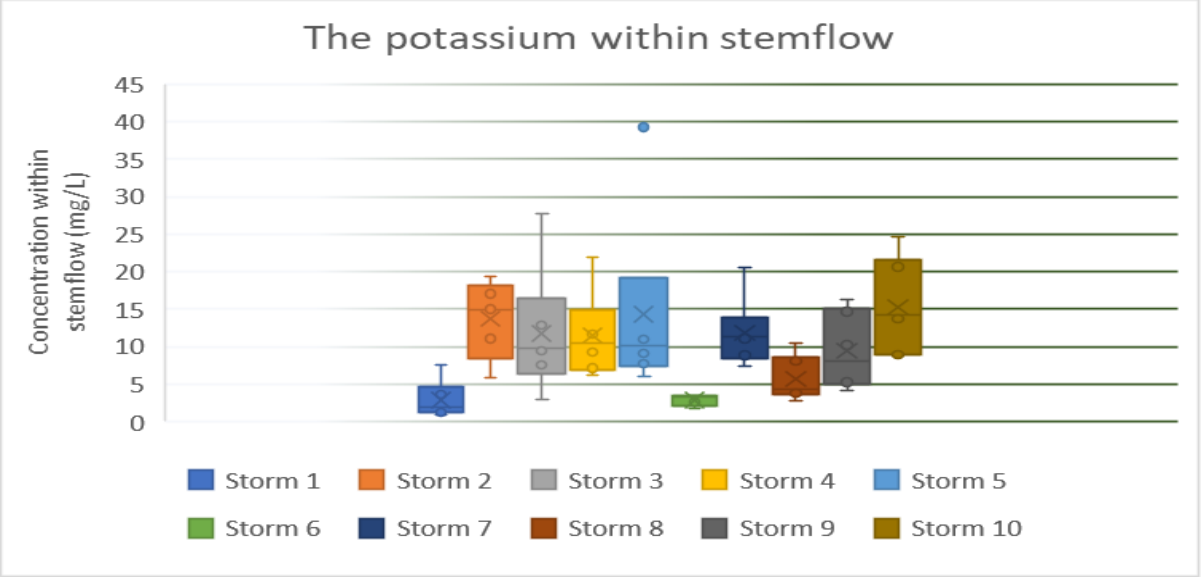

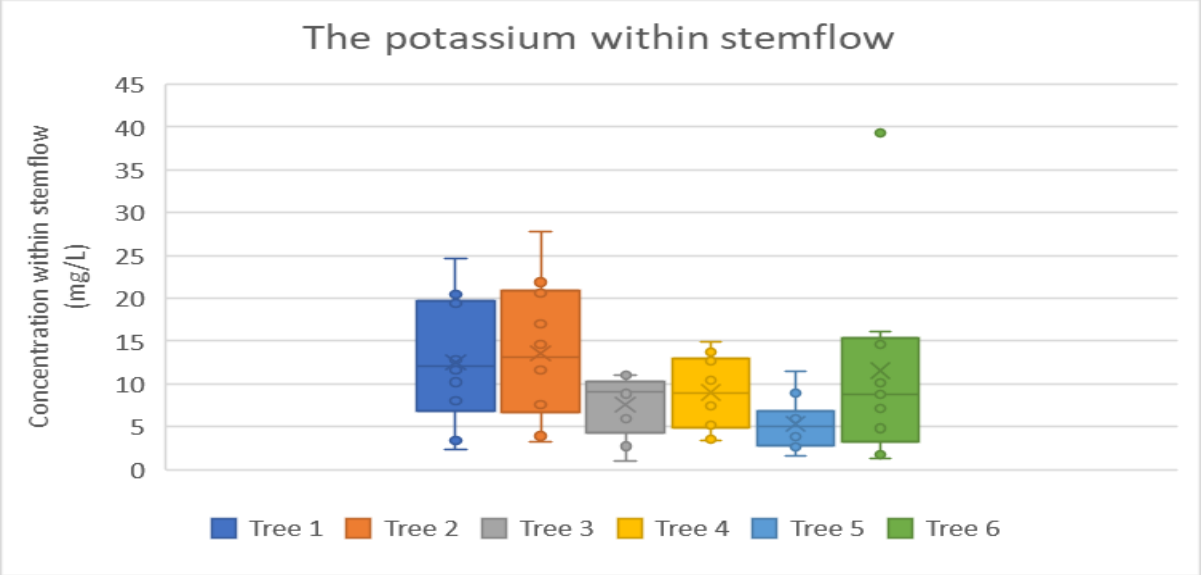

Figure 26K&l: A box and whisker graph showing the distributions of Potassium concentrations both between storms (above) and between trees (below). An X represents the mean; the line through the box represents the median; the box in the interquartile range and the whiskers are the full range.

There are two noticeable storms (S1 and S6) where the quantities take are visibly lower than the other storms, with low ranges also. Most storms have a low skew for their interquartile range, with S2, S5, and S7 having a higher skew, however with S5 this is attributable to the external outlier (Figure 26k), which is over 11mg/L higher than the next highest reading. This is the same external outlier seen within figure 26j. Every other tree has an internal outlier on both sides of their interquartile range, which contributes to the relatively even skew seen within them. Quantitively, it

is apparent that T1 and T2 produce the most potassium, with T6 having occasionally high values, while on the opposite end, T5 is consistently low.

3.3.7 Bromide

Bromide averages 0.45mg/L and shows a weak seasonal influence with higher values and ranges before full bloom (Figure 26m). There is a similar trend to other salt originating ions with low values and ranges for S6, and S8, with S1 only showing a reading within T3.

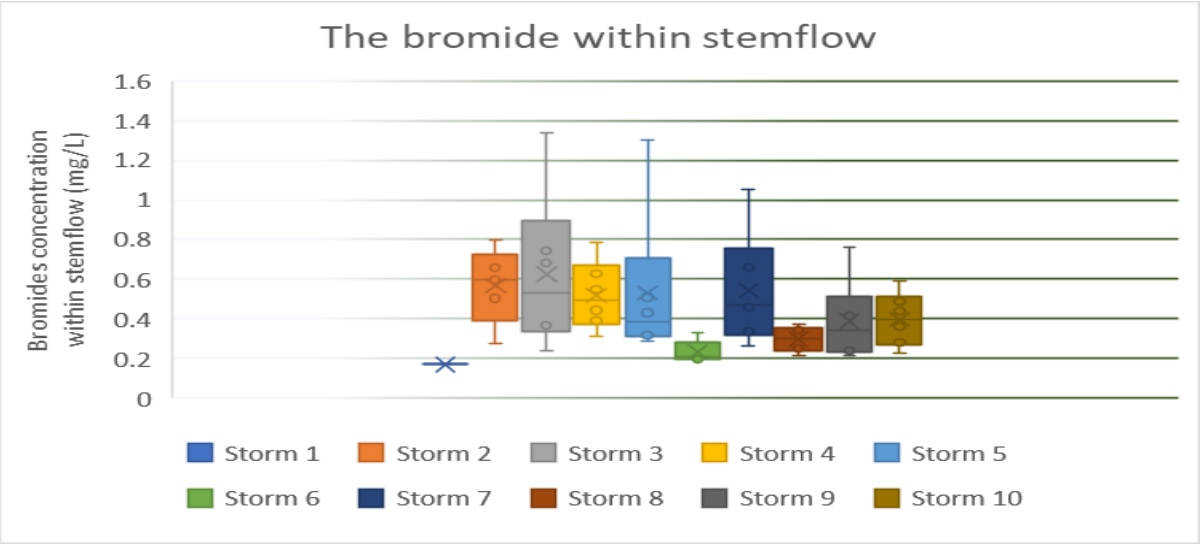

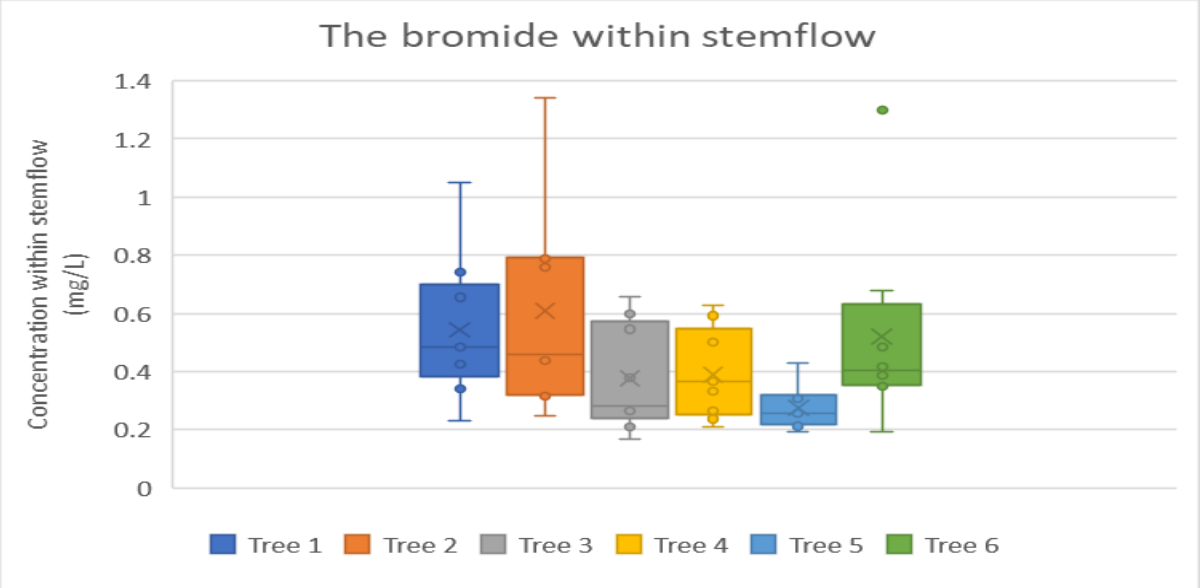

Figure 26m&n: A box and whisker graph showing the distributions of Bromide concentrations both between storms (above) and between trees (below). An X represents the mean; the line through the box represents the median; the box in the interquartile range and the whiskers are the full range.

There were often lower skews (Figure 26m) for the inter-quartile range (S3, S5, S6, S7, S9, and S10) because of singular values that were especially high within each storm, with S2 showing the reverse. Out of these seven storms, only S10 had no similar result within another ion, with S3, S5, and S9 having similar results in four previous ions. The instance in S5 is also the external outlier from T6 seen before in ammonium, potassium and chloride. Furthermore, while there was a value that caused a low skew within S6, that same storm contained a recording which caused a high skew in T6. The trees showed similar behaviours to most other salts, with T2 having a large range and a lower skew, similar to T1 and T5. However T1 is similar to T3 and T4 in that it has an internal outlier on both sides of the interquartile range.

3.3.8 Fluoride

Fluoride averages 0.14mg/L, with S1, S5, S7, and S8 uniformly below this mark while S2 is consistently above this.

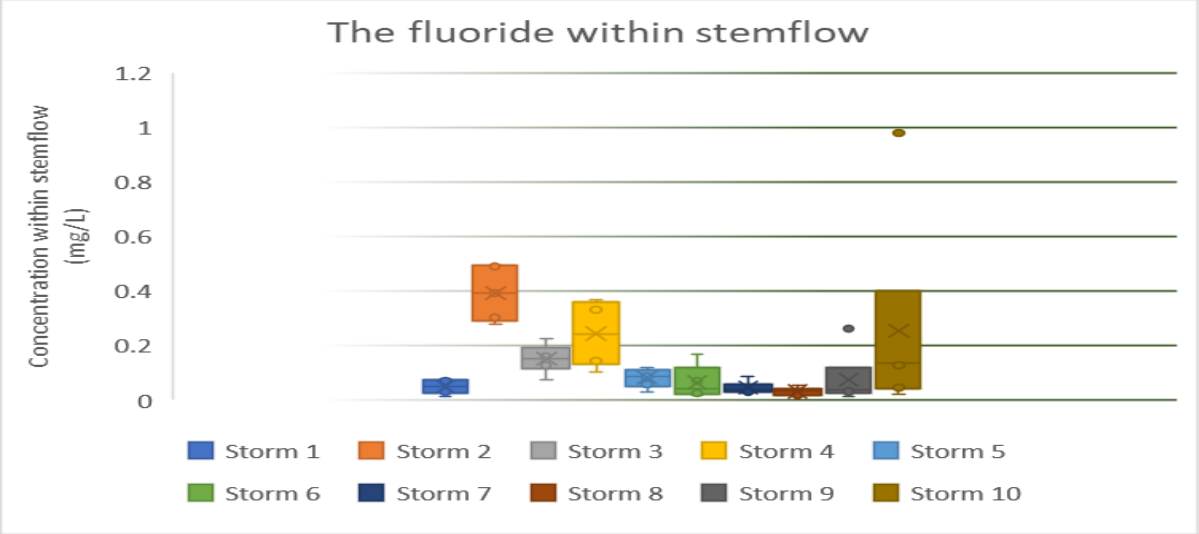

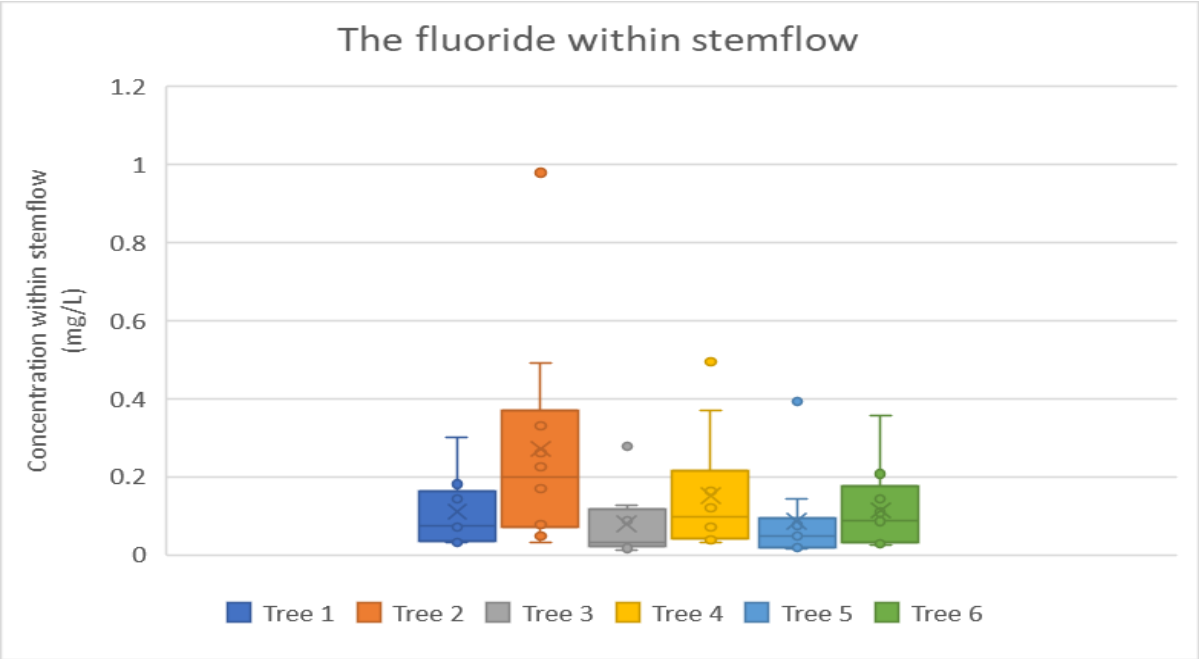

Figure 26o&pl: A box and whisker graph showing the distributions of Fluoride concentrations both between storms (above) and between trees (below). An X represents the mean; the line through the box represents the median; the box in the interquartile range and the whiskers are the full range.

Fluoride shows a partial seasonal influence, with ranges and values being noticeably higher in S2, S3, and S4, while S10 had the largest inter-quartile range and single value at 0.978mg/L (Figure 26o), being almost double the second largest value. This value is also the outlier for T2 (Figure 26p), while the external outlier in S9 was from the same tree. These same trees have caused low skews for magnesium and sodium for S9 and for ammonium for S10, while the skews are especially small within fluoride compared with other ions. The trees have consistently low skews (Figure 26p), with

the three external outliers from T3-5 all coming from S2. This is also the first ion where T5 doesn't have the lowest concentrations, with T3 having slightly smaller outliers and ranges.

3.3.9 Ammonium

Ammonium averages 2.86mg/L across all its readings, with a stronger inter-storm dependency over a seasonal influence. This is noted in the stark differences in both range and quantities recorded within each storm (Figure 26q), where some storms are consistently below 0.4mg/L, while others are consistently above 2.5mg/L.

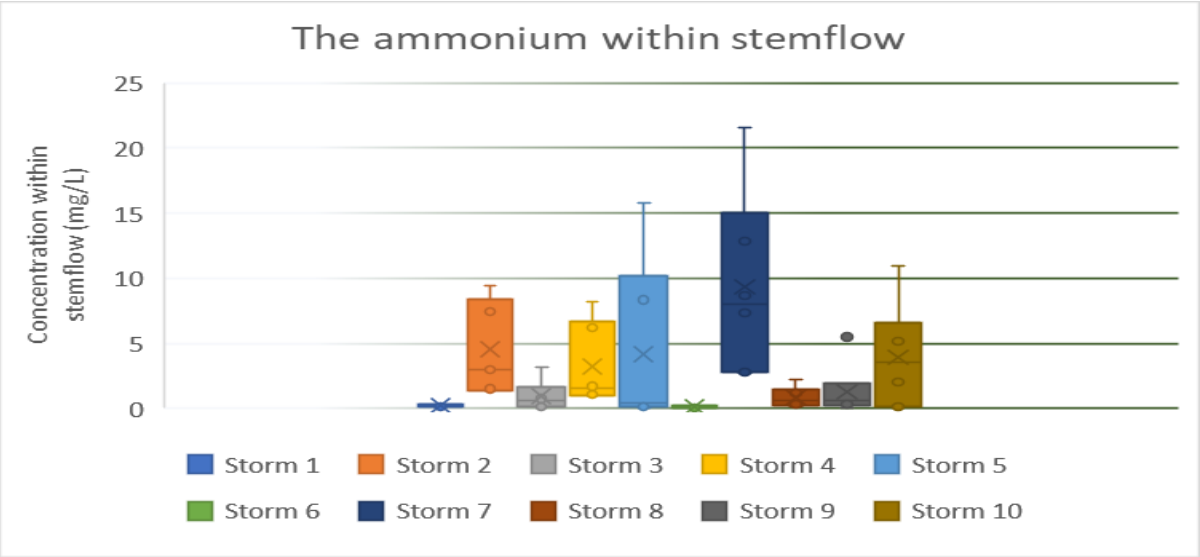

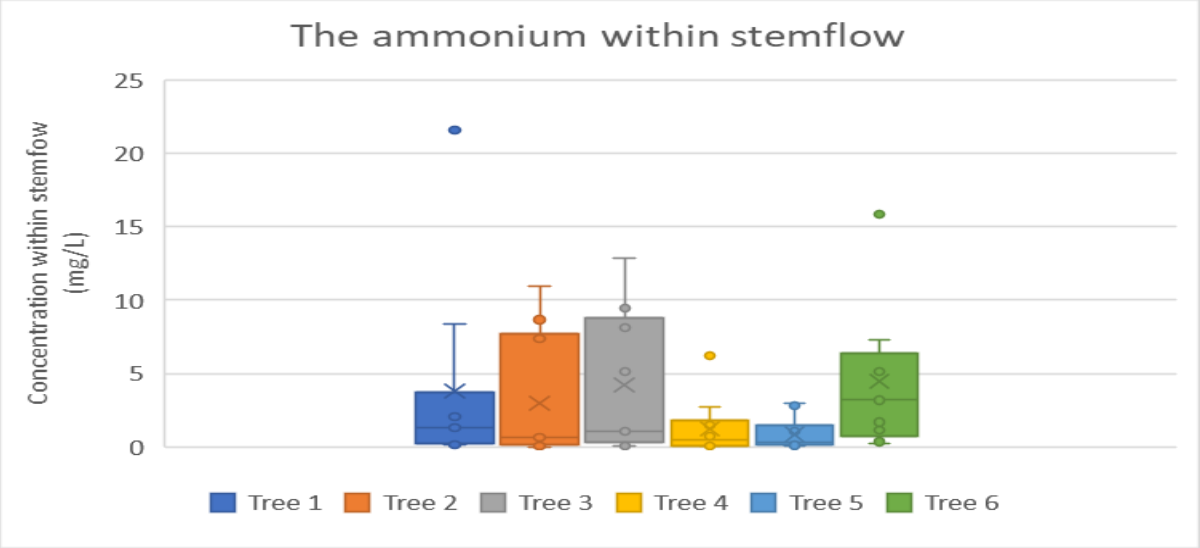

Figure 26q&r: A box and whisker graph showing the distributions of ammonium concentrations both between storms (above) and between trees (below). An X represents the mean; the line through the box represents the median; the box in the interquartile range and the whiskers are the full range.

There is the tendency for some storms (S2, S3, S4, S7, S8, and S10) to have a singular high value between 2-3x of the average, which skews the average for that storm. However, the only external outlier value was within S9, as the other storms had a secondary high value to support it. This low skew carries onto the trees (Figure 26r) as the only tree with a relatively even range is T6. However, unlike the storms, each tree has an outlier value, which mostly contribute to S7 unusually high ammonium readings, while the others contribute to the skew seen in S2, S4, and S5. The trees at site 1 produce more ammonium than at site 2 (Figure 26r), with trees 4 and 5 have consistently low values, with only 1 each above average, however they were also only the lowest value 3 times combined (T4 – 2; T5 – 1). Storms 1 and 6 stand out as being noticeably inactive when it comes to ammonium, while T6 produces uniquely high quantities.

3.3.10 Nitrite

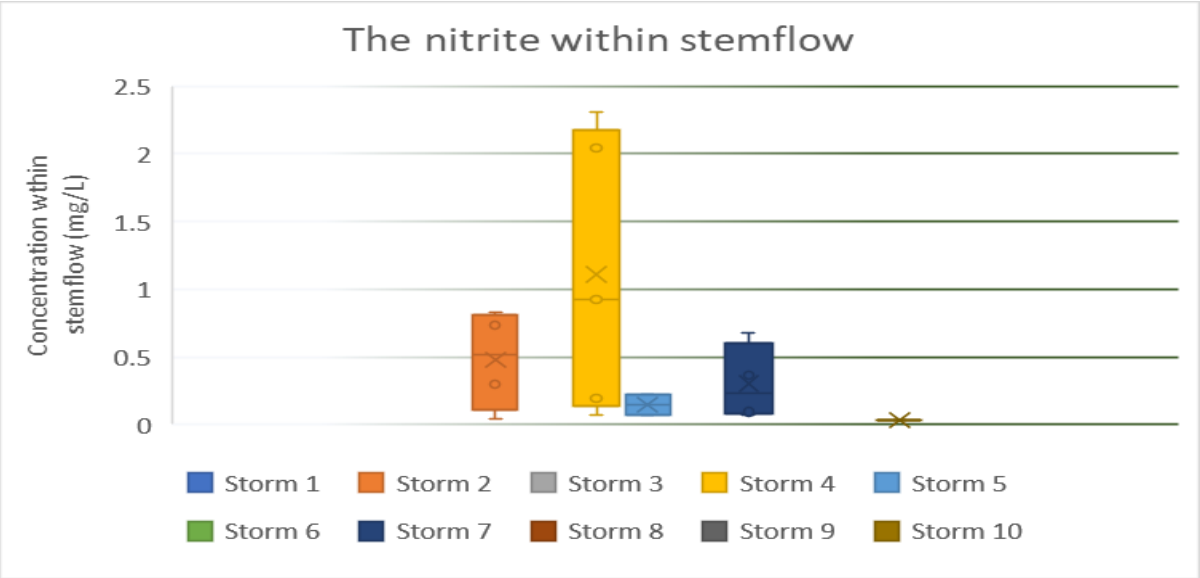

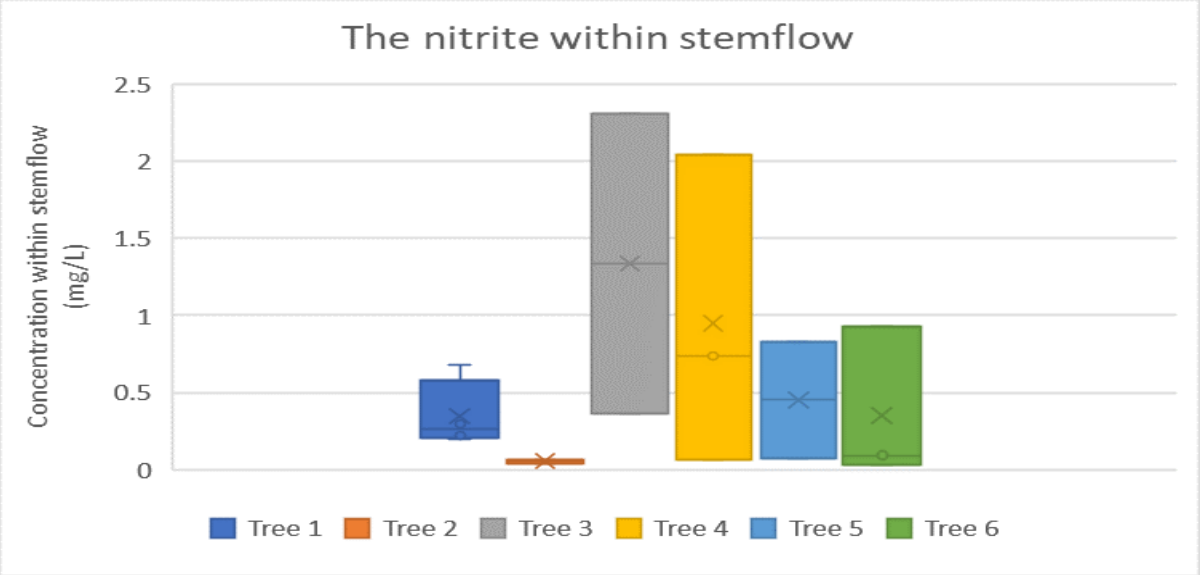

Figure 26s&t: A box and whisker graph showing the distributions of Nitrite concentrations both between storms (above) and between trees (below). An X represents the mean; the line through the box represents the median; the box in the interquartile range and the whiskers are the full range.

Nitrite was only detectable within five storms (S2, S4, S5, &, and S10) with Storms 1, 3, 6, 8, and 9 not producing any detectable results (Figure 26s). However, nitrite was produced by each tree between 2-4 times each (Figure 26t), so it was the least prevalent ion with an average quantity when it was detected was 0.56mg/L. This produces large disparities between the storms and the trees, with unique results of T3 and T4 being the largest producers. Comparing the storms shows no

exceptional skews, with the stark difference in the sizes of interquartile ranges. A characteristic that is unique is that T2 is the lowest producer of Nitrite.

3.3.11 Nitrate

Nitrate averages 1.95mg/L and shows similar patterns but larger values in the five storms where nitrite is present (S2, S4, S5, S7, and S10), while still being present in all ten storms (Figures 26o & 26s).

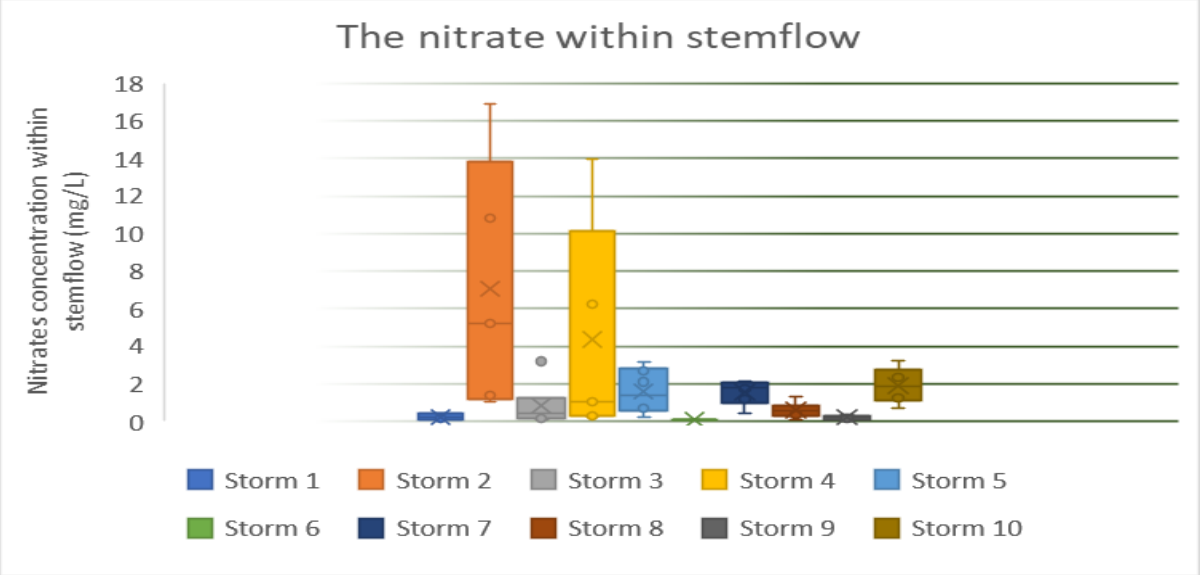

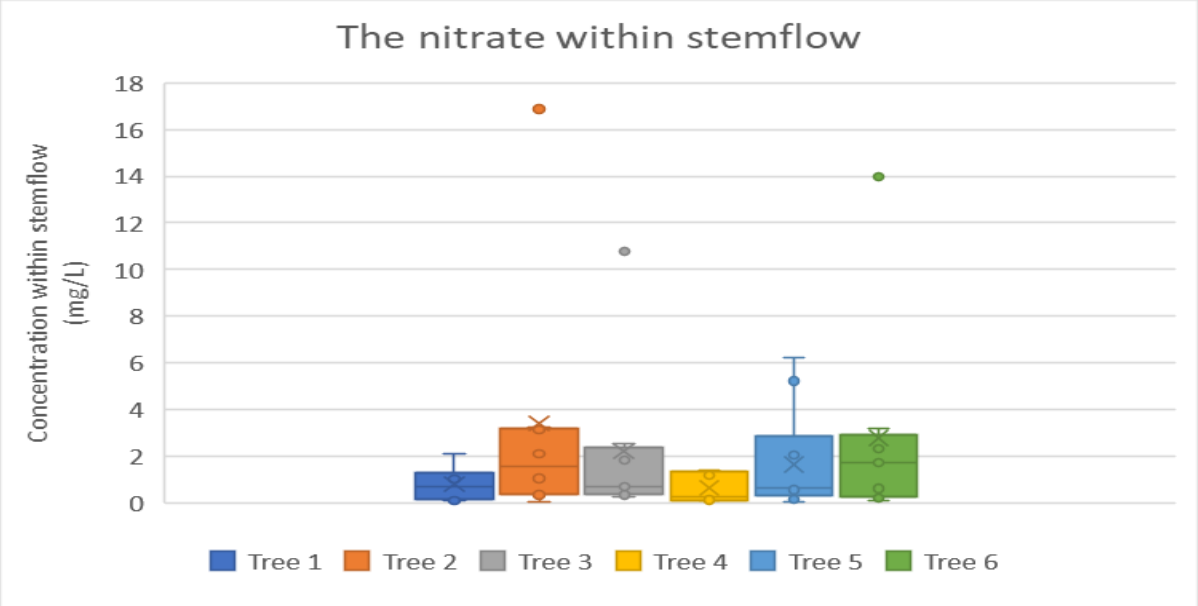

Figure 26u&v: A box and whisker graph showing the distributions of Nitrate concentrations both between storms (above) and between trees (below). An X represents the mean; the line through the box represents the median; the box in the interquartile range and the whiskers are the full range.

There is one external outlier within S3 that shows a similarity to ammonium, with a further similarity in the low skew seen within S2. The low skew from S4 is a more common characteristic, however a similarity with the tree at fault leaves the similarity to magnesium. There are three further external outliers, one from T2, T3, and T6 (Figure 26v), with the first 2 from S2 and the third from S4, which contributes to the exceptional interquartile ranges seen within Figure 26u. Tree 5 further produces the most prominent range with an internal outlier from S2, while the other trees show no apparent pattern of behaviour.

3.3.12 Phosphate

Phosphate averages 2.28mg/L and is completely absent from S1, with 18 occurrences where it was below detection levels.

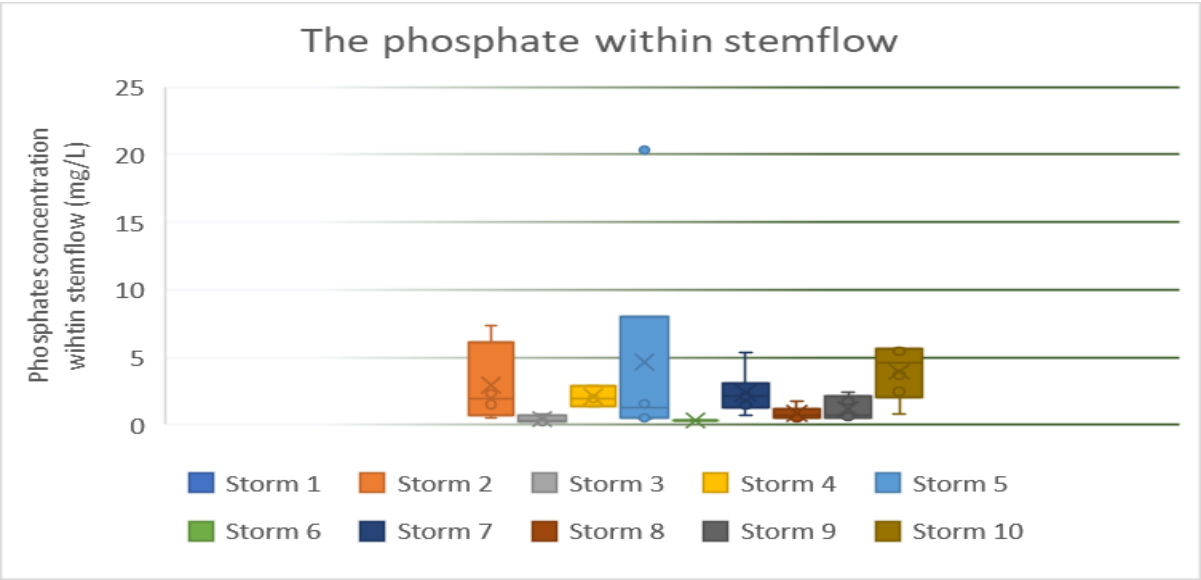

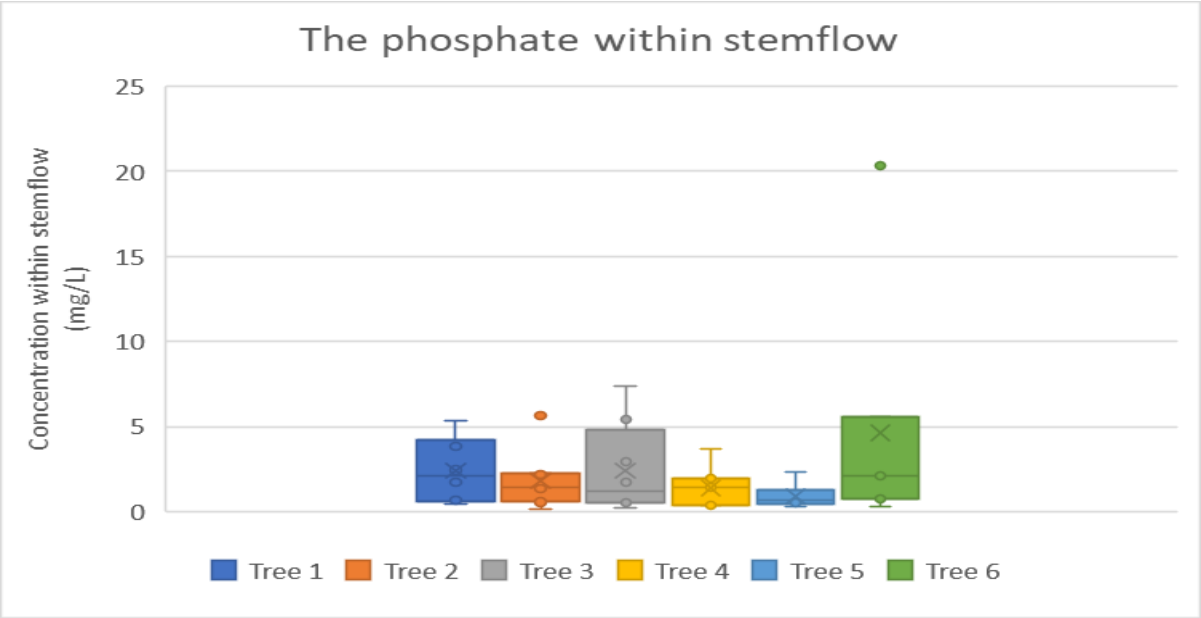

Figure 26w&x: A box and whisker graph showing the distributions of Phosphate concentrations both between storms (above) and between trees (below). An X represents the mean; the line through the box represents the median; the box in the interquartile range and the whiskers are the full range.

There appears to be a stronger storm-to-storm dependency as the ranges are different in consecutive storms (Figure 26w). The external outlier from S5 gives phosphate a similarity to five previous ions, and its secondary nature as the external outlier for T6 (Figure 26x) strengthens the similarity with three of those ions. The low skews seen in S2, S7, S8, and S9 (Figure 26w) give phosphate a strong similarity to ammonium, where the tree with the highest recording in each storm was identical in all 9 storms. A contrast can be made between the trees where if there is an

external outlier, there will be a higher interquartile range skew. This is shown as where the ranges extend up (T1, T3-5 in Figure 26x) they correspond with similar low interquartile range skews for S2 and S7 (Figure 26w).

3.3.13 Overall evaluation of the ions within stemflow

The statistical differences of the ions between both the trees and the storms only produced significant differences between the largest ions for the trees, while some of the lesser ions like phosphate were extremely unsignificant, with p levels as high as 0.735. This consistency shows that tree factors such as the architecture, epiphytes, topographical situation are the lesser component unless one is dealing with large quantities of a particular ion, like one is with sodium and chloride. The consistency of significance within ions and storms shows that each ion is responding to some meteorological variable.

	Significance level (p)	
Ion	Between storms	Between Trees
Na	0.03	0.011
NH4	0.005	0.1531
K	<0.001	0.1102
Ca	<0.001	0.3545
Mg	0.002	0.1715

	Significance level (p)	
Ion	Between storms	Between Trees
F	<0.001	0.127
Cl	0.0013	0.002
NO2	0.04	0.553
Br	<0.001	0.554
NO3	0.004	0.670
PO4	<0.001	0.735
SO2	<0.001	0.517

Tables 9a&b: The statistically significant difference levels of each ion, using the Kruskal-Wallis test both between storms and between trees using the null hypothesis below.

Null hypothesis: Each storm/tree will have the same quantities of ions ($P < 0.05$).

3.4 The ions within rainfall

Within the ionic compositions of the rainfall, 8 of the 12 ions are found within every sample, with 7 of those being salt ions (Na^+, K^+, Ca^+ Mg^+, Cl^-, Br^-, SO_4^{2-}) and the other, NH_4^+ The only salt ion without

a consistent prevalence is fluoride, which was present in rainfall collected during storms S2, S3, and S10. Meanwhile, Nitrate is missing on two occasions (S3 and S5), Nitrite is consistently absent, with the exception of contamination for S2RF1, while phosphate occurs in the final 3 storms with an additional occurrence in S4.

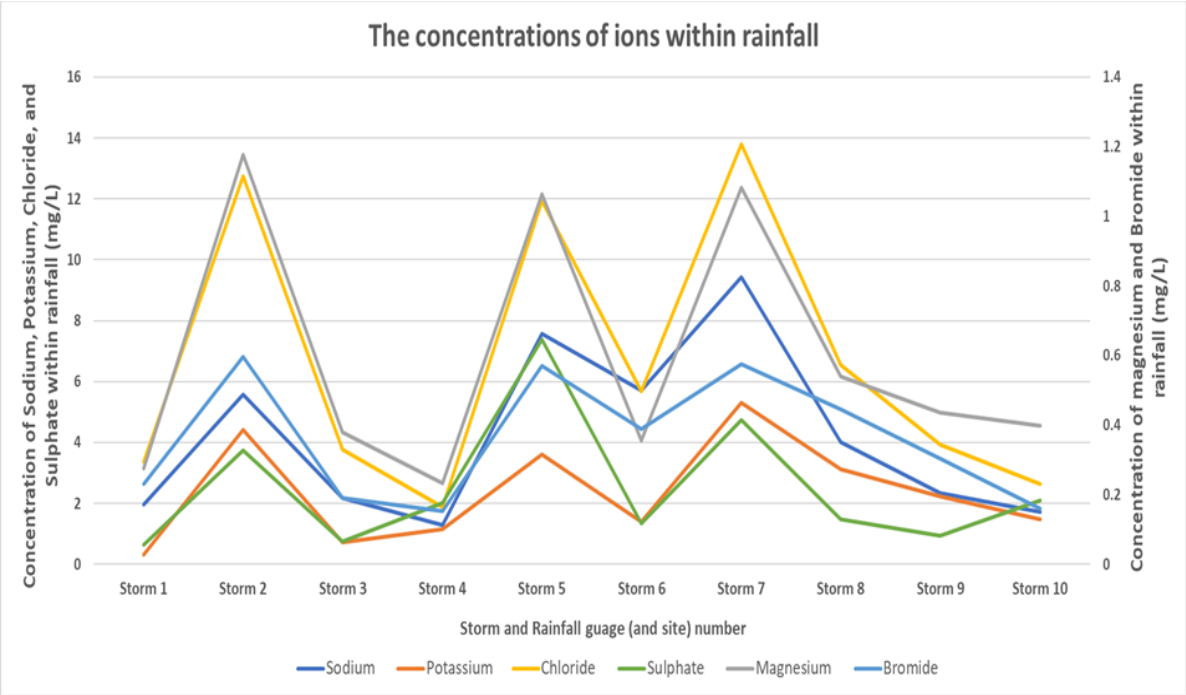

Figure 27: The quantities of the major salt ions within rainfall.

The six major salt ions (list the ions) appear to behave in a fairly concurrent manner, with higher quantities in S2, S5, and S7 (Figure 27). There are low concentrations for S3 and S4, and a noticeable drop in concentration for S6, while the concentrations decrease through S8-10 with sulphate having the only increase from S9-10. The concentrations of all the ions within rainfall appear to partially concur with stemflow quantities (Figures 26a-x), with low S1, S6, and S8 and high S2 concentrations. While the storms characteristics differ to the ions in S3, S4, S9, S10 which saw large values within stemflow values but low rainfall concentrations. The remaining storms S5 and S7 show high rainfall concentrations with all six ions in figure 27, whereas similar high stemflow concentrations are only found within Potassium, Sulphate, and Bromide. Ammonium and Nitrates pattern are partially similar (Figure 28), having high concentrations for S7, however their second highest values came a storm earlier in S4, but also showing the general decrease through S8-10.

Nitrate also shows a similar high concentration within S2 and S9RF1, with ammonium showing a similar increase in S10.

The other five ions (Figure 29) show separate patterns to the previous ions, with calcium's most prominent feature being a large preference for site 1 over site 2, with a 7x difference being the largest. Phosphate and Fluoride have sporadic occurrences, with both values either supporting high stemflow concentrations as in Fluoride (Figures 26k&l) or supporting consistent occurrences above detection level for Phosphate (Figure 26w&x).

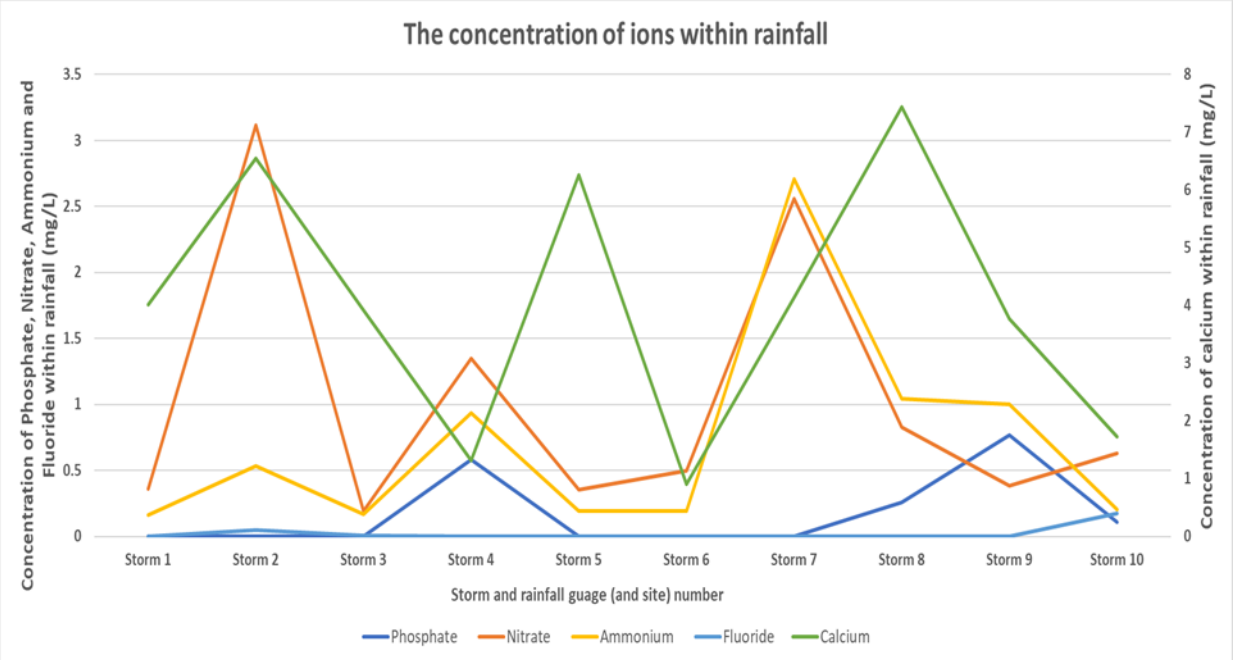

Figure 28: The quantities of Calcium, Nitrate, Ammonium, Fluoride, and Phosphate within rainfall.

3.4.1 Impact of rainfall on stemflow ionic composition

Rainfall impacts the ionic composition of stemflow mainly by providing the input of the fluid solvent (water) that transports the ions from the tree surface to the base of the tree. Comparing the rainfall ion concentration with the stemflow ionic concentration, there was no instance where that the ion was quantitatively greater in mg in the stemflow than in the total amount of rainfall obtained from

any tree and storm combination. So we cannot definitively state that intake of ions occurred other than when those ions were present in stemflow and not in rainfall for any respective tree and storm combination.

The most reliable metric that indicates some deposition/leaching are the disparities between the stemflow percentages and the quantities of ions recorded within stemflow. This can be expressed by calculating the quantity of an ion that would have fallen on a tree by multiplying the concentration in the rainfall (mg/L) by the estimated volume of water that will have fallen on the tree within any storm. For example, if 1% of the rainfall is recorded as stemflow, but less than 1% of the sodium from that rainfall is within the stemflow , then that sodium must still be on the tree or diverted into another form of runoff (throughfall). This occurred at least once for each ion, being more common in Nitrate (half of samples) and Ammonium (a third of samples), while phosphate occurred only 3 times in S8 and S9. The salt ions can be broken into 2 categories, one with sparce occurrences (5 or under – Na, K, Mg, F, Cl), and more common occurrences (10 or more – Ca, Br, So42). Within the sparse occurrences, fluoride is unique in having all its occurrences in S10, while the other storms share the 5 storm-tree combinations, with S8T3 being found in all 4. Where the common occurrences differ is that instead of having individual trees within a storm, they have most or all of the trees with those storms (Commonly S5, S6, S8).

3.5 The movement of stemflow

When comparing the movement of water droplets at different bark angles (Figure 31), there was a statistically significant difference between the angles in the dried samples ($P = <0.001$); however, there was not a significant difference in the field samples ($P = 0.1842$). Furthermore, no significant difference was found between any angles in the field, while only the difference between 45° and 60° was not statistically significant at the 0.1% confidence level within the dried samples; however, this then passed at the 1% confidence level. When comparing the droplet repetitions, there was a significant difference between field and dried samples ($p = <0.001$). However, this significance was primarily attributable to the first droplet, as statistically significant differences between droplets 3, 4, or 5 were not found. Furthermore, droplet two only had significant differences between droplets 4 and 5 in the dried samples and droplet five within the field samples. However, as both dried and field samples are statistically significantly different, this variable is used to compare droplets' speeds

over dried and field bark samples. The angles used within this experiment are as follows, with the outer bark facing upwards. The resulting proportions within each time category are then shown as they develop.

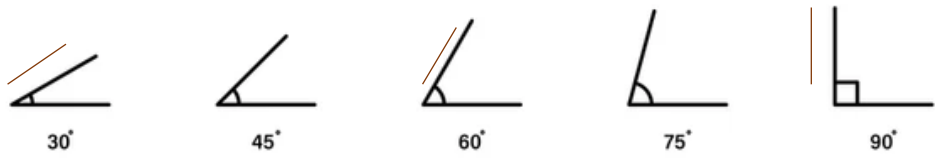

Figure 29: An illustration of the angles of bark used to test water movement behavioural differences, with the brown line denoting the positioning of the bark sample.

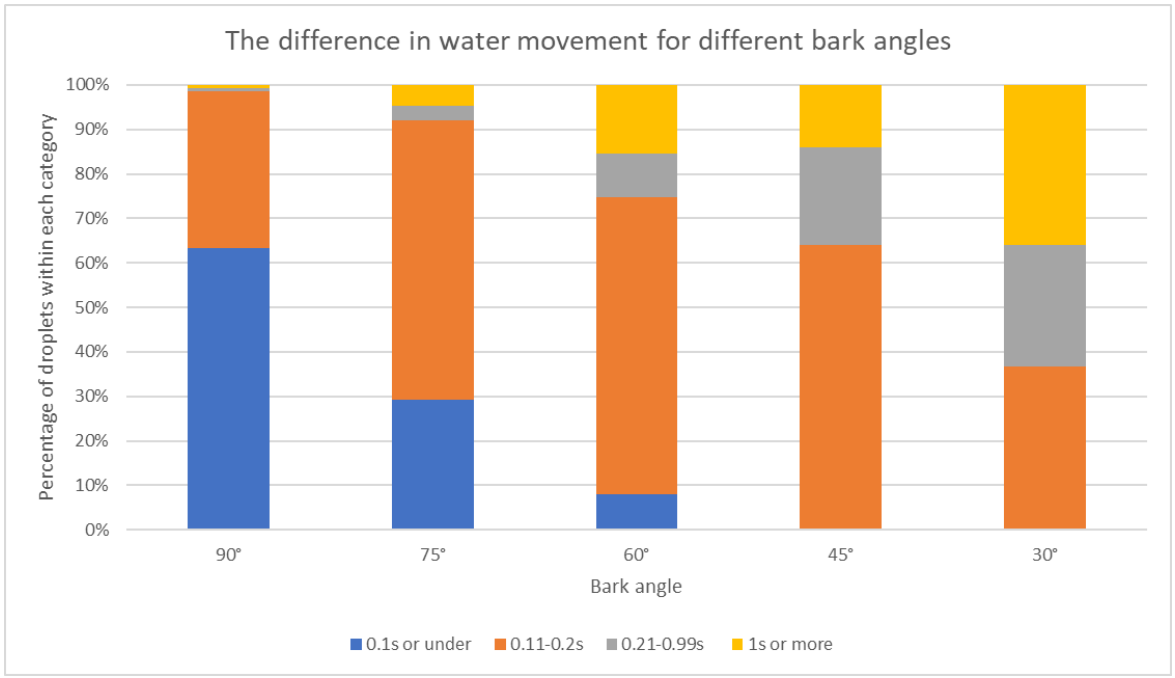

Figure 30: The number of droplets within each temporal category.

Figure 30 shows that when bark samples are set to 90 degrees, the droplets were consistently fast, with 98% of their droplets completing the distance in or under 0.2s. This proportion drops to 91% when samples are set to 75° ; 75% for 60 degrees; 63% for 45 degrees; and 37% for 30 degrees. Whereas, when the bark sample becomes more horizontal (30 degrees), gravity has less of an influence, with 0.6% of droplets taking more than a second to cover the bark length within 90-

degree samples; 4.66% in 75 degrees; 15.33% for 60 degrees; 14% for 45 degrees; and 38% for 30 degrees. The bark angle further impacted the travel velocity. For any instance where the average and standard deviation for a droplets velocity were higher for a gentler slope than on a steeper slope, the droplet at fault was 3SD higher in its velocity than the average within its specific category (First, second, third… droplet : angle of bark slope). Overall, the bark angles' influence on droplet movement is clear, with significant decreases in speeds throughout the droplets and no 5th droplet having similar or lesser speeds than the first. There is also a clear variability in behavioural dynamics between the first and fifth droplets as the first droplets have far more extreme anomalies when compared to the fifth droplets which show a far steadier incline with their droplet times.

The acceleration with successive droplets is attributable to the lubricated travel channels, as when one applied a surface saturation, there was a noticeable and consistent drop in velocity. This drop in speed is not recorded because of the difficulty in accurately measuring and the lack of a defined obvious movement. Overall, the bark angles' influence on stemflow s speed is clear, with significant decreases in speeds throughout the droplets and no 5th droplet having the similar or lesser speeds than the first. When comparing the dried and field samples, there is a statistically significant difference ($p = 0.043$), meaning bark moisture impacts stemflow speeds, with dried bark found to be slower.

3.6 Hygroscopicity and bark water loss

3.6.1 Hygroscopic nature of bark

The experiment involving the observation of bark's moisture exchange with the atmosphere with increasing relative humidity shows bark samples increase in weight by an average of 1% when the relative humidity was increased from 50 to 60%; 1.5% when the relative humidity was increased from 60-70%; and 3.5% when the relative humidity was increased from 70-80%. Figure 31 demonstrates the increases in relative humidity will cause increasingly more water to be stored in a piece of bark as the percentage of weight increase will grow with each consecutive increase of relative humidity. The initial condition of the bark did not impact later weightings; however it is responsible for the two outlier values as the piece of bark held onto water for longer than other pieces of a different physical condition but in the same climatic conditions.

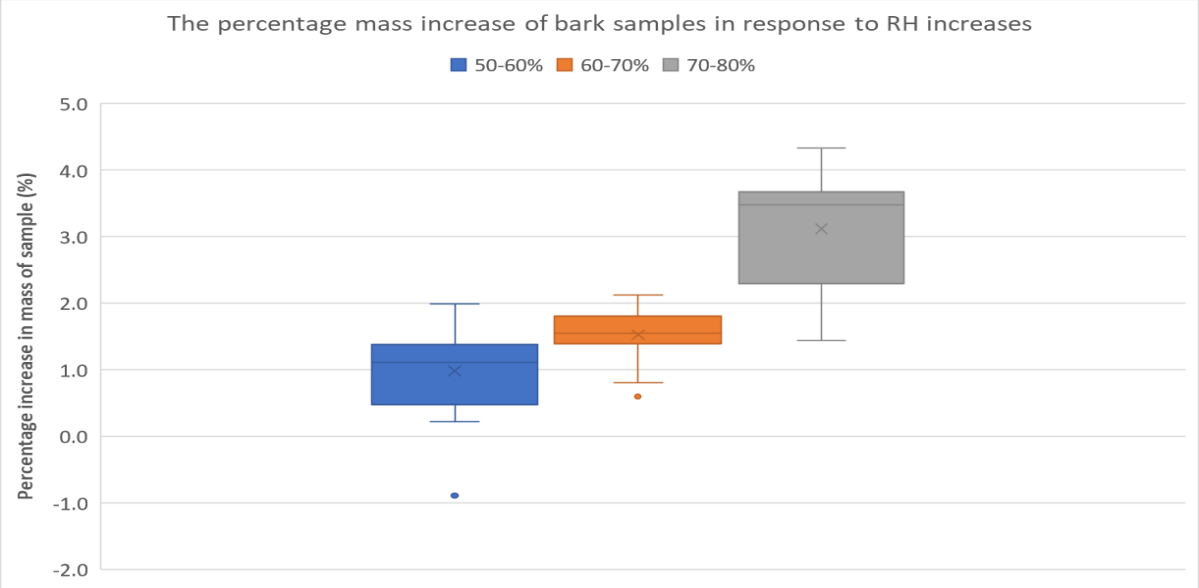

Figure 31: A box and whisker diagram showing the percentage of bark samples moisture content change with increase in relative humidity RH (P = <0.01, H = 29.4)

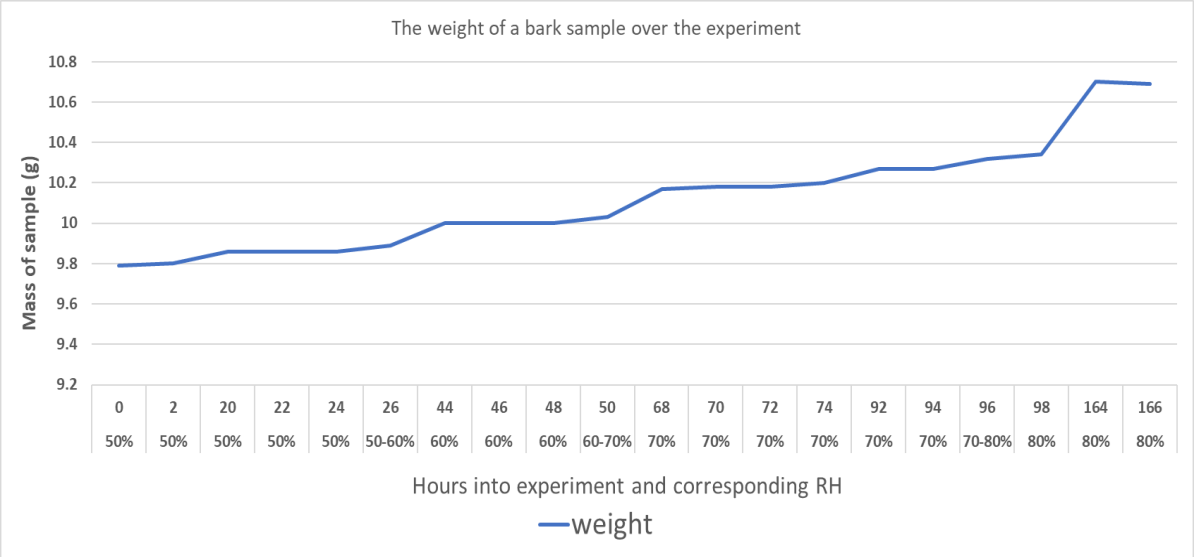

Figure 32: Examples of the increase in mass of a bark sample through the increasing relative humidity's.

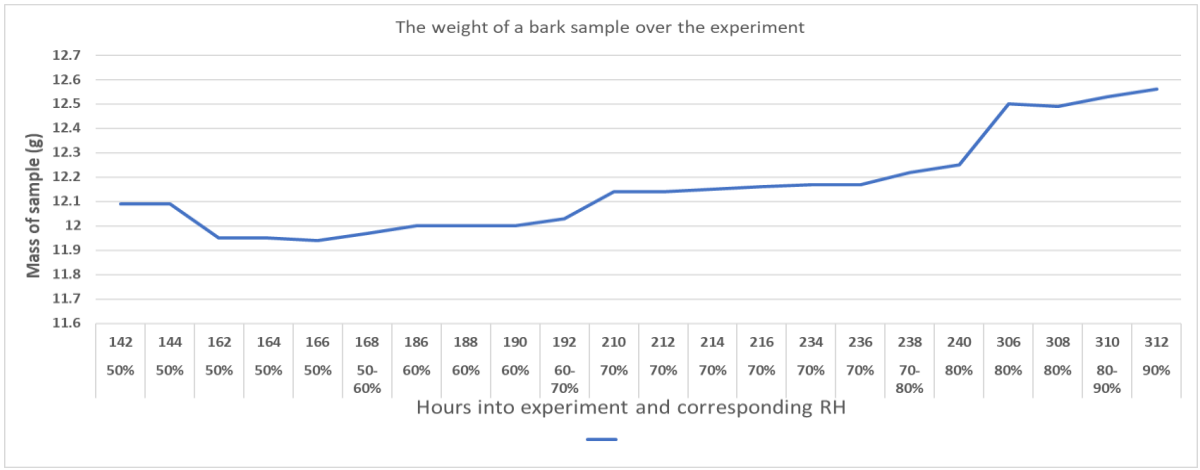

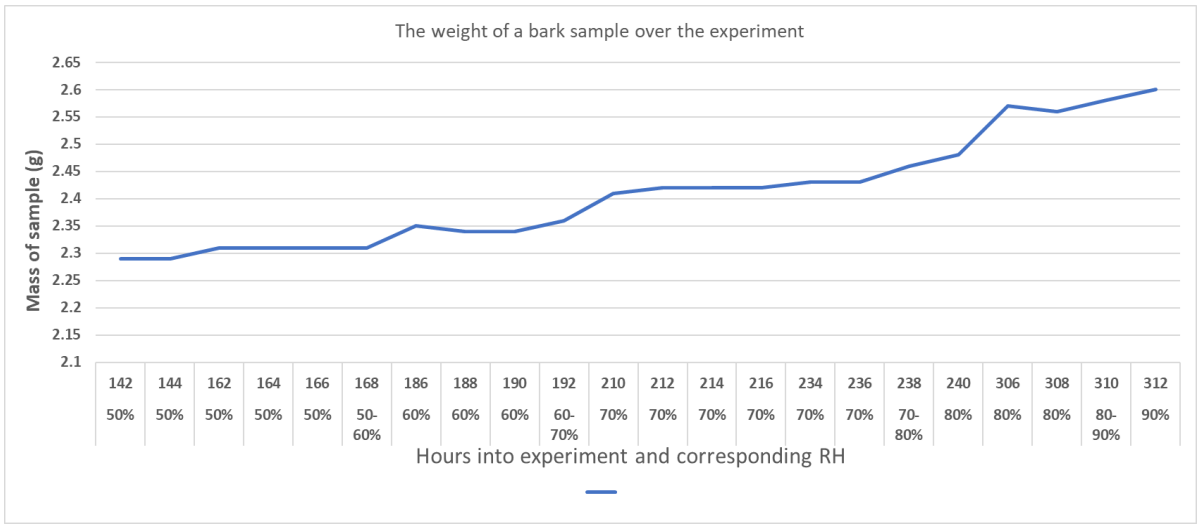

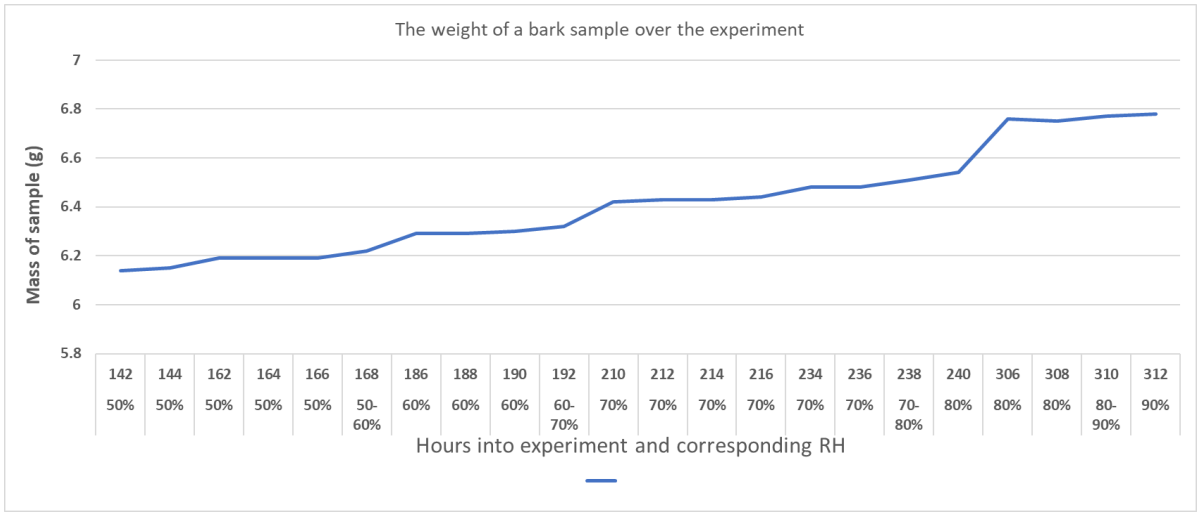

Figure 33: Further examples of the behaviour of bark through different circumference and consequentially different weight categories.

Hygroscopic intake is shown where water is taken in quickly initially and will be tail off until the stable weight at each relative humidity level. The initial intake (First 2 hours) gently increased through the three increases (Figures 32 & 33), with the timings of the increase sometimes being sharper if they done overnight or over weekend. This does show that an uninterrupted placement within a higher relative humidity could give higher weights, which can be seen in the slight decrease of mass between hours 164-166 in figure 32, which combined an uninterrupted period of 66 hours with the largest average increases (Figure 32). The tail towards the stable weight became longer as the relative humidity's increased, taking roughly 24, 48, and 72 hours respectively, until a stable weight was recorded. The reaction to humidity behaves relative to the current humidity, with greater humidity spikes having a faster response. The experiment was repeated with the wet samples, with similar results.

3.6.2 Barks moisture content

The oven drying experiments (see section 2.3.5) where one placed samples of bark in an oven at 105°C and left them for roughly 72 hours demonstrated that firstly: The moisture in any bark surface depends on the surface complexity as moisture is stored in small gaps within the fibrous interior and the percentage of epiphytic coverage on the surface of the bark. A threshold seems to lie around a circumference of 30cm, where a higher epiphytic population holds more water to be lost, whereas this is reversed in lower circumferences. Table 12 shows that even when bark is from and held in identical conditions, there can still be discrepancies in the moisture content of the bark. This complicates the definitions of “moist” and “dried” sample used in the methodology and indicates that bark moisture is too sensitive a variable to achieve statistical significance using this experiment. The temperature of 105^{o}C was likely too high to stop deformation of this natural material, one recommends further studies to limit to between 50-60^{o}C over a longer timeframe.

Sample circumfrence + number	Starting weight	Moss cover	Final weight	% change
50+cm BS1	15.60g	10%	9.22g	-40.90
50+cm BS2	15.60g	15%	8.83g	-43.40
40 to 50cm BS1	9.01g	1%	5.81g	-35.52
40 to 50cm BS2	9.01g	5%	5.43g	-39.73
30 to 40cm BS1	9.27g	40%	5.34g	-42.39
30 to 40cm BS2	9.27g	60%	5.03g	-45.74
20 to 30cm BS1	4.14g	0%	2.14g	-48.31
20 to 30cm BS2	4.14g	5%	2.21g	-46.62
10 to 20cm BS1	4.35g	10%	2.00g	-54.02
10 to 20cm BS2	4.35g	50%	2.10g	-51.72

Table 10: The mass loss of moisture in bark samples with different circumference and moss cover

4. Discussion

4.1 The weather during the study period

The rainfall results show that the period March-July 2022 was one of the driest in the last 40 years, with only 61% of the rainfall expected to fall being received in these five months. Therefore, it provides the context that the following discussion points should be understood in, with the results indicative of likely future results as the effects of contemporary man-made climate change produce more of this unusual weather. This weather is likely to come in more pronounced extremes as April-June is noted as a dry time in Swansea, notably as dry spells during the investigation period of 17 and 13 days, with a separate storm 20mm in depth and others over 20 hours long. These large storms are also presented when the number of rainy days exceeds the historical average, so most storms are getting smaller, with individual large downpours. However, the overall depth of the rainfall does not mean that the ions within stemflow are dense as they have the same if not more transport, but with fewer occasions where they are sufficiently washed from the surface, potentially leading to conditions noted in arid climates (Van stan & Gordon, 2018). The drier weather pattern changed in June, where the month was consistently wetter than the historical average, which could demonstrate more historically average ionic levels for June's storm still with a prior dry period of almost a week. The droughts allowed for extended periods of sun, demonstrated through the 1-2°C above the historical average throughout the four months. While this is particularly pronounced in March, this seems consistent with predictions averaging around 1.5°C, further putting the results within the context of climate change (Levia, 2003).

Most storms were not overall unusual but had their individual characteristics, with eight having southerly winds from the sea, and the other two having each a north-westerly and easterly direction. The wind in any storm was a complex component as pressure systems ultimately changed the angle of the incoming rainfall, with the SD of the wind ranging from 9.73° in S3 to 87.14° in S4. This intricacy means that only the average can be considered, as the methods were not designed to encompass the time-sensitive nature of this variable. The storm length is usual compared to the historical average. The storms have a preponderance for the morning, like the earlier preference for early in the month. This likely means that the rainfall encounters bark with higher moisture content, so less rainfall is lost to evapotranspiration forces. However, it will remain inconclusive as to the extent to which this counteracts the large dry periods and their inflated quantities of ions. Another sensitive variable with stemflow quantity is noted where rainfall gauges and weather station data

can be similar but ultimately are not identical, so the dilution variable can only be theorised from the data, while the exact amount of water received from the tree is precisely unknown, so factors such as

4.2 Storm depth and its categorisation of stemflow

The obvious difference between trees T1, T2, T4, and T5 and T3 & T6 meant that categorising them provided further behavioural themes within both groups (Figures 24 & 25). The first category shows that when a storm is above 10mm in depth, the values for stemflow are consistently between approximately 800-1000ml, where 1000ml appears to be the upper limit for this category of tree (Figure 24a & 25a) where additional water could be lost as throughfall or other metrics. It is worth noting that both of these storms did not come after a long drought, with both having roughly 10mm of rainfall in the week prior. This upper limit exists within moist conditions, and different values would likely appear if a storm this size preceded an extended drought.

The lower limit of around 800ml is common (Figure 24a & 25a), with lower outliers differentiating the following category in S3 and S4, where T2 shows a value of 448ml in S3 and T4 shows a value of 299ml in S4. Where T2 shows a value of 448ml, this likely represents the epiphytic life and its response to the long dry period before S2, with the smaller storm not quenching its thirst, meaning S3 had to compensate still partially. For T4s 299ml value in S4, the tree's architecture, which has a levelled appearance attributable to the very horizontal branches and the diverse wind directions, could have created an abnormally high throughfall quantity. This theory is contradictory to the previous argument about a diverse wind direction. However, T4 does demonstrate a reduction in its FR from S3 to S4, so there may be canopy or tree characteristics that favour a diverse wind direction for the production of stemflow.

The following category where stemflow volumes struggle to break 200ml could represent two influences, peak storm volume (%) and early onset of this for S8 and an extended dry period where values cannot match. Whereas for S10, the strongest argument is the one similar to S2, where the storm's size cannot overcome the length of the prior dry period, reducing the overall quantity of stemflow produced. The influence that these storms share is a predisposition to have a strong hygroscopicity argument as S10 had the lowest consistent relative humidities and lowest value

recorded during one of our ten studied storms, while S8 was the only afternoon onset storm, which means it might have been met with far dryer bark than if it had arrived twelve hours earlier.

The final category comprises the smallest four storms (S2, S5, S7, and S9), where S2, S5, and S9 have the same large ranges seen in the second category (S3 & S4), and S7 shows similar behaviour to the third category (S8 & S10). The most apparent reasoning for this is the same as S8, as S7 occurred shortly after S6. Therefore, alongside the small depth within its storm, all the systems were likely still sodden from the downpour. The further three trees in this category each appear to respond to different causes that have been discussed within prior trees, being S2 and its long dry period, highlighting the effect of epiphytes with a low T1 & T2 volume, but a T4 & T5 volume over 5x this amount, with the higher threshold for stemflow generation being noted, with a similar difference in S5. The final storm (S9) shows the effect of an existing saturation in removing the effect of epiphytes as a stemflow reduction variable for dry periods and very small storms. All of these variables in volumetric stemflow production indicate some consistency when storms are above 10mm, whereas under, the characteristics causing each tree to produce a lower quantity intuitively match their physical characteristics.

4.3 How the funnelling ratio and $SF_{\%}$ control stemflow's volume

As the FR indicates the extent to which the water flow from branches is incorporated to the total stemflow volume, one can postulate the key factors that can affect the FR are the tree characteristics together with the meteorological conditions. Trees 4 and 5 showed consistently higher SF% values in comparison to all other trees. They are the only trees with SF% comparable with studies such as Durocher (1990) and Bellot *et al*., (1990). Tree no 5 (Figure 22) has consistent values of FR above 1 for all investigated storms, the potential explanation of hydrological efficiency of the tree is lack of epiphytes on tree bark. The FR of the remaining trees is variable depending on the storm, tree 2 and tree 6 are the least efficient, with only 3/10 of their results above 1. The first potential influence is the lack of epiphytes on T5, which would support why T4 also has a consistently high FR. The lack of epiphytes could explain why the trees respond differently to S2 & S5, supporting results found in Chen *et al* (2019), where the long dry period followed by an inadequate storm to quench the thirst, similar to T3, which had little moss and fungal epiphytes. This

theory could be carried forward through S6-8, where the abundance of water negates the influence of the epiphytes giving similar behaviours throughout all six studied trees.

The effects of wind can be a contributing factor as S4 is the only storm where all six trees are above one, with an extremely large SD in its wind direction, meaning it had an extremely diverse wind direction, owing to the orientation of the pressure systems to Swansea at the time. This diverse wind angle will have generated much more PFPs than the average storm, likely leading to a higher FR. This efficiency supports results found in Crockford and Richardson (2000). The next highest wind direction SD occurred in S6, where high rainfall intensities likely cause throughfall, meaning that a diverse wind direction will increase a tree's FR. The causes behind a low FR were found to be extremes as S2 & S7 both had the lowest FR (below 1 in 4/6 trees) and had separate (dry periods and peak storm volumes (%)). Peak storm volume is more consistent as S5 and S8 (where the peak storm volume (%) is above 50%) had another seven instances of FR<1, and S4 also has the lowest peak storm volume (%) at 17%.

The extremes causing a low FR were found to be congruent with $SF_{\%}$, as 11/12 of the highest and lowest values were seen within the four smallest storms (Table 9 - S2, S5, S7, & S9), which partially supports results from Levia and Germer (2015). The results her, however, show a curve similar to a cosine, whereas Levia and Germer (2015) found a more linear relationship. The single outlier is the same for FR and $SF_{\%}$ as the highest value for T6 was found in the largest storm (S6 – 20mm). However, T6 is also the tree with the highest correlations to rainfall characteristics, which may indicate that its FR and $SF_{\%}$ values are the ones with the least external influence. As T6 is the smallest tree, this could indicate that a tree's ability to produce stemflow becomes less dependent on weather conditions and more on tree characteristics (epiphytic coverage, branch architecture, topographical situation) as the tree grows more mature, just as they become less susceptible to being killed by this same extreme weather or by herbivores as they age. This contrast could further indicate that stemflow as a process has two distinct phases in that it starts as a way of providing nutrients to the sapling and, as the tree grows, becomes a way of delivering those same nutrients to epiphytic life as a tree becomes more a communal host than an individual.

The further fluctuations in $SF_{\%}$ appear to be rainfall related (Muzylo *et al*., 2012) as the large values from S4 does not show any remarkable values (Table 9), with the continued effect of epiphytic coverage showing with T4 & T5s distinctively large $SF_{\%}$ values. This is except S7, where they dip to levels consistent with the other four trees, highlighted the effect of epiphytes which would have likely not had the chance to dry out from the large S6 a day prior. This trend continues to S8 and S9,

where the larger T1 and T2 follow the pattern inside an extremely wet fortnight (>40mm), where S9 shows high $SF_{\%}$ values in T1 and T2. This theory could indicate that for the largest of oak trees if they are also dense in epiphytes, that stemflow does not occur outside of extreme storms as the threshold for an $SF_{\%} > 0.5\%$ for T2 appears to be this 40mm in 14 days, while this tree is only estimated to be roughly 40 years old.

Both of these aforementioned factors represent a tree's ability to produce stemflow, which ultimately comes down to the volume of water produced. T1 mostly covered its full range with its interquartile range (Figure 23), with no obvious skew and the only outlier coming from S7. This storm also produced a high interquartile skew for T4 & T5. Indicating again that as the peak storm volume (%) increases, it causes a reduction in FR and $SF_{\%}$ (Cayvela *et al.,* 2018), which further translates to an overall reduced volume of stemflow. On the other end, T2 has an outlier above its range producing 200ml more stemflow with just over half of the total storm depth. However, there were reasonable storms the three days prior (2.8mm 61h prior; 8.5mm 34h prior), so there is the potential, because of the long water retention of oak bark and the corticolous lichen, that remnants of previous storms have inflated S1 stemflow volume.

The two trees that stand out are T3 & T6 (Figure 23), which failed to produce more than 400ml of stemflow within the range of the studied conditions despite being a similar height and age to T4 & T5. One theory is that the vascular epiphyte is siphoning the stemflow away from the main trunk and, therefore, the stemflow collar. It achieves this by providing a gravitationally favourable mode of transport with a smoother bark surface. Since the epiphyte wraps around the full trunk, it likely siphons off a large portion of the stemflow (Chen *et al*., 2019) . In the case of T6, an argument of size and situation can be made as it is the smallest and most sheltered tree within the studied six. However, it could also strengthen the argument of the epiphytic influence as it was by far the most densely covered tree in site 2 (Pypker *et al.,* 2006). This epiphytic argument is not strong enough to cover a small difference in size and coverage between T5 & T6. Still, it explains the average 400ml difference between the two trees, so the sensitive difference in the situation makes up this difference or the cause of the difference remains unknown within the dataset.

The following category where stemflow volumes struggle to break 200ml could represent two influences, peak storm volume (%) and early onset of this for S8 and an extended dry period where values cannot match. Whereas for S10, the strongest argument is the one similar to S2, where the storm's size cannot overcome the length of the prior dry period, reducing the overall quantity of stemflow produced. The influence that these storms share is a predisposition to have a strong

hygroscopicity argument as S10 had the lowest consistent relative humidities and lowest value recorded during one of our ten studied storms, while S8 was the only afternoon onset storm, which means it might have been met with far dryer bark than if it had arrived twelve hours earlier.

The difference between the response to the storms in T1, T2, T4, and T5 to the lesser producing T3 & T6 shows a logarithmic relationship in the larger sub-section and an exponential in the smaller sub-section. The difference between these seems to indicate an evolution of stemflow that will peak at some point in a tree's lifetime and revert to a reliance on storm characteristics over storm depth. stemflow in older oak trees, therefore, becomes a question of bark saturation as they will have the capturing capacity to produce more. However, their PFP will also be longer and require a deeper saturation. The current lack of papers on this topic could indicate that stemflow is rarely produced in suitable quantities for these trees or that because of the bark morphology, the stemflow is only travelling a short distance on the trunk, which would not reveal many ionic behaviours relating to the tree.

4.4 The behaviours of each ion within stemflow throughout the fieldwork period

Between mid-March and early June, the concentration of ions within the stemflow samples responds to varying climatic influences, such as wind speed and direction, rainfall duration and intensity and the prior dry period before the storm. As the ionic data is quantitative, it is compared with quantitative climatic data. The most prominent insight from the data is the difference between the sites, where site 2 on average produced 9.1% more volumetric stemflow , but was only denser in Nitrite (13% higher) and Phosphate (7.6% higher) within their ionic signatures. The remaining ten ions were between 17.2-53.8% (average 36.5%) higher at site 1, with the difference of age of the cumulative age of the three trees at either site being 35.1% higher at site 1, which indicates quite strongly that one of the main controls in stemflow's ionic signature is the size and therefore, scavenging capability of a tree. The following section will quantitatively explain the ions against the climatic variable where the strongest relationship exists. The deviations from this relationship are explained with analyses involving additional climatic components.

4.4.1 Sodium

Sodium and chloride largely appear attributable to sodium chloride, the most common sea salt which comprises up to 90% of salt compounds within seawater (Jeong *et al.,* 2017). Further sodium compounds are discussed within section 4.5. The behaviour of sodium as an individual appears to rely primarily on the dry period between storms in order to either be deposited on the bark surface (DD – see section 1.3) or suspended within the atmosphere (WD – see section 1.4). The prior dry

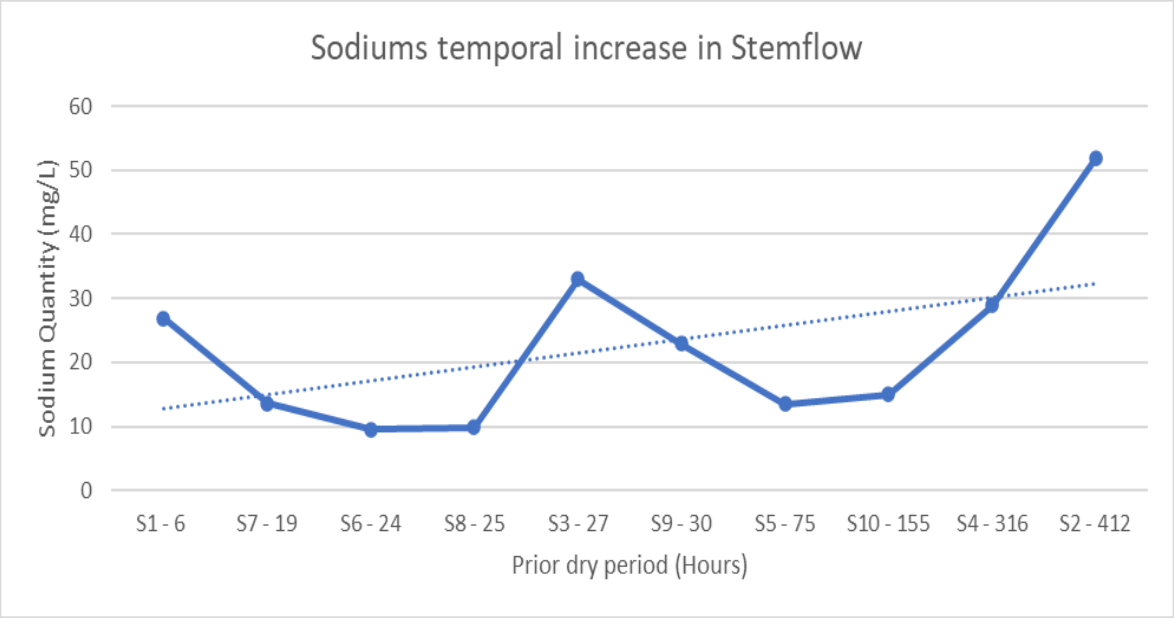

periods can be broken into three categories: up to and including 24 hours (Storms 1, 6, and 7), between 25-120 hours (Storms 3, 5, 8, and 9) and 120+ hours (Storms 2, 4, and 10).

There was an interesting correlation between the strength of the wind and the amount of ions, which could develop ideas put forth in Mohan (2016) and reveal a primary control over the quantities of ions.

RF gauge	Sodium in Rainfall	Wind speed
S7RF1	8.368	1.88
S5RF1	5.725	2.06
S5RF2	9.431	2.06
S9RF1	2.669	2.6
S9RF2	2.019	2.6
S8RF1	4.228	2.99
S8RF2	3.781	2.99
S6RF1	3.384	3.59
S1RF1	1.637	4.12
S1RF2	2.281	4.12
S3RF1	2.114	4.86
S3RF2	2.231	4.86

Table 11 (left): The relationship between sodium in rainfall (mg/L) and windspeed (m/s). S – Storm; RF rainfall gauge or site 1 or 2.

Figure 34 (above): The relationship between stemflow sodium and dry period prior to storm.

Within the <24 hours category, because of the short deposition and suspension window, the sodium values are low with S1 being larger than expected but also having a particularly large and long storm. There is some indication that a lesser wind allows the sodium ions to stay close to the coast, allowing for deposition onto our site and in/below-cloud scavenging above. This indicates that for these short prior dry periods, a wind speed averaging below 2m/s allows for the ion travel to mostly land or be suspended at our site around 1km from the coast. Within the dry periods between 25-120 hours, there was a sharp increase in the sodium for S3. This relationship could develop data found in Eaton *et al.* (1973). This relationship again indicates that in these shorter dry periods, high winds have the capability to deposit sodium more readily, while the lesser winds let sodium suspend within the atmosphere, to be removed by rainfall. However, one could also note that S3 could be the results of an incomplete washing of ions from S2 and its especially long prior dry period. Figure 1b shows the first three storms as the only ones above the linear increase does indicating some seasonal influence as it was shortly after S3 when the trees began to bloom (Chapter 3 – Figure 1).

For storm events with dry period of more than 72 hours there is a constant increase of Na concentration in stemflow throughout the three occurrences (Figure 35), which indicates that sodium concentrations will generally be higher where there are more prolonged prior dry periods. However the rate of this increase could be supported by the ratios of the incoming winds or could simply be a result of the dramatically longer timespan in which deposition can take place. The orientation of wind could also partially explain the quantities of sodium as northerly winds would theoretically transport less sodium because it would be an inland source. This is supported by figure 1b, which shows storm 10 (Figure 1b – 155) as sharply below the linear increase, with 30% of days being northerly, compared to 23% where Storm 4 (Figure 1b – 316) is fractionally below and 5% where Storm 2 (Figure 1b – 412) is considerably above. Furthermore, the total amount of wind,

which is the sum of the averages for each day during the dry periods, also supports storm 2 having the highest sodium. Therefore, a lower wind allows for sodium to become suspended and transported to our site close to the shoreline, with the wind directions and proportions of which in each dry period indicating how many days deposition could occur on. As sodium is coming partially from rainfall, storm length is a secondary factor after the length of dry period, which could be the reason why Storms 4 and 10 vary so much despite having similar dry periods and wind source proportions. This is substantiated by storms 1 and 3 (Figure 1b - 33 and 38) being above the trendline with 21 and 11 hours respectively for storm duration, while storm 5 (figure 1b - 75) being the furthest below the trend and with the shortest duration of 2 hours.

4.4.2 Chloride

Chloride behaves in a similar way to sodium, having peaks large quantities in earlier storms which indicates that these ions are travelling as part of the sodium chloride molecule, the most common salt compound in seawater (Jeong *et al*., 2017). This overall indicates that chloride, like sodium, is primarily dependent on wind for its quantity within stemflow. The differences between the two ions can be seen with a more pronounced S2 & S3 for chloride, which likely represents the lack of washing from the exceptionally long dry period discussed within sodium's section above and the difference in inter-quartile range for trees where T2 & T5 show lower inter-quartile ranges compared to high ones in sodium. This could partially explain the more pronounced values seen in S2 & S3 which if removed, drastically reduce this difference. The evidence that these ions have travelled as a compound is compelling down to the fact that the average quantities over all storms both come within 5% of their respective molar masses, which does still leave room for travel as singular or different compounds.

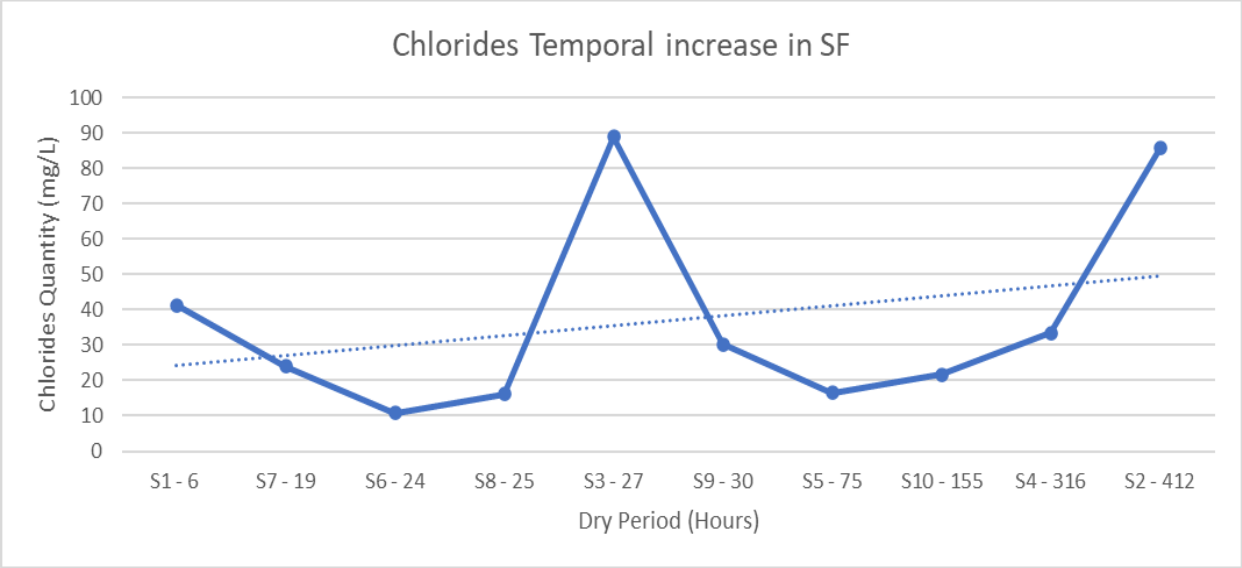

Figure 35: The similar relationship between the sum of chloride quantities and dry period before each storm.

The peak seen with S3 could be attributable to the high winds (Figure 1a), which would transport the lighter sodium further than the heavier chloride, because of chloride having 54% more mass per ion. However, this higher weight requires more energy to transport, therefore it is less likely to travel long distances for deposition. This higher energy requirement could also lend itself to the fluid argument as it will be more likely to be deposited before reaching a stemflow collection bucket. Therefore, the difference between sodium and chlorides 27 and 30 hour long dry period could be attributed to the shorter storm length in S2, which allows for the long dry period to only be partially washed.

4.4.3 Magnesium and Sulphate

Magnesium and Sulphate responds to dry period prior to storm in a similar way to chloride and sodium, with the large spike at 27 hours on the x-axis, followed by a trough at 30 hours (Figure 37). This drop equalled a 7.6x drop for sulphate and a 3.4x drop for magnesium. With magnesium's molecular weight being slightly above sodium and a response only slightly greater further substantiates the control of wind within the deposition process, specifically regarding sea salts. The molar mass of 96.06g/mol for sulphate does not support the same wind speed hypothesis presented within sodium therefore the more likely cause is the smaller portion sulphate makes up of sea salt.

The elevated levels of sulphur dioxide in the atmosphere ahead of storm 5 alongside elevated levels of sulphate within the rainfall (2nd and 3rd highest values) indicates that sulphur had simply not been deposited and was still airborne. This could be the result of the fairly low winds, combined with the higher molar mass allowing sulphur to stay airborne for longer. However, the unnatural projection into the atmosphere by polluting omissions could be giving the sulphate different travel characteristics (Reynolds *et al*., 2004).

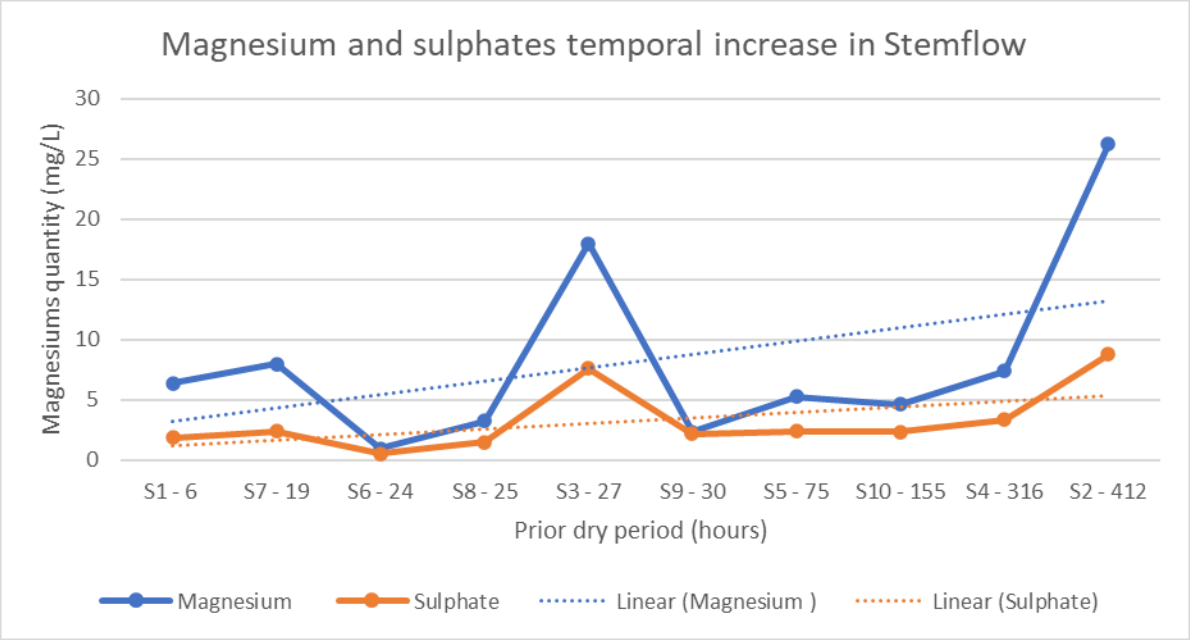

Figure 36: The relationship between magnesium and sulphates quantity in stemflow and the length of the dry period leading up to the storm.

This theory between the ions molar mass and wind speed is partially supported by S3T2 having the highest value seen within sulphate, which could be attributable to the trees larger size therefore catchment ability of airborne particulates. There is an apparent decrease in the total sulphate contents when the trees begin to bloom, showing sulphates role in forming amino acids and proteins (Stewart, 2010). This theory is supported by results in Xu *et al*., (1996), who found statistically significant relationships between sulphate levels and rates of photosynthesis, which is substantiated further as sulphur is known to be involved in the creation of chlorophyll.

The consistency throughout the four predominant sea salt ions (Sodium, Chloride, Magnesium, and Sulphate) shows that high winds result in a higher deposition rate for each of these ions. This is

shown in the sharp decrease between the dry period of 27 and 30 hours. In the three instances of longer dry periods (155, 316, and 412 hours), a consistent increase indicates that once a threshold is met, the duration of potential deposition is the primary variable. The most notable difference between the 2 compounds (NaCl and MgSO42-) is the difference in S7 where NaCl is beneath the linear increase, while MgSO42- is above. Being a day after a 20mm storm, the lack of washing as an argument is void, however the starkly different wind angles could have activated flow paths that had been unused in some time as this was the first SE storm in over 2 months so the deposition window for that orientation was significant.

4.4.4 Potassium

Potassium was a unique salt, likely only part of the compound potassium chloride, which indicated a lot of singular travel especially in later storms. Potassium tends to have a negative quantitative relationship to climatic variables, the highest being to storm intensity. Ultimately, this indicates that potassium exists already on the plant, highlighting the role it has within photosynthesis and the influence of inter-plant potassium exchange. The negative relationship potassium has with storm intensity partially supports results found within Levia *et al*., (2020) that showed a logarithmic relationship between duration submerged and leaching quantities. It appears that between a storm intensity of 0.482-0.7mm/H one can expect a higher-than-expected quantity of potassium within stemflow .

4.4.5 Calcium

Calcium was different when compared to the other salts as it had full storm or site values where the rainfall concentrations were higher than the corresponding stemflow values and over a third of the total values in stemflow were less than in rainfall, hinting a large amount of WD. As the storms following the storms where rainfall values exceeded stemflow values did not have this phenomenon, this could indicate that calcium's deposition is particularly large within specific storms and is washed for the next few preceding storms, however, any climatic reasoning for this was not obvious. Like other salt ions, the highest correlations between the observed concentrations and the known storm characteristics were with the length of the dry period prior to the storm, as this metric provides a

greater deposition window. Following on from the length of prior dry period, the length and average hourly intensity of the storm is then the main control on calcium's concentration. This was observed as the storms with the highest intensities favoured less calcium than lower hourly intensities, excluding instances where the prior dry period is especially long. Similarly, shorter storms generally had lesser calcium concentrations, with the prevailing theory being calcium is deposited further down in the tree's architecture in these lesser storms which causes lower stemflow values below these storm length and intensity thresholds.

4.4.6 Bromide

Bromide needs a dry period of over one day in order for stemflow values to be greater than rainfall values. This inverse relationship to dry period differentiates bromide from the common argument made for the major salt ions, indicating that DD of this ion occurs substantially after 24 hours. This is substantiated by bromides stemflow quantities relationship to average hourly rainfall intensity providing greater concentrations of bromide in lower rather than higher rainfall intensities, which again indicates that it is being primarily washed out of the atmosphere during WD. The indication of washing from the atmosphere during WD strengthens the theory that bromide largely travels as an individual ion (see section 4.5) as its potential pairings with sodium and magnesium do not show a similar behaviour, both having a weak relationship to rainfall intensity. Bromides absence from S1 could indicate a strong washing effect in the days prior, which consequently to bromides relatively low quantity within sea salinity, did not have the chance to then populate in any significant number. However, attributable to its presence in the rainwater, it is also possible that this is attributable to an error in processing by the ion chromatograph. The retention of bromide by the trees appears to be triggered by extended dry periods and released by prolong periods within regular rainfall, however more study should be done to confirm this or identify if it is coincidental. However this trend is present in other ions and could indicate a response by the tree to the extended droughts.

Figure 37: The apparent retention of ions after the prolonged droughts prior to S2 & S4.

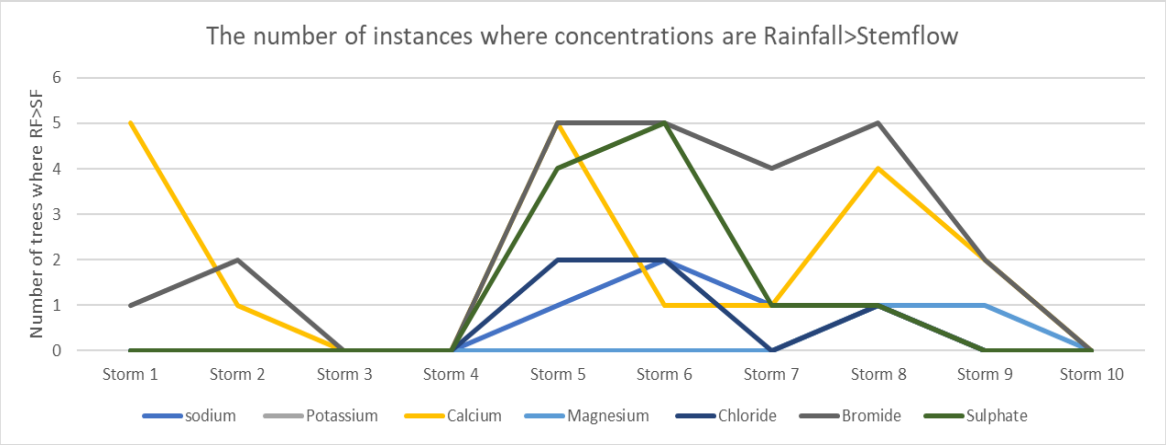

4.4.7 Fluoride

Fluoride had a strong relationship (R^2 = 0.63) with prior dry period, which indicates similar to other salt ions that are taken from the sea and deposited, that the fluoride ions increase with a larger window of deposition. There was a secondary control of the storm length, however this was not as clear because of starkly different values within equal storm lengths. These values did hint at a level of dilution as higher total rainfalls often equalled a lower concentration of fluoride. This is supported within the noticeable jump in fluoride values between 6 to 9mm, which then drops off, likely because of the aforementioned dilution.

4.4.8 The nitrogen compounds

The nitrogen compounds are undeniably linked to each other through the nitrogen cycle. Nitrate is linked to nitrite through the nitrate reduction process, while the opposite of this process is called nitrification (Sparacino-Watkins *et al*., 2013). Ammonia is linked to nitrite and nitrate via nitrate/nitrite ammonification. The order of this process is Nitrate -> Nitrite -> Ammonia, which explains why there is often low amounts of nitrite in most storms, with higher dry periods allowing nitrite to reach the collection buckets, which would prevent ammonification that can only occur below the euphotic zone in water. The budget for these nitrites comes from the nitrates, which have a clear relationship to prior dry period as all values from under 36 hours are negative, meaning rainfall values were greater than stemflow , while all values above 36 hours are positive. This corresponds with nitrites absence between 24-48 hours in prior dry period. The results from stemflow movement show that stemflow moves faster on saturated bark, which would indicate that there is a longer timeframe in which nitrite could undergo ammonification to form ammonia, however this does also indicate that the duration for bark to return to its unsaturated state is between 48-72 hours. Outside of prior dry period, nitrite and ammonium both have their strongest relationships being a negative one to average hourly storm intensity, which again highlights the order of the nitrogen cycle as the higher intensities would wash away the ions before it can undergo the next stage of the process.

4.4.9 Phosphate

Phosphate showed negative relationships with all the variables apart from the prior dry period, which again indicates that an extended deposition period allows for more phosphate to potentially be deposited. The strongest relationship was with total storm rainfall, which would support the theory of phosphate originating from fertilizers and also the release from foliage as stated in Neal *et al.* (2003).

4.5 Ionic composition of rainfall

4.5.1 The major salt ions

The quantities of ions in the rainfall showed a consistent pattern within Na^{+}, Cl^{-}, Mg^{+}, SO_4^{2}-. K^{+}, and Br^{-}. All of these ions being salt ions indicates that the ratio at which different salt ions are suspended from Swansea Bay are consistent with the ratios of the salt ions that make up its salinity. The storms showed their peak values in S2, S5, and S7 (Figure 27), which were also the three smallest storms. The concentrations of ions within the rainwater were not drastically different despite the stark difference in the prior dry period, which could indicate that the amount of ions suspended in the atmosphere does not gradually increase over time, with DD keeping this at a somewhat consistent level, supporting discussion points made between prior dry period and stemflow s ionic quantities. The four largest storms (S1, S3, S4, and S6) were also visibly lower (figure 27) which supports the earlier argument and indicates that dilution does impact this.

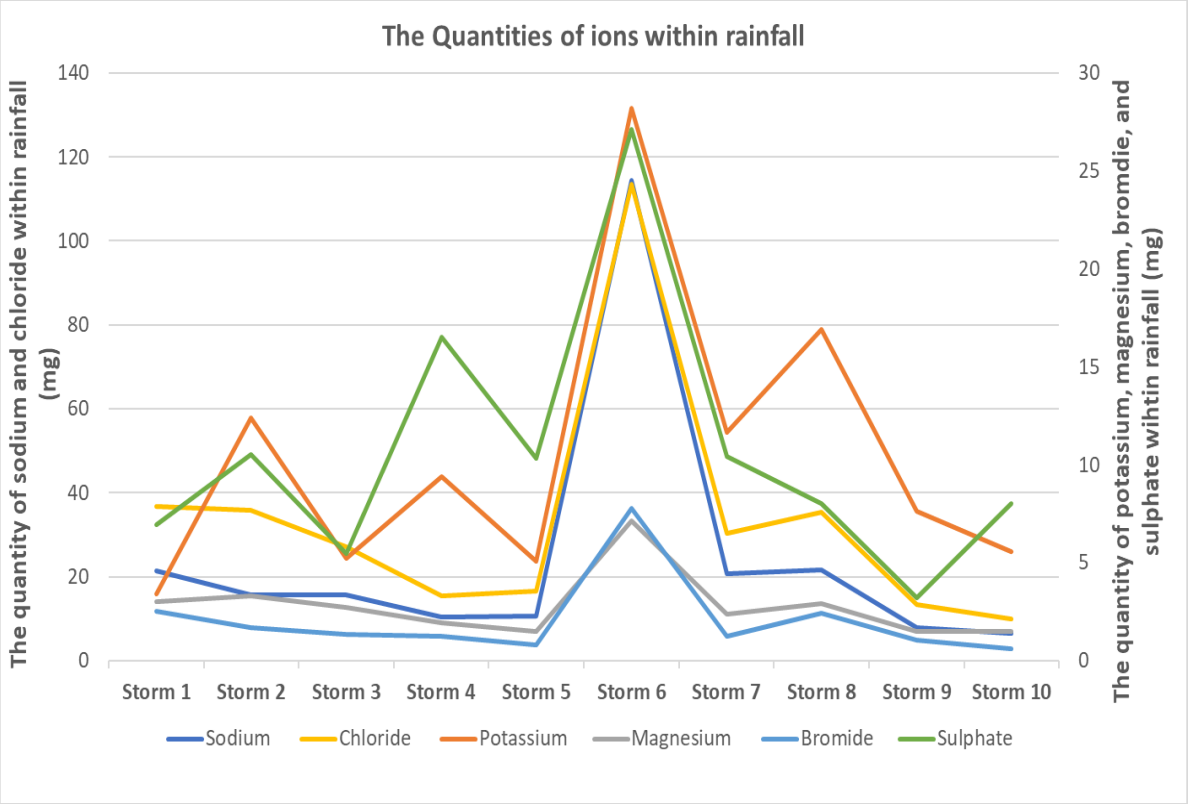

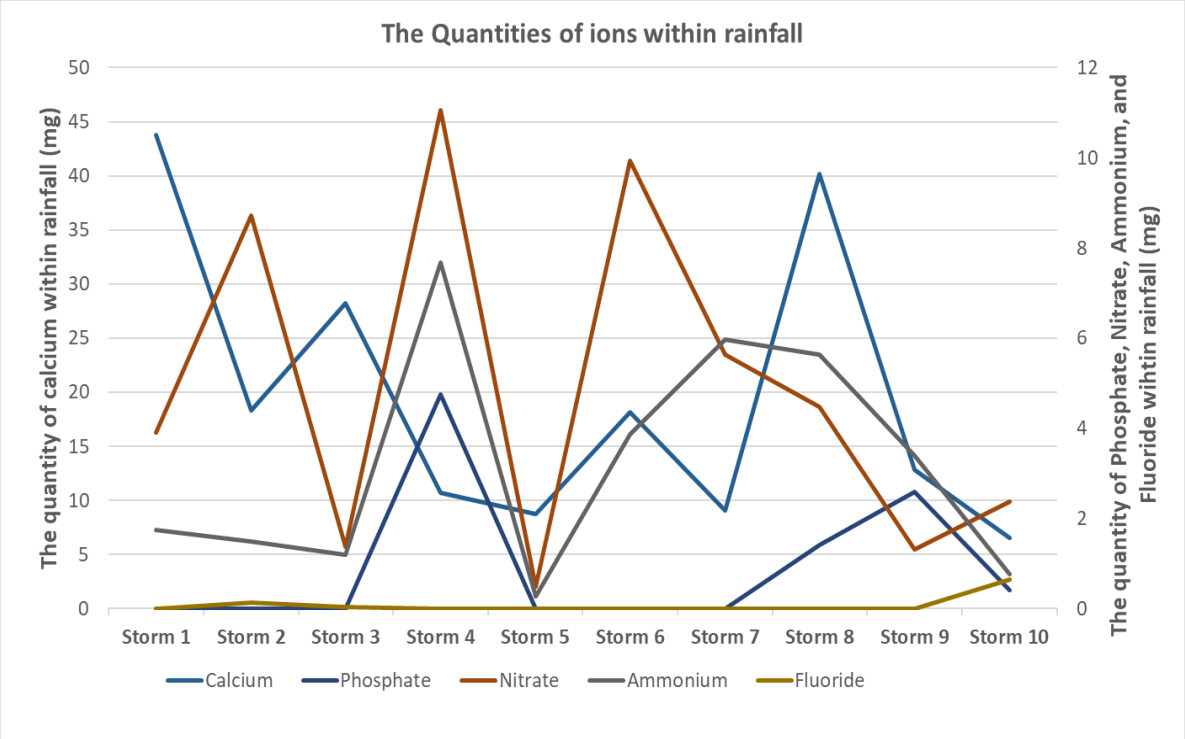

Figure 38a&b: The overall quantities of ions (mg) within rainfall with the same separation as figures 27 & 28.

What figure 34 highlights is that while the concentrations (mg/L) are lower within larger storms, the overall quantity of ions being delivered are higher. This does not necessarily negate the prior point about a stable level of ions, as higher storms may instead offer a more thorough washing of the atmosphere, which could then affect later storms (S7), as the quantity within the atmosphere would have not recovered. This effect of dilution indicates that there is a base level of ions most storms will have, and that the increase of ions within a storm, related against the storm volume is a logarithmic relationship, that is partially controlled, like stemflow volume and ions, by climatic conditions in the days and weeks prior to the storm. There was a consistent decrease in the concentration of ions within rainfall through S8-10, with sulphate breaking this trend in S10 for both concentration and overall quantity, with a similar difference of behaviour within S4. For the five other ions, this could be a result of the full bloom of the leaves retaining more ions that they catch, or that for the ions that they do catch, more are being lost to throughfall as the leaves become more hydrophobic over the course of their life (Klamerus-Iwan and Witek, 2018). In the case of sulphate, this could indicate that there were elevated levels of sulphur in the atmosphere from a polluting source, which could also partially explain the lower correlation values between the 2 constituent ions (discussed in section 4.5).

4.5.2 The minor ions

For the other five ions that were recorded within rainfall (Ca, PO43-, NO3-, NH4+, and F-), ammonium and nitrate appear to have a similar behaviour with peaks in S2, S4, and S7 and lows in S1 , S3, S5, and S6. What is interesting is the difference in response to S10. This shows that the Dissimilatory nitrate reduction to ammonium process was reduced prior to this storm, so the store of nitrogen as nitrate persisted, contrary to the main hypothesis that dissimilatory nitrate reduction to ammonium increases during summer (Marchant *et al*., 2014). This could indicate that the hot and dry conditions had damaged the populations of microbes that perform dissimilatory nitrate reduction to ammonium, showing one of the many effects of climate change within this study. Calcium was one of the more interesting ions within rainfall, having stark 6x differences between the two sites for three storms (S3, S8, S9), which indicates there is a significant source for this calcium that is available for site 1, but blocked from site 2. This could be from exposed rock that is being weathered and suspended or local soil erosion that makes up the difference between site 1 & 2 on top of the sea salt aerosols that will undoubtedly be present within the quantities. Phosphate and Fluoride do not appear to have a strong influence within the rainfall quantities, only appearing in a minority of storms.

4.6 The potential travel of compounds

4.6.1 The salt ions

The ratios of salt originating ions (Fluoride, Chloride, Bromide, Sulphate, Sodium, Potassium, Calcium, and Magnesium) and the correlations between their quantities gives an indication of the compounds present before dissolving within the stemflow samples, while the nitrogen compounds (Nitrite, Nitrate, and ammonium) give indications of oxidation levels present on the bark surface. Phosphate is the outlier, not falling into either of these categories, but being required by photosynthesis as one of the building blocks of DNA. Certain ions, such as fluoride, potassium and sulphate have predominant unidimensional reasons for their quantities in terms of how they could be deposited. There are other possibilities for their quantities, as shown in table X but the explanations in Figure 1a are the overwhelming reason. For each storm, the unidimensional ions will be calculated first, with their known molecular ratios calculated through the molar mass of the

compound and the individual atoms. This reveals if the ion has travelled as part of a compound or as an individual through DD or WD. For the more common ions, exceptional correlations (0.95+) indicate deposition as that compound. The remaining salt of Calcium could originate in the form of fluorspar, Gypsum or as Calcium Ammonium Nitrate, which is used as a fertilizer. The calcium within the rainfall is most likely part of calcium carbonate.

Ions	Fluoride	Sulphate	Potassium
Most likely source	As part of Sodium Fluoride (NaF - 54.75:45.25), which is used to flourinate water to prevent dental problems	As part of Magnesium Sulphate (MgSO4 - 20.19:79.81), otherwise known as Epsom salt, which is the second most prevelent in the sea	Potassium is likely deposited as part of Potassium Chloride (KCL - 52.43:47.57)

Table 32: The reasons for the quantities of the following three ions and the ratios of their weight in their 1:1 compound pairing based on their molar masses

The correlations between the salt ions shows that deposition of sodium chloride, the most common sea salt, is consistently high, resulting in chloride being the highest reading in 38/58 of the samples, with sodium representing another seven. Potassium started to overtake in the latter storms, substantiating its role within photosynthesis, as this overtake started after storm 5, whereas blooming commenced around storm 4.

Salt Compound	Storm 1	Storm 2	Storm 3	Storm 4	Storm 5	Storm 6	Storm 7	Storm 8	Storm 9	Storm 10
Sodium Chloride	0.998	0.990	0.985	0.990	0.917	0.965	0.995	0.975	0.997	0.987
Magnesium Sulphate	0.993	0.942	0.994	0.687	0.852	0.077	0.636	0.897	0.269	0.777
Magnesium Chloride	0.988	0.958	0.992	0.583	0.644	0.952	0.643	0.893	0.948	0.953
Potasssium Chloride	0.970	0.909	0.994	0.898	0.594	0.408	0.113	0.675	0.604	0.967
Magnesium Bromide		0.906	0.952	0.307	0.960	0.967	0.510	0.918	0.979	0.408
Sodium Bromide		0.864	0.897	0.738	0.552	0.977	0.392	0.932	0.958	0.494
Calcium Chloride	0.991	0.723	0.906	-0.104	0.572	0.141	0.348	0.980	0.631	0.786
Calcium Sulphate	0.995	0.871	0.916	0.109	0.924	-0.694	0.789	0.854	0.282	0.746

Table 13: The correlations between each of the constituents within a salt compound. The areas blacked out are attributable to bromide only being detectable inT3 within S1.

The consistently high correlation between sodium and chloride, with the lowest being a 0.909 in S5 shows that most sodium and chloride are occurring as dissolved sodium chloride (common salt). The second most common salt, Magnesium Sulphate, otherwise known as Epsom salt, appears to be the main mode of compound transport for both magnesium and sulphate in S1, S2, S3, S5, and S8. The dips in correlations could support the argument of atmospheric sulphur pollution within S4 and S10, while persisting dilution could partially explain S6, S7, and S9. However, one must consider magnesium's role in greening chlorophylls (Hasaneh *et al.,* 2020) and sulphurs in the production of amino acids (Brown, 1982), which would alter quantities reaching the stemflow collar and being counted within the overall concentrations. This could explain why the correlations appear to decrease throughout the fieldwork period. However a further explanation could be the high correlations in Magnesium Chloride that coincide with low correlations within Magnesium Sulphate, where a similar argument can be made for magnesium bromide, however the high correlations are likely coincidental as only a fraction of magnesium could have ever travelled as part of the magnesium bromide compound in any storm because of the far lower bromide quantities, similar to sodium bromide. Calcium likely has a near equal proportion of sea salt and terrestrial inputs through calcium chloride, and calcium sulphate, otherwise known as gypsum, where the argument for a heavier gypsum input is through the stronger correlations in S1-7, where calcium chloride increases through the final three storms. This could be a result of the dry conditions earlier in the fieldwork period allowing for greater suspension of terrestrial minerals to then be incorporated within stemflow .

The ion of fluoride either travels as an individual; as part of the sodium fluoride, as pairings with the other anions are rare or don't occur naturally. Within fluoride, with its pairing of sodium, there was no occurrence where the quantity of sodium cannot handle its 1:1 pairing with fluoride, so one cannot state whether fluoride has travelled in a compound or an individual because both are equally possible within the data.

4.6.2 The nitrogen compounds

The nitrogen compounds of Nitrate, Nitrite, and ammonium form different stages of the wider nitrogen cycle, therefore, indicate levels of this biotic activity during this study. Nitrite was only detectable in 5 storms (Storms 2, 4, 5, 7, and 10) and 16/58 of the stemflow samples. This could simply mean most nitrite present at those times has been oxidised to form nitrate. This can be

shown as Nitrite is only present without nitrate on one occasion, whereas nitrate is present without nitrite on 35, showing that oxidation promptly occurs on the studied trees.

The rate of these reactions is shown forth most in storm 2 where an elevated rainfall ammonium content corresponds with the highest nitrate contents for both trees 2 and 3, while the second highest rainfall ammonium corresponded with the highest nitrite content within trees 1 and 2, with storm 4 site 2 high ammonium levels corresponding with high nitrite and nitrate figures. This indicates some level of nitrate reductase within storm 4 as nitrite was greater than nitrite during storm 4 site 1. Because of nitrites predominant absence from rainfall, one can assume that atmospheric nitrite will readily react to form nitrate because of the abundance of oxygen, therefore nitrite values simply represent values that have not yet reacted. As nitrate reductase is mostly common in crop plants while nitrification is common within *Comammox, Nitrobacter, Nitrospira, and Nitrosomonas* bacteria.

4.6.3. Phosphate

Phosphate presence in the stemflow is considered to be because of fertilisers, as it is not a marine salt or nitrogen compound, but instead forms in integral part of the DNA helix found in living matter on Earth. This means that a strong proportion of the phosphate could be released upon rainfall impact (Neal *et al*., 2003). The phosphorus cycle does not include the atmosphere, instead it consists of a slow-moving erosion and geologic uplift of phosphate minerals (Filippelli, 2008). Within the Clyne Valley field site, the most likely natural sources are the deposits of Wavellite found on the Gower peninsula, with a less likely source being pyromorphite, which is common within Carmarthenshire. However, this would likely result in some correlation to fluoride, which is most likely within storm 6, so the more likely explanation for phosphates values, and a reason it appears within rainfall would be pollution from fertilizers containing phosphorus from nearby farms and greenhouses. This is substantiated by ammonium phosphate (a common fertilizer) having the 4th highest average correlation throughout the 10 storms.

4.7 The hygroscopicity of oak bark

4.7.1 Absorption of water

Bark is the part of the tree that directly interacts with the outside environment, with 10-30% of the total water holding potential being occupied by barks hygroscopic abilities (Ilek *et al.,* 2016). The results from this study show that dry bark was able to absorb moisture up to 18% of its own weight at 80% relative humidity, with potential 100% stable weight between 22.95-31.61% higher. The implications for this at thestudy sites, which has consistently high humidity's, is that the bark is likely saturated to near 100% of its hygroscopic abilities, losing some of this each day alongside the average daily relative humidity drop. Furthermore, this indicates that storms taking place in the morning or night have less of the total bark water storage capacity to fill, and the total rainfall threshold for generating stemflow is smaller. This could partially explain the low stemflow levels seen within S8, as discussed in section 4.2. With regards to the studied storms, a variation in relative humidity was only observed in Storms 2, 7, 8, 9, and 10. Storms 2, 7, 8, and 9 were towards the ends of single day drops in humidity lasting around 12 hours or under. Storm 10 is an anomaly, being one of 2 northerly storms, and for likely encountering and having to overcome the lowest bark moisture content attributable to a 41 drop in relative humidity, where it remained under 70% and got as low as 37.6%. Because of this there is the potential for more of the influences of hygroscopicity within this storm.

The passive intake or removal of moisture occurred until the bark reached a stable weight that increased with increasing relative humidity, which were seen at every relative humidity. Therefore one can state that bark will seek to equilibrise with the surrounding atmosphere and that the time taken to equilibrise is longer with higher relative humidity's and intuitively with larger deviations in relative humidity. With the timescales that were observed, it is unlikely that bark fully equilibrises with the surrounding atmosphere. The increasing timeframes to stabilisation were linear and similar to results documented by Ilek *et al*. (2021). Saturation of the bark appears to inhibit its hygroscopic abilities, with the less porous bark having greater variations in mass, these findings are consistent with the current literature (Ilek *et al.,* 2016), however, results show that their assumption that bark hygroscopicity does not vary vertically was not consistent with our findings. More research should be undertaken to decide which theory holds true throughout different tree species of bark.

Results from this study differ from academic literature (Oberhuber *et al*., 2020) regarding porosity and moisture intake. The results clearly show that the higher circumference classifications absorb a lesser percentage of their original weight when the relative humidity was increased. These samples were more fractured with furrows so have a higher surface area, however the unfractured lower circumferences, absorbed 1.36-3.69x more water relative to their starting weights. A possible explanation for this is that there could be a higher Hydroxyl to Cellulose ratio in unbroken oak bark

compared to the furrowed surface area (Hill *et al.,* 2009). However, with Scots Pine trees, the outer layer of bark was found to be very hygroscopic (Oberhuber *et al*., 2020), so one could assume that oak bark has similar properties. Furthermore, the reaction to relative humidity increases was uniformly sharper as the humidity's increased, with the reaction being 1.98x when comparing 60-70% and 70-80%.

4.7.2 Desorption of water

The desorption of water found within oak bark was found to have quite a high spatial sensitivity as two adjoining 15.6g bark samples could have a 0.39ml+ discrepancy in moisture content. This indicates that while the responsive behaviour to atmospheric moisture is consistent, the starting point of the bark is not. This is intuitive because of the complicated structure of trees, meaning different surface areas of the bark are receiving varied amounts of energy at any one point, combined to their sheltered status from any orientation of rainfall. This indicates that stemflow could have idiosyncratic conditions for each storm, which would make its volumetric and ionic fluctuations inherently random if one attempts to combine the myriad of variables on a small spatial scale. Therefore, an understanding on a full-tree scale is more appropriate, in which the discrepancies are averaged out.

Where the results shown in section 3.6.2 demonstrated a discrepancy, higher moss covers showed higher moisture losses, this was similarly the circumference where furrows appeared, therefore this sudden increase in surface area would likely be the reason for this trend reversal. Therefore, the hygroscopicity of bark likely effects storms in Clyne woods later in each day, however in locations where a less regular fluctuation exists, the hygroscopicity of bark could play a more dynamic role in stemflow production. The role that this plays within the ionic fluctuations is likely more significant within the sea-salts over terrestrially sourced ions.

4.8 The movement of water on the bark's surface

4.8.1 Stemflow movement on the bark's surface

The results obtained from experiment 2.3.3 suggest that stemflow movement was higher (faster) on the bark surface than within the fibrous interior. Within bark, the movement was uneventful, showing little indication of any significant gravitational pull. The bark appeared to dry at similar rates depending on the initial moisture content at different angles, indicating that any loss in mass was attributable to the surrounding atmosphere or the barks own hygroscopicity. The statistical analysis showed an insignificant difference in each 5min time category or the bark angle, which strongly indicates that stemflow is a bark-surface process, with interior bark water fluctuating the generational threshold of stemflow .

Interior bark water movement		
Statistical result	Time caetgory	Bark angle
p value	0.45	0.1617
H statistic	18	5.14
N2	NaN	0.0091

Table 14: The statistical results of the interior bark water movement experiment.

Therefore, an in-depth look at stemflow on the bark surface was undertaken during experiment 2.3.3, which revealed behavioural dynamics one has classified as flow path generators, flow path followers, and obstacle blockers. The architecture of these PFP changes depends on the rainfall's inclination. However, it can be thought of as streams transferring energy (and ions) from higher in the canopy, either to be deposited further down the tree's architecture or within the soil matrix. Stemflow was observed to follow the path set by previous drops overwhelmingly. These observations are consistent with previous work (Crockford *et al.* 1996), which indicates that the specific spatiality of the PFP, itself dependent on rainfall inclination throughout the storm, will leave a large part of the bark's surface area predominantly un-leached and therefore, unrepresented within stemflow's ionic composition. However, this largely applies to the underside of bark (Herwitz, 1987), with the upper side becoming somewhat uniformly saturated over a storm if within the storm's rain shadow. This surface saturation revealed different dynamics when there was a less obvious PFP, affecting splash and overall speed differences. This change in surface stemflow dynamics in turn affects impacts stemflow's ionic composition because of the time-dependent relationship with its physical contact with the bark and evapotranspiration rates. Furthermore, it suggests that the mixing rate between PFP and blocker droplets may be indications of the eventual ionic composition and how molecules of subsequent droplets behaved as they flowed along the PFP.

4.8.2 Preferential flow path generation

The results of the experiment where single water drops were deposited on the bark to measure the speed of movement and path of travel show that the first drops arriving on the bark determine the orientation of the preferential flow path PFP; they come into contact with dry bark and leave a trail of water behind them for subsequent droplets to follow, showing a level of hydrophilicity for oak bark. The initial droplet or droplets will follow the most gravitationally favourable path from the point of contact to the end. As fluid trails behind them, one can state that they are losing mass throughout their flow, limiting the length one droplet can potentially travel. The direction of travel is determined by the bark micro-relief structure and sensitive discrepancies in the hydrophobicity of the bark surface but will guide the droplet down the most gravitationally favourable path. The micro-relief characteristics that commonly differentiate stemflow movement are the furrows. The small differences in hydrophobicity could cause small and sharp movements where the surface of the bark where the gravitational influence was weaker. If one postulates droplets entering any given bark area outside a furrow, it will not enter the furrow because of the slight upcurve. This micro-relief structure gravitationally prevents it unless the incoming droplet velocity holds enough kinetic energy to enter the furrow, but not enough to fully dislodge itself from the bark surface. The furrow curves were observed to guide stemflow parallel and perpendicular, dependent on where the highest potential energy was guided concerning the branch's overall curve. The slight moisture discrepancies refer to deviations on the mm^2 scale attributable to slight deviations in the evapotranspiration losses compared to the water intake.

The observation of water movement on bark suggests that stemflow is most likely to enter a furrow inhabited by epiphytes; this travel is firstly absorption, then once the epiphytes water holding capabilities are close to maximum, there is a quick saturation along the arms of the moss. The same arms can stop a droplet and slowly absorb it using its gametophytes from inside a furrow. Travelling within non-epiphyte furrows was more complicated attributable to the more intricate structure; this caused numerous instances where a droplet could be held until dislodged by a subsequent droplet (See section 4.1.2). This dislodging commonly happened so the droplet would exit the furrow as the plentiful micro-ridges within the furrow often provided a platform. Furthermore, the slight curve that prevented entering, often promoted droplets leaving furrows. This preference for ridge travel disagrees with the little literature on stemflow movement, as Levia *et al*. (2020) assumed that stemflow travels through interconnecting furrows. However, the difficulty of individual droplets entering, alongside the ease of exiting furrows without epiphytes, demonstrates that travel

predominantly occurs on unbroken bark. Therefore, the bark will likely absorb stemflow entering a furrow, allow the droplet(s) to succumb to evapotranspiration forces, or dislodge the droplet, producing throughfall. This behaviour substantiates intuitive knowledge of stemflow in the porous versus smooth antithesis (Levia and Frost, 2003). Trees with smooth bark have higher FR with smaller thresholds for stemflow generation because of the lack of furrowed stemflow disturbance.

4.8.3 Blocking and separating Droplets

Academic literature has established that smoother bark produces a greater FR (Van Stan *et al*., 2016), as fewer obstacles could cause stemflow to be absorbed or transpired on its journey. One reason for this is "blocking droplets", which are stemflow droplets that follow a PFP that block a pathway obstacle on the bark surface. This blocking droplet is partially mixed by subsequent drops, leaving enough to continue to block said obstacle. This observation is one of the contributing factors to the statistically significant difference found between angles for dry bark and not for moist bark. This is likely because for dry bark, every droplet that progresses a PFP is in some way a “blocking droplet” to the complicated topography found on oak bark. The only angles that were not statistically significant in the bark was the 45° to 60° difference, which is interesting as this is the barrier between being more horizontally and vertically inclined, which likely indicates some sensitive behavioural dynamics in this spatial barrier. The differentiation between Wenzel and Carrie-Baxter (sometimes called Fakir) state droplet flows reveal which obstacles are significant enough to warrant blocking (Mohammadrezaei *et al*., 2022), and which droplets require part of the droplet to remain, somewhat increasing the quantitative cost of PFP generation.

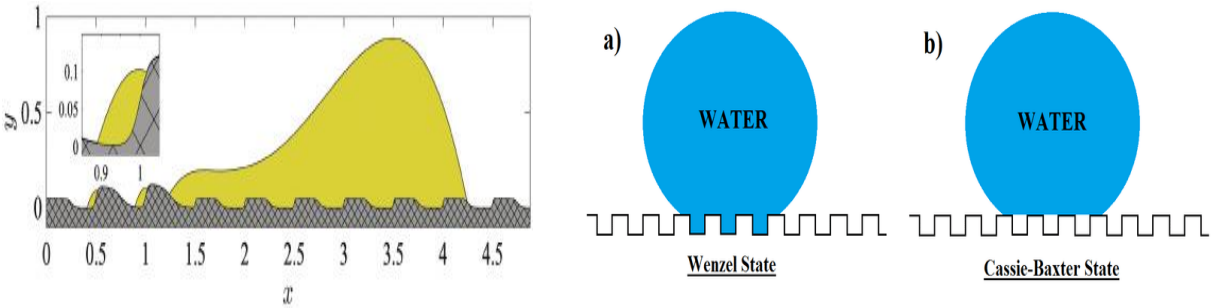

Figure 40a&b: A diagram showing the difference between Wenzel and Carrie-Baxter droplets (right), with an illustration example of a "blocking droplet" (left).Reference

Intuitively, the mass of these blocking droplets corresponds to the size of the obstacle, concerning the obstacle's interference relative to the strength of existing the gravitational pull on the PFP. Furthermore, blocker droplets can become dislodged independently through decelerated stemflow additions from the PFP. However, if these obstacles exist outside the main trunk or the upper side of branches, the drop will likely become throughfall. The role obstructions play in producing throughfall from stemflow are known as drip points (Crockford and Richardson, 2000); therefore, blocker droplets are more likely towards the topside of branches before stemflow can travel to its preferred underside. On branch undersides, attributable to the increased potential energy of the droplet, obstacles likely need a chokepoint to allow stemflow to continue (drip points briefly discussed in the introduction).

Independent drips were seen when drops occurred that were visually unrelated to any administered drop and without the visible bulge of the droplet travelling along the PFP. These drops are possibly attributable to slower flows experienced by the remnant PFP trail, which has the potential to overcome an obstacle if the trail behind is significant enough to provide the necessary excess stemflow to overcome the obstacle. Depending on the storm's intensity and the saturation of the PFP, blocker droplets could represent hotspots of ion exchange attributable to the potentially long and stable contact with the bark surface. Therefore, while representing a reason for lower FR in oak bark, they similarly demonstrate why oaks have higher stemflow ionic densities. Furthermore, while contact with only one side is predominant, contact with both sides is possible in certain circumstances, increasing ionic compositions. This double-sided contact is also a possible reason why drops occasionally separate while on a PFP; however, this occurs mostly at lower angles. The 2-side contact could also instead be a PFP chokepoint, where a gap is big enough to allow water through very slow velocities. However, if another drop arrives before this can complete, it will cause the choked droplet to act as a blocking droplet. At higher angles, another possibility is the higher travel velocity (Bao and Kang, 2021); the droplet has a higher chance of becoming dislodged, where it falls freely; with each repeat of this, the chances of droplet separation grow upon recontact.

4.8.4 Preferential flow path followers

Once the PFP is formed, attributable to the preferential adhesion, droplets will follow this flow path without much deviation if the remainder of the bark remains dry. If enough time lapses between droplets, there is the chance that the path will have flowed away, meaning a second droplet will

have to recreate the PFP, the second time likely being the same as the first. There is no instance where following a PFP causes significant droplet deceleration, with acceleration, measured by dividing the time taken from start to finish ranging from 1.15x to 4007.9x from the first to the fifth droplet. However, there were instances where a droplet would move faster at a lower angle, with these droplets being outliers (3SD) within their chosen categories. This could indicate either the droplet was applied and rode higher on the PFP, reducing the drag with the barks surface causing the quick flowtime, or that other droplets were applied in such a way that they had to overcome the adhesion of the barks surface before they could accelerate and flow down the PFP.

At angles higher than 30 degrees, most of the fifth drops were primarily gravitationally induced. This acceleration demonstrates that the lubrication from previous droplets gives a hydrophilic travel channel for the droplets. This further provided a channel of a consistent hydrophobicity, meaning the droplet could accelerate through the channel dependent on the branch angle for gravities input. This channel slowly travels, resulting in drips unrelated to applied droplets; this effect could be revealed in further dyed water experiments to see how the channel flows without additional droplets, but how fluid travelled slowly but continuously down the channel. This molecular movement indicates that ions are denser lower down in the architecture as some will be deposited before travelling the full length of the PFP. Therefore, the results support that stemflow 's volumetric majority is generated in the canopy's upper half (Bialkowski and Buttle, 2015), and stemflow ’s qualitative majority is generated in the bottom half.

Furthermore, the path was appeared to replace after roughly 3 to 5 droplets. This replacement rate substantiates that the storm intensity impacts the stemflow s composition (Muzylo *et al*., 2012), as the time differential between droplets on a path would impact the time frame in which ion exchange can occur. The replacement rate was partially attributable to the size of the droplet, as smaller droplets had a more laminar flow while the larger droplets had a rolling flow. The mixing rate was greater towards the end of the path, indicating that the circular motion upwards into the droplet requires some acceleration, likely from molecules' acceleration downwards and back in the roll. Therefore, the spatiality of mixing starting between a PFP follower and the PFP path equals the drop diameter above a threshold, differentiating rolling from laminar stemflow. There is a less regular adherence to the PFP once the bark becomes saturated as secondary PFPs become open and, in some instances, gain gravitational preference. These PFP deviations were more prevalent on porous samples than on smoother barks attributable to the available possible paths. However, in most instances, the PFP became wider, as the direction of travel was similar to a triangle. The wider bottom was equal to the width of the splash and slowly became narrower until equal to the width of

a travelling drop. If the surface had become saturated after the PFP had been formed, the remaining droplets formed within the vicinity would follow this same path roughly.

Furthermore, as long as droplets enter a bark area in roughly the same area, they will likely follow the same path unless the surface saturation has generated blocking droplets that enable more gravitationally favourable PFP. There was a noticeable decrease in speed when there was a surface saturation, likely attributable to the wider splash radius on the surface, compared to the hydrophobic bead on dryer samples. This deceleration indicates a wider catchment of leached surface area than the channelled underside PF, if true, further indicating the temporal: ionic density relationship.

5. Concluding points

5.1 Concluding Stemflow volume and its controls

Both the FR and $SF_{\%}$ of a tree gives an insight into what conditions may lead to more efficient stemflow production. The main control is how the coverage of epiphytic life and its relationship with the prior dry period before the storm modifies how much rainfall becomes stemflow. It does this by

acting as a barrier that must be compensated with a volume of water before stemflow can progress further down the trunk of the tree, meaning a higher epiphytic coverage will increase the threshold for stemflow production. An influence of the storm characteristics can circumvent this in two ways. Firstly it can have a high peak storm volume (%), which will produce more throughfall than stemflow and is one of the reasons that small storms do not produce much stemflow. The stemflow volumes from each tree also support the notion of a high peak storm volume (%) will reduce the Fr and $SF_{\%}$ and ultimately the volume of stemflow received. Secondly a storm could have a diverse wind direction, which will produce stemflow that follows a diverse range of PFPs, which can circumvent any concentration of epiphytic life, therefore, producing more stemflow . This diverse wind direction depends on the extent to which the tree stands alone, as our trees, while free standing by respect to their canopy, were still in the shade of other trees, which would reduce a trees response to a diverse wind direction. This dependency is seen within S4 T4 where with a diverse wind direction that caused a high FR and $SF_{\%}$ in other trees, the architecture of T4 meant that it ended up producing more throughfall, which is supported by the high volumes on the other end of the wind direction spectrum. Ultimately, the seasonal element within stemflow appeared to be misguided as the changing of the foliage surface did not have the same importance as individual storm characteristics. This could indicate that evergreen trees would produce a more seasonal pattern as our independent variable would remain more stable.

The stark difference between T1, T2, T4, and T5 and T3 & T6 stemflow volumes both supports the influence of epiphytes on production of stemflow, while highlighting sensitive differences in a trees topographical situation in placing drastically lower volumetric limits on a trees ability to produce stemflow. This is interesting as lichen and moss are often noted for their absorption abilities, but a vascular epiphyte may have a greater ability to siphon stemflow away from the trunk. However, this is inconclusive because of the lack of studies to support or reject this theory, and because of the void samples from that tree prohibiting insight of this in the larger storms within our study. For the four trees without these volumetric limits, the theories have more merit, with a clear upper limit within a fairly large size and age gap. This similarity again highlights the role of epiphytes, especially in the densely covered T2, where dry preceding conditions produced stemflow volumes a fraction of T4 & T5, but also where the larger size of the trees at site 1 has a larger threshold for producing stemflow regardless of the prior conditions. Whereas T4 & T5 show how a high peak rainfall volume (%) could have a larger impact on smaller trees who also don’t have the epiphytic life to slow down any potential stemflow.

The behaviours of the trees show 2 stages of stemflow development, one where stemflow will always increase with a larger storm (S3 & S6) and one where stemflow has a limit on its production (T1, T2, T4, and T5). This limit of production is limited to the ten studied storms with the largest having an average intensity of 2.5mm/h which would produce more throughfall. Therefore the larger volumes of stemflow could be possible in longer storms with near equal stemflow volumes seen in S1 & S4 with about half of the overall storm input. This indicates that it may be rainfall intensity that take the role of peak storm volume (%) in larger storms, but that any hour where rainfall intensity >1mm/h will reduce the FR and $SF_{\%}$ and consequently, the overall stemflow volume. The results and conclusions related to storm characteristics and stemflow volume were one of the stronger results within this study. They agreed with previous academic works such as Muzylo *et al., (*2012); and Levia and frost (2003), meaning the results have strengthened these theories about rainfalls characteristics on stemflow.

5.2 Concluding notes on bark's hygroscopicity and its impact on stemflow volume

Hygroscopicity was difficult to identify throughout the studied storms, as the relative humidities stayed consistently high, with the argument made about morning and afternoon onset storms being inconclusive because of the coincidental 9/10 morning onset storms. Storm 8, the only afternoon onset storm, was especially low with its stemflow volume, however more than one instance is required for a conclusion and there were other variables that could have compounded or also caused these low values. Storm 10 was similarly especially low, with low relative humidities, indicating a hygroscopic influence. However, it is more likely that this was supporting the long and hot dry period, that will have dried the bark out regardless of its hygroscopic abilities. Nevertheless, this variable being apparent where it was going to be the most visible could warrant further study. Meanwhile the presence of water within the barks structure and the spatiality of it proved to be either random or of such a delicate nature that study on the spatial space of a full tree would be useless, but on smaller scales could indicate some interesting fluid and porous medium physics. A study directly comparing morning and afternoon onset storms could enhance understanding, potentially requiring an extended fieldwork period to ensure a sufficient number of significant morning onset storms, as achieving an equal number of stemflow-producing morning and afternoon storms may be challenging.

5.3 The meteorological conditions and tree characteristics that quantitatively control ions

The most apparent control over the overall quantity of ions that was present within a stemflow volume was the size of the overall tree, as the difference in ages and overall quantities of ions were remarkably similar where the overall volume was not. This shows that larger trees will scavenge more ions from their surrounding atmosphere and will likely retain more of them as the ability to produce large volumes of stemflow is hampered by the increasing number of obstacles it accounts for. Ultimately, the seasonal element within stemflow appeared to be too short a timeline, with Neal *et al*., (2003) showing many ions have near decadal patterns in their quantities, with the Springs unusually hot and dry behaviour further damaging any patterns through a gradual heating up into summer occurring.

The four largest salt ions (Na, Cl, SO24, and Mg) each appear to have their main control as the prior dry period, as this provides the window of opportunity in which an ion can be deposited. These are then complimented by secondary variables to explain the fluctuations, for example wind speed and external pollution, with further tertiary variables causing some of the more minute fluctuations. Fluoride had a similar deposition window control, but that amounts in rainfall were often negligible meaning that fluoride mainly quantifiably exists within DD. The nitrogen ions appear to behave in a similar manner, with only an unexpected jump in nitrate within S10 which hints at a damage to the microbe populations, or an effect of climate change within the study period, and one that warrants further study to determine which environmental factors could damage the dissimilatory nitrate reduction to ammonium process. What quantities of these ions also show is that rainfall can interrupt this process, producing the values of nitrite found in S2, S4, S5, S7, and S10. However, the conditions or rainfall characteristics remained unclear. Phosphate seemed unrelated to many of the other ions, meaning its foliage input is most likely (Neal *et al*., 2003). Potassium was interesting as it reduced as any storm characteristic increased, while it was consistently higher in stemflow than in the rainfall, which indicates a fair bit of deposition, but also that it is retained better than any other ion by the trees, strongly highlighting its role within photosynthesis and that plants leach any molecule associated with this process at a lesser rate in order to promote it. Calcium appears to have a principal situational control, as proximity to terrestrial sources drastically increased the WD input within some storms solely at site 1. A support for this is with the decrease as the weather

becomes wetter, which would decrease the amount of mineral suspension from this source as it became sodden more frequently. Bromide likely fell victim to a processing error within S1, which makes any conclusion relating to storm size negligible. The consistently higher concentrations within rainfall over stemflow indicates that bromide is being retained on the tree, with the trigger for this being long dry periods, and with this being present amongst a further five ions indicates that this could be a strong variable to study to understand how trees will react to the extremes of climate change.

5.4 The potential travel as compounds

There was strong evidence to show that the ions travelled through DD as part of a salt compound as the consistency of Sodium Chloride and strong performance of Magnesium sulphate, while the other salt compounds have individual storms where they had strong correlations indicate compound travel. The overall trend supports earlier hypothesis, being that the absence of leaves, interrupts the flows of ions less, giving the consistent high values in the first three storms which are seldom matched in the following seven. This is followed by a large drop in all but the potassium chloride salt, which shows again the retention of ions by the tree, which would disrupt correlations or hint at singular ion travel. The last being some diluting and washing remnants of S6 within the quantities seen in S7, which would also disrupt any strong correlations forming within any of the salt compounds.

Results and discussion about the nitrogen compounds shows than dissimilatory nitrate reduction to ammonium can be interrupted by rainfall leaving trace amounts of nitrite within stemflow samples, with a decrease in the rate of dissimilatory nitrate reduction to ammonium potentially showing a further effect of climate change within this study so an area that should warrant further research. Phosphate did have the potential to have been carried as sediment form nearby phosphate containing minerals, but the quantities indicated more strongly that it was pollution from the use of fertilizers in nearby agriculture and the release from foliage surfaces during the stemflow process.

5.5 The movement of stemflow

The movement of stemflow was primarily gravitationally influenced, with steeper bark surfaces causing an acceleration in droplet travel. This was through all of the modes of travel, including PFP generators, PFP followers, and blocking droplets, and would follow the most gravitationally favourable path according to the sensitive topography of the barks surface. This means that the path was liable to change when the bark changed angle, and alongside the gradual change of branches, both in their inclination and surface characteristics, likely means that the PFPs on a trees surface change gradually over time but will still follow the same overarching gravitational rules. The droplets: PFP generators and blocking droplets are often one of the same, simply depending on if there is a large enough blockage to require a full droplet ,or the extent to which a droplet runs out of fluid if there is a Wenzel-state droplet (figure 41). There is the potential for further travel if there is enough hydrophobicity to have a Carrie-Baxter state droplet for some duration of its travel. What categorises blocking droplets is their stationary nature, that is then partially mixed and dislodged by the following droplet. PFP followers contribute the least to the ionic properties of stemflow as they have a faster travel, and an unknown level of mixing as the droplet is dispersed along the PFP making it indistinguishable by the end of the bark sample.

The drying of a PFP reveals how ions are gradually transported down a tree, as the small amounts of water that act as blocking droplets (Figure 41) will have ions within them but will deposit them when these droplets are lost to evaporation. This drying may also be through slow travel downwards as seen through drips unrelated to any administered droplets, however this is inconclusive because of the lack of recording any timescales in which it happened.

5.6 Limitations of the study

It should be noted that this study and the results and discussion points within it are limited to the specific climatic zone in which they took place. Furthermore, because of the complex nature of trees, the results presented represent a very small fraction of what is possible within the realm of the ionic composition of stemflow within young oak trees owing to the plethora of variations that could have a sizable impact on stemflows ionic signature.

6. **Bibliography**

Aleksandra, S.-C., Krzysztof, K. and Aleksander J., K. (2010). Influence of Quercus robur Throughfall on Elemental Composition of Pleurozium schreberi (Brid.) Mitt. and Hypnum cupressiforme Hedw. Polish Journal of Environmental Studies, 19(4), pp.763–769.

Andreas, E.L., Vlahos, P. and Monahan, E.C. (2016). The potential role of sea spray droplets in facilitating air-sea gas transfer. IOP Conference Series: Earth and Environmental Science 35 (1), p. 012003.

Anna, I. and Jarosław, K. (2014). Hydrological properties of bark of selected forest tree species. Part I: the coefficient of development of the interception surface of bark. Trees, 28(3), pp.831–839.

Aryal, B. and Neuner, G. (2009). Leaf wettability decreases along an extreme altitudinal gradient. Oecologia, 162(1), pp.1–9.

Asman, W.A.H., Pinksterboer, E.F., Maas, H.F.M., Erisman, J.-W., Waijers-Ypelaan, A., Slanina, J. and Horst, T.W. (1989). Gradients of the ammonia concentration in a nature reserve: Model results and measurements. Atmospheric Environment (1967), 23(10), pp.2259–2265.

Badenoch-Jones, J., Summons, R.E., Djordjevic, M.A., Shine, J., Letham, D.S. and Rolfe, B.G. (1982). Mass Spectrometric Quantification of Indole-3-Acetic Acid in Rhizobium Culture Supernatants: Relation to Root Hair Curling and Nodule Initiation. Applied and Environmental Microbiology, 44(2), pp.275–280.

Bao Q., Kang H.Y., (2021). Numerical simulation of droplet impacting and sliding on hydrophobic granular surfaces. Mathematical Problems in Engineering 2021 (1), p.5534003.

Beck, H.E., Zimmermann, N.E., McVicar, T.R., Vergopolan, N., Berg, A. and Wood, E.F. (2018). Present and future Köppen-Geiger climate classification maps at 1-km resolution. Scientific Data 5 (1), pp 1-12.

Behera, S.N., Sharma, M., Aneja, V.P. and Balasubramanian, R. (2013). Ammonia in the atmosphere: a review on emission sources, atmospheric chemistry and deposition on terrestrial bodies. Environmental Science and Pollution Research 20 (11), pp.8092–8131.

Beria, H., Larsen, J.R., Ceperley, N.C., Michelon, A., Vennemann, T. and Schaefli, B. (2018). Understanding snow hydrological processes through the lens of stable water isotopes. WIREs Water, 5(6).

Bialkowski, R. and Buttle, J.M. (2015). stemflow and throughfall contributions to soil water recharge under trees with differing branch architectures. Hydrological Processes, 29(18), pp.4068–4082.

Blow, F.E. (1985). Quantity and hydrologic characteristics of litter under upland oak forests in eastern Tennessee. The Journal of Science and Technology for Forest Products and Processes, 52(5), pp.190–195.

Brooker, M.P. and Johnson, P.C. (1984) 'The behaviour of phosphate, nitrate, chloride and hardness in twelve welsh rivers,' Water Research, 18(9), pp. 1155–1164.

Brown K.A., (1982). Sulphur in the Environment: A review. Environmental Pollution Series B, Chemical and Physical 3 (1). Page 47-80.

Budke, J.M., Bernard, E.C., Gray, D.J., Huttunen, S., Piechulla, B. and Trigiano, R.N. (2018). Introduction to the Special Issue on Bryophytes. Critical Reviews in Plant Sciences, 37(2-3), pp.102–112.

Bytnerowicz, A. and Fenn, M.E. (1996). Nitrogen deposition in California forests: A review. Environmental Pollution, 92(2), pp.127–146.

C. Donald Ahrens and Henson, R. (1994). Meteorology today : an introduction to weather, climate, and the environment. 5th ed. Boston, Ma: Cengage.

Cardon, M.E., McGee, G.G. and Kiernan, D.H. (2019). Variation in Acer saccharum Marshall (Sugar Maple) Bark and stemflow Characteristics: Implications for Epiphytic Bryophyte Communities. Northeastern Naturalist, 26(1), p.214.

Carlyle-Moses, D.E., Iida, S., Germer, S., Llorens, P., Michalzik, B., Nanko, K., Tischer, A. and Levia, D.F. (2018). Expressing stemflow commensurate with its ecohydrological importance. Advances in Water Resources, 121, pp.472–479.

Carlyle-Moses, D.E. and Schooling, J.T. (2015). Tree traits and meteorological factors influencing the initiation and rate of stemflow from isolated deciduous trees. Hydrological Processes, 29(18), pp.4083–4099.

Cayuela, C., Llorens, P., Sánchez-Costa, E., Levia, D.F. and Latron, J. (2018). Effect of biotic and abiotic factors on inter- and intra-event variability in stemflow rates in oak and pine stands in a Mediterranean mountain area. Journal of Hydrology, 560, pp.396–406.

Chand I., Bhargava P.K., (2005). Estimation of Angle of Deflection of rain driving prone stations in India. Journal of Asian Architecture and Building Engineering 4(1): 223-229.

Chen, L., Wang, L., Martin, C.E. and Lin, T. (2019). Mediation of stemflow water and nutrient availabilities by epiphytes growing above other epiphytes in a subtropical forest. Ecohydrology, 12(7).

Cheng, I., Al Mamun, A. and Zhang, L. (2021). A synthesis review on atmospheric wet deposition of particulate elements: scavenging ratios, solubility, and flux measurements. Environmental Reviews, 29(3), pp.340–353.

Chuyong, G.B., Newbery, D.M. and Songwe, N.C. (2004). Rainfall input, throughfall and stemflow of nutrients in a central African rain forest dominated by ectomycorrhizal trees. Biogeochemistry, 67(1), pp.73–91.

Coulthard, T.J., Ramirez, J.A., Barton, N., Rogerson, M. and Brücher, T. (2013). Were Rivers Flowing across the Sahara During the Last Interglacial? Implications for Human Migration through Africa. PLoS ONE, 8(9), p.e74834.

Crockford, R.H. and Richardson, D.P. (2000). Partitioning of rainfall into throughfall, stemflow and interception: effect of forest type, ground cover and climate. Hydrological Processes, 14(16-17), pp.2903–2920.

Crockford, R.H., Richardson, D.P. and Sageman, R. (1996). Chemistry of rainfall, throughfall and stemflow in a eucalypt forest and a pine plantation in south-eastern Australia: 3. stemflow and total inputs. Hydrological Processes, 10(1), pp.25–42.

Croft, B., Lohmann, U., Martin, R.V., Stier, P., Wurzler, S., Feichter, J., Posselt, R. and Ferrachat, S. (2009). Aerosol size-dependent below-cloud scavenging by rain and snow in the ECHAM5-HAM. Atmospheric Chemistry and Physics, 9(14), pp.4653–4675.

Del Arco, J.M., Escudero, A. and Garrido, M.V. (1991). Effects of Site Characteristics on Nitrogen Retranslocation From Senescing Leaves. Ecology, 72(2), pp.701–708.

Dempsey, F. (2018). A Survey of Regional-Scale Blocking Patterns and Effects on Air Quality in Ontario, Canada. Atmosphere, 9(6), p.226.

Dentener, F.J. and Crutzen, P.J. (1994). A three-dimensional model of the global ammonia cycle. Journal of Atmospheric Chemistry, 19(4), pp.331–369.

Dickson, A.G. and Goyet, C. (1994) *Handbook of methods for the analysis of the various parameters of the carbon dioxide system in sea water. Version 2*.

Draxier, R.R. and Hess, G.D. (1998). An overview of the HYSPLIT_4 modelling system for trajectories, dispersion and deposition. Australian Meteorological Magazine, 47(4), pp.295–308.

Duce, R.A., Liss, P.S., Merrill, J.T., Atlas, E.L., Buat-Menard, P., Hicks, B.B., Miller, J.M., Prospero, J.M., Arimoto, R., Church, T.M., Ellis, W., Galloway, J.N., Hansen, L., Jickells, T.D., Knap, A.H., Reinhardt, K.H., Schneider, B., Soudine, A., Tokos, J.J. and Tsunogai, S. (1991). The atmospheric input of trace species to the world ocean. Global Biogeochemical Cycles, 5(3), pp.193–259.

Dunkerley, D. (2014). stemflow production and intrastorm rainfall intensity variation: an experimental analysis using laboratory rainfall simulation. Earth Surface Processes and Landforms, 39(13), pp.1741–1752.

Durocher, M.G. (1990). Monitoring spatial variability of forest interception. Hydrological Processes, 4(3), pp.215–229.

Eaton, J.S., Likens, G.E. and Bormann, F.H. (1973). Throughfall and stemflow Chemistry in a Northern Hardwood Forest. The Journal of Ecology, 61(2), p.495.

Ellis, W.B. (1999) 'Books: Ullmann's Encyclopedia of Industrial Chemistry, 6th Edition,' *Journal of* Industrial Ecology, 3(2–3), pp. 192–195.

Elmendorf, S.C., Henry, G.H.R., Hollister, R.D., Björk, R.G., Bjorkman, A.D., Callaghan, T.V., Collier, L.S., Cooper, E.J., Cornelissen, J.H.C., Day, T.A., Fosaa, A.M., Gould, W.A., Grétarsdóttir, J., Harte, J., Hermanutz, L., Hik, D.S., Hofgaard, A., Jarrad, F., Jónsdóttir, I.S. and Keuper, F. (2011). Global assessment of experimental climate warming on tundra vegetation: heterogeneity over space and time. Ecology Letters, 15(2), pp.164–175.

Erisman, J.W., Vermetten, A.W.M., Pentecost Farmer, E.F., Asman, W.A.H., Waijers-Ijpelaan, A. and Slana, J. (1987). Atmospheric ammonia: distribution, equilibrium with aerosols and conversion rate to ammonium. In *Ammonia and Acidification. Symp. EURASAP, Bilthoven, The Netherlands* (pp. 13-15).

Farmer, A.M., Bates, J.W. and Bell, J.N.B. (1991). Seasonal variations in acidic pollutant inputs and their effects on the chemistry of Stemflow, bark and epiphyte tissues in three oak woodlands in N.W. Britain. New Phytologist, 118(3), pp.441–451.

Filippelli, G.M., (2008). The Global Phosphorus cycle: Past, present, and future. Elements 4 (2): Page 89-95.

Fleischbein, K., Wilcke, W., Goller, R., Boy, J., Valarezo, C., Zech, W. and Knoblich, K. (2005). Rainfall interception in a lower montane forest in Ecuador: effects of canopy properties. Hydrological Processes, 19(7), pp.1355–1371.

Ford, E.D. and Deans, J.D. (1978). The Effects of Canopy Structure on Stemflow, Throughfall and Interception Loss in a Young Sitka Spruce Plantation. Journal of Applied Ecology, 15(3), pp.905-918

Frank, G., Trautner, F. and Tschiersch, J. (1991). Determination of scavenging efficiency by using fluorescent aerosol. Journal of Aerosol Science, 22, pp.S537–S540.

Frevert, T. and Klemm, O. (1984). Wie ändern sich pH-Werte im Regen- und Nebelwasser beim Abtrocknen auf Pflanzenoberflächen? Archives for Meteorology, Geophysics, and Bioclimatology Series B, 34(1-2), pp.75–81.

Fritz, Ö., Brunet, J. and Caldiz, M. (2009). Interacting effects of tree characteristics on the occurrence of rare epiphytes in a Swedish beech forest area. The Bryologist, 112(3), pp.488–505.

Gabelica, V. and Marklund, E. (2018). Fundamentals of ion mobility spectrometry. Current Opinion in Chemical Biology, 42, pp.51–59.

Gall, J.E., Boyd, R.S. and Rajakaruna, N. (2015). Transfer of heavy metals through terrestrial food webs: a review. Environmental Monitoring and Assessment 187 (4), pp1-21.

Garcia-Estringana, P., Alonso-Blázquez, N. and Alegre, J. (2010). Water storage capacity, stemflow and water funneling in Mediterranean shrubs. Journal of Hydrology, 389(3-4), pp.363–372.

Gonzalez-Ollauri, A., Stokes, A. and Mickovski, S.B. (2020). A novel framework to study the effect of tree architectural traits on stemflow yield and its consequences for soil-water dynamics. Journal of Hydrology, 582, p.124448.

Gotsch, S.G., Draguljić, D. and Williams, C.J. (2017). Evaluating the effectiveness of urban trees to mitigate storm water runoff via transpiration and Stemflow. Urban Ecosystems, 21(1), pp.183–195.

Hasanah Y., Mawarni L., Hanum H., Nasution M.R., (2020). The role of magnesium sulphate in the formation of chloropyll and density of stomata of soybean varieties (Glycine max (L.) Merril). IOP Conference Series: Earth and Environmental Science 454: p.012158

Hauck, M. (2010). Ammonium and nitrate tolerance in lichens. Environmental Pollution, 158(5), pp.1127–1133.

Henskens, F.L., Green, T.G.A. and Wilkins, A. (2012). Cyanolichens can have both cyanobacteria and green algae in a common layer as major contributors to photosynthesis. Annals of Botany 110 (3), pp.555–563.

Herwitz, S.R. (1985). Interception storage capacities of tropical rainforest canopy trees. Journal of Hydrology 77(1-4), pp.237–252.

Herwitz, S.R. (1988). Buttresses of tropical rainforest trees influence hillslope processes. Earth Surface Processes and Landforms, 13(6), pp.563–567.

Herwitz, S.R. and Slye, R.E. (1995). Three-dimensional modeling of canopy tree interception of wind-driven rainfall. Journal of Hydrology, 168(1-4), pp.205–226.

Holden, J. (2017). An introduction to physical geography and the environment. Harlow, England: Pearson.

Holder, C.D. (2012). Effects of leaf hydrophobicity and water droplet retention on canopy storage capacity. Ecohydrology, 6(3), pp.483–490.

Huang W., Plistil A., Stearns S.D., Dasgupta P.K., (2021). Gradient nano pump based suppressed ion chromatography using PEEK open tubular columns. Talanta Open 3: p.100029

Hutchinson, I. and Roberts, M.C. (1981). Vertical Variation in stemflow Generation. Journal of Applied Ecology, 18(2), p.521.

Iida, S., Wheeler, K.I., Nanko, K., Shinohara, Y., Sun, X., Sakai, N. and Levia, D.F. (2021). Canopy structure metrics governing stemflow funnelling differ between leafed and leafless states: Insights from a large-scale rainfall simulator. Hydrological Processes, 35(8), e14294.

Ilek, A., Kucza, J. and Morkisz, K. (2017). Hygroscopicity of the bark of selected forest tree species. iForest - Biogeosciences and Forestry, 10(1), pp.220–226.

Imai S., Onoda M., Endo R., Okawa T., (2022). Changing sliding characteristics of a droplet on a slope by the shape and orientation of mircotrangular projections for droplet transportation. Sensors and Actuators: A Physical 336: p.113380.

Jeffrey, L.C., Maher, D.T., Chiri, E., Leung, P.M., Nauer, P.A., Arndt, S.K., Tait, D.R., Greening, C. and Johnston, S.G. (2021). Bark-dwelling methanotrophic bacteria decrease methane emissions from trees. Nature Communications, 12(1), 2127.

Jensen, A.M., Mintschenko, H. and Ræbild, A. (2020). Transpiration reduction and absorption of intercepted water in Leyland cypress (× Cupressocyparis leylandii) and European common oak (Quercus robur). European Journal of Forest Research 139(4), 585-593.

Jeong, S., Naidu G., Leiknes T., Vigneswaran S., (2017) 4.3 Membrane biofouling: Biofouling assessment and reduction strategies in seawater reverse osmosis desalination. In *Elsevier eBooks*, pp. 48–71.

Jickells, T.D., Baker, A.R. and Chance, R. (2016). Atmospheric transport of trace elements and nutrients to the oceans. Philosophical Transactions of the Royal Society A: Mathematical, Physical and Engineering Sciences, 374(2081), p.20150286.

Johnson, M.S., Lehmann, J., Steenhuis, T.S., Vargem de Oliveira, L. and Fernandes, E.C.M. (2005). Spatial and temporal variability of soil water repellency of Amazonian pastures. Soil Research, 43(3), p.319-326.

Khalid, S., Shahid, M., Dumat, C., Niazi, N.K., Bibi, I., Gul Bakhat, H.F.S., Abbas, G., Murtaza, B. and Javeed, H.M.R. (2017). Influence of groundwater and wastewater irrigation on lead accumulation in soil and vegetables: Implications for health risk assessment and phytoremediation. International Journal of Phytoremediation, 19(11), pp.1037–1046.

Khan, N., Ali, S., Shahid, M.A. and Kharabian-Masouleh, A. (2017). Advances in detection of stress tolerance in plants through metabolomics approaches. Plant Omics, 10(03), pp.153–163.

Klamerus-Iwan, A. and Witek, W. (2018). Variability in the Wettability and Water Storage Capacity of Common Oak Leaves (Quercus robur L.). Water, 10(6), p.695.

Kraus, T.E.C., Dahlgren, R.A. and Zasoski, R.J. (2003). Tannins in nutrient dynamics of forest ecosystems - a review. Plant and Soil 256 (1), pp.41–66.

Krupa, S.V. (2002). Sampling and physico-chemical analysis of precipitation: a review. Environmental Pollution, 120(3), pp.565–594.

Larsen, H.M.E. and Rasmussen, H.N. (2021). Bark extract influence on spore germination in corticolous lichen Xanthoria parietina in vitro. Mycological Progress, 20(3), pp.313–323.

Larsen, H.M.E., Rasmussen, H.N. and Nord-Larsen, T. (2017). The water holding capacity of bark in Danish angiosperm trees. In IUFRO Division 5 Conference 2017.

Lei, Y.D. and Wania, F. (2004). Is rain or snow a more efficient scavenger of organic chemicals? Atmospheric Environment, 38(22), pp.3557–3571.

Leith, I.D., Mitchell, R.J., Truscott, A.-M. ., Cape, J.N., van Dijk, N., Smith, R.I., Fowler, D. and Sutton, M.A. (2008). The influence of nitrogen in stemflow and precipitation on epiphytic bryophytes, Isothecium myosuroides Brid., Dicranum scoparium Hewd. and Thuidium tamariscinum (Hewd.) Schimp of Atlantic oakwoods. Environmental Pollution, 155(2), pp.237–246.

Levia Jr., D.F. and Herwitz, S.R. (2000). Physical properties of water in relation to stemflow leachate dynamics: implications for nutrient cycling. Canadian Journal of Forest Research, 30(4), pp.662–666.

Levia, D. and Frost, E. (2003). A review and evaluation of stemflow literature in the hydrologic and biogeochemical cycles of forested and agricultural ecosystems. Journal of Hydrology 274(1-4), pp.1–29.

Levia, D.F. (2003). Winter stemflow leaching of nutrient-ions from deciduous canopy trees in relation to meteorological conditions. Agricultural and Forest Meteorology, 117(1-2), pp.39–51.

Levia, D.F. (2004). Differential winter stemflow generation under contrasting storm conditions in a southern New England broad-leaved deciduous forest. Hydrological Processes, 18(6), pp.1105–1112.

Levia, D.F. and Germer, S. (2015). A review of stemflow generation dynamics and Stemflow-environment interactions in forests and shrublands. Reviews of Geophysics, 53(3), pp.673–714.

Levia, D.F. and Herwitz, S.R. (2002). Winter chemical leaching from deciduous tree branches as a function of branch inclination angle in central Massachusetts. Hydrological Processes, 16(14), pp.2867–2879.

Levia, D.F. and Herwitz, S.R. (2005). Interspecific variation of bark water storage capacity of three deciduous tree species in relation to stemflow yield and solute flux to forest soils. CATENA, 64(1), pp.117–137.

Levia, D.F., Michalzik, B., Näthe, K., Bischoff, S., Richter, S. and Legates, D.R. (2014). Differential stemflow yield from European beech saplings: the role of individual canopy structure metrics. Hydrological Processes, 29(1), pp.43–51.

Levia, D.F. and Underwood, S.Jeffrey. (2004). Snowmelt induced stemflow in northern hardwood forests: a theoretical explanation on the causation of a neglected hydrological process. Advances in Water Resources, 27(2), pp.121–128.

Levia, D.F., Van Stan J.T., Siegert C.M., Inamdar S.P., Mitchell M.J., Mage S.M., McHale P.J., (2011) 'Atmospheric deposition and corresponding variability of stemflow chemistry across temporal scales in a mid-Atlantic broadleaved deciduous forest,' Atmospheric Environment, 45(18), pp. 3046–3054.

Levin, Z. and Cotton, W.R. (2009). Aerosol pollution impact on precipitation. Earth Science Reviews.

Likens, G.E. and Frederick Herbert Bormann (1994). Biogeochemistry of a forested ecosystem. New York Berlin Heidelberg London Paris Tokyo Hong Kong Barcelona Budapest Springer.

Liu, X., Ye, C., Li, X., Cui, N., Wu, T., Du, S., Wei, Q., Fu, L., Yin, J. and Lin, C.-T. (2018). Highly Sensitive and Selective Potassium Ion Detection Based on Graphene Hall Effect Biosensors. Materials, 11(3), p.399.

Liu Y., Fu B., Shen Y., Liu C., Liu H., Zhao Z., Zhang L., (2019). Environmental effect of heavy metals deposition in arid city. *Global NEST Journal* 21 (3), pp 405-409

Lui, D.-L. (2010). Particle deposition onto enclosure surfaces. In: Developments in Surface Contamination and Cleaning Particle Deposition, Control and Removal. pp.1–56.

Magyar, D., Van Stan, J.T. andScavenging ratioidhar, K.R. (2021). Hypothesis and Theory: Fungal Spores in stemflow and Potential Bark Sources. Frontiers in Forests and Global Change 4, p.623758.

Marchant H.G., Lavik G., Holtappels M., Kuypers M.M.M. (2014). The fate of Nitrate in intertidal permeable sediments. PLOS ONE 9 (8), p.e104517.

Mariraj Mohan, S. (2015). An overview of particulate dry deposition: measuring methods, deposition velocity and controlling factors. International Journal of Environmental Science and Technology 13 (1), pp.387–402.

McCarroll D., (2016) “correlation“. In Simple statistical tests for geography 1st edition. Chapman and Hall, New York.

McJannet D., Wallace J., Reddell P., (2007). Precipitation interception in Australian tropical rainforests: 1. Measurement of stemflow , throughfall and cloud interception. Hydrological Processes 21 (13): 1692-1702.

Mitchell, R.J., Truscot, A.M., Leith, I.D., Cape, J.N., Van Dijk, N., Tang, Y.S., Fowler, D. and Sutton, M.A. (2005). A study of the epiphytic communities of Atlantic oak woods along an atmospheric nitrogen deposition gradient. Journal of Ecology, 93(3), pp.482–492.

Mohammadrezaei S., Siavashi M., Asiaei S., (2022). Surface topography effects on dynamic behaviours of water droplet over a micro-structured surface using an improved-VOF based lattice Boltzmann method. Journal of Molecular Liquids 350:118509.

Mohan, S. (2015) 'An overview of particulate dry deposition: measuring methods, deposition velocity and controlling factors,' *International Journal of Environmental Science and Technology*, 13(1), pp. 387–402.

Morillas, H., Maguregui M., Garcia-Florentino C., Marcaida L., Madariaga J.M., (2016) 'Study of particulate matter from Primary/Secondary Marine Aerosol and anthropogenic sources collected by a self-made passive sampler for the evaluation of the dry deposition impact on built heritage,' *Science of the Total Environment*, 550, pp. 285–296.

Munger, J.W. and Eisenreich, S.J. (1983). Continental-scale variations in precipitation chemistry. Environmental Science & Technology, 17(1), pp.32–43.

Mużyło, A., Llorens, P. and Domingo, F. (2011). Rainfall partitioning in a deciduous forest plot in leafed and leafless periods. Ecohydrology, 5(6), pp.759–767.

Nadkarni, N.M. (1984). Epiphyte Biomass and Nutrient Capital of a Neotropical Elfin Forest. Biotropica 16 (4), pp.249–256.

Neary, A.J. and Gizyn, W.I. (1994). Throughfall and stemflow chemistry under deciduous and coniferous forest canopies in south-central Ontario. Canadian Journal of Forest Research, 24(6), pp.1089–1100.

Niinemets, U. and Tamm, U. (2005). Species differences in timing of leaf fall and foliage chemistry modify nutrient resorption efficiency in deciduous temperate forest stands. Tree Physiology, 25(8), pp.1001–1014.

Nowlan, C.R., Martin, R.V., Philip, S., Lamsal, L.N., Krotkov, N.A., Marais, E.A., Wang, S. and Zhang, Q. (2014). Global dry deposition of nitrogen dioxide and sulfur dioxide inferred from space-based measurements. Global Biogeochemical Cycles, 28(10), pp.1025–1043.

Oakes, M.M., Burke, J.M., Norris, G.A., Kovalcik, K.D., Pancras, J.P. and Landis, M.S. (2016). Near-road enhancement and solubility of fine and coarse particulate matter trace elements near a major interstate in Detroit, Michigan. Atmospheric Environment, 145, pp.213–224.

Odum, E.P. (1959). Fundamentals of ecology. Australia: Cengage Learning.

Oka, A., Takahashi, J., Endoh, Y. and Seino, T. (2021a). Bark Effects on stemflow Chemistry in a Japanese Temperate Forest I. The Role of Bark Surface Morphology. Frontiers in Forests and Global Change 4, p.654375.

Oka, A., Takahashi, J., Endoh, Y. and Seino, T. (2021b). Bark Effects on stemflow Chemistry in a Japanese Temperate Forest II. The Role of Bark Anatomical Features. Frontiers in Forests and Global Change 4, p.657850.

Pallardy, S.G. and Kozlowski, T.T. (2007). Physiology of woody plants. Boston: Elsevier, Lexington, Ky.

Papen, G.C., Gardner, C.S. and Pfenninger, W.M. (1995). Analysis of a potassium lidar system for upper-atmospheric wind–temperature measurements. Applied Optics, 34(30), pp.6950-6598.

Paramanov, M., Gronholm, T. and Virkkula, A. (2011). Below-cloud scavenging of aerosol particles by snow at an urban site in Finland. Boreal Environment Research, 16, pp.304–320.

Petroff, A., Mailliat, A., Amielh, M. and Anselmet, F. (2008). Aerosol dry deposition on vegetative canopies. Part I: Review of present knowledge. Atmospheric Environment, 42(16), pp.3625–3653.

Polymenakou, P.N. (2012). Atmosphere: A Source of Pathogenic or Beneficial Microbes? Atmosphere, 3(1), pp.87–102.

Ponette-González, A.G. (2021). Accumulator, Transporter, Substrate, and Reactor: Multidimensional Perspectives and Approaches to the Study of Bark. Frontiers in Forests and Global Change 4, p.716557.

Ponette-Gonzalez, A.G., Weathers, K.C. and Curran, L.M. (2010). Water inputs across a tropical montane landscape in Veracruz, Mexico: synergistic effects of land cover, rain and fog seasonality, and interannual precipitation variability. Global Change Biology 16(3), pp.946–963.

Ponmurugan, P., Ayyappadasan, G., Verma, R.S. and Nayaka, S. (2016). Survey, distribution pattern and elemental composition of lichens in Yercaud hills of Eastern Ghats in southern India. Journal of Environmental Biology, 37(3), pp.407–412.

Ptatscheck, C., Milne, P.C. and Traunspurger, W. (2018). Is stemflow a vector for the transport of small metazoans from tree surfaces down to soil? BMC Ecology, 18(1), 1-11.

Pypker, T.G., Unsworth, M.H. and Bond, B.J. (2006). The role of epiphytes in rainfall interception by forests in the Pacific Northwest. I. Laboratory measurements of water storage. Canadian Journal of Forest Research, 36(4), pp.809–818.

Radzi Abas, M., Ahmad-Shah, A. and Nor Awang, M. (1992). Fluxes of ions in precipitation, throughfall and stemflow in an urban forest in Kuala Lumpur, Malaysia. Environmental Pollution, 75(2), pp.209–213.

Rosier, C.L., Moore, J.D., Wu, T.H. and Van Stan, J.T. (2015). Forest Canopy Precipitation Partitioning: An Important Plant Trait Influencing the Spatial Structure of the Symbiotic Soil Microbial Community. In: H. Bais and J. Sherrier, eds., Plant microbe interactions. Amsterdam: Academic Press, pp.215–240.

Rovelli, G. Jacobs M.I., Willis M.D., Rapf R.J., Prophet A.M., Wilson K.R., (2020) A critical analysis of electrospray techniques for the determination of accelerated rates and mechanisms of chemical reactions in droplets. Chemical Science, 11(48), pp. 13026–13043.

Sæbø, A., Popek, R., Nawrot, B., Hanslin, H.M., Gawronska, H. and Gawronski, S.W. (2012). Plant species differences in particulate matter accumulation on leaf surfaces. Science of The Total Environment, 427-428, pp.347–354.

Sansalone, J.J. and Cristina, C.M. (2004). First Flush Concepts for Suspended and Dissolved Solids in Small Impervious Watersheds. Journal of Environmental Engineering, 130(11), pp.1301–1314.

Sardans J., Penuelas J., (2015). Potassium: A neglected nutrient in global change. Global Ecology and Biogeography 24 (3): 261-275

Schlesinger W.H., Bernhardt E.S., (2020) Chapter 12 - The Global Cycles of Nitrogen, Phosphorus and Potassium, Biogeochemistry (Fourth Edition). Pages 483-508

Schlesinger, WilliamH. and Hartley, AnneE. (1992). A global budget for atmospheric NH3. Biogeochemistry 15(3), pp.191-211.

Shearman, T.M. and Varner, J.M. (2021). Variation in Bark Allocation and Rugosity Across Seven Co-occurring Southeastern US Tree Species. Frontiers in Forests and Global Change 4, p.731020.

Sheridan, C.D., Puettmann, K.J., Huso, M.M.P., Hagar, J.C. and Falk, K.R. (2013). Management, Morphological, and Environmental Factors Influencing Douglas-Fir Bark Furrows in the Oregon Coast Range. Western Journal of Applied Forestry, 28(3), pp.97–106.

Spribille, T., Tuovinen, V., Resl, P., Vanderpool, D., Wolinski, H., Aime, M.C., Schneider, K., Stabentheiner, E., Toome-Heller, M., Thor, G., Mayrhofer, H., Johannesson, H. and McCutcheon, J.P. (2016). Basidiomycete yeasts in the cortex of ascomycete macrolichens. Science, 353(6298), pp.488–492.

Stokes, G.G. (1851). On the effect of the internal friction of fluids on the motion of pendulums. Cambridge Philosophical Society 8.

Tonello, K.C., Campos, S.D., de Menezes, A.J., Bramorski, J., Mathias, S.L. and Lima, M.T. (2021). How Is Bark Absorbability and Wettability Related to stemflow Yield? Observations From Isolated Trees in the Brazilian Cerrado. Frontiers in Forests and Global Change 4, p.650665.

Tucker A., Levia D.F., Katul G.G., Nanko K., Rossi L.F. (2020). A network model for stemflow solute transport. Applied Mathematical Modelling 88, pp266-282.

Van Stan, J.T. and Gordon, D.A. (2018). Mini-Review: stemflow as a Resource Limitation to Near-Stem Soils. Frontiers in Plant Science 9, p.312219.

Van Stan, J.T., Klamerus-Iwan, A. and Dymond, S.F. (2021). Editorial: Bark-Water Interactions. Frontiers in Forests and Global Change 4, p.802586.

Van Stan, J.T., Lewis, E.S., Hildebrandt, A., Rebmann, C. and Friesen, J. (2016). Impact of interacting bark structure and rainfall conditions on stemflow variability in a temperate beech-oak forest, central Germany. Hydrological Sciences Journal, 61(11), pp.2071–2083.

Van Stan, J.T. and Pypker, T.G. (2015). A review and evaluation of forest canopy epiphyte roles in the partitioning and chemical alteration of precipitation. Science of The Total Environment, 536, pp.813–824.

Voigt, G.K. (1960). Distribution of rainfall under forest stands. Forest Science, 6(1), pp.2–10.

Wang, X.-P. ., Wang, Z.-N. ., Berndtsson, R., Zhang, Y.-F. . and Pan, Y.-X. . (2011). Desert shrub stemflow and its significance in soil moisture replenishment. Hydrology and Earth System Sciences, 15(2), pp.561–567.

Ward, R.C. and M Robinson (2011). Principles of hydrology. England: Mcgraw-Hill Pub. Company.

Wesely, M. (2000). A review of the current status of knowledge on dry deposition. Atmospheric Environment, 34(12-14), pp.2261–2282.

Xu, D., Ge, B., Wang, Z., Sun, Y., Chen, Y., Ji, D., Yang, T., Ma, Z., Cheng, N., Hao, J. and Yao, X. (2017). Below-cloud wet scavenging of soluble inorganic ions by rain in Beijing during the summer of 2014. Environmental Pollution, 230, pp.963–973.

Yuan, C., Gao, G. and Fu, B. (2016). stemflow of a xerophytic shrub (Salix psammophila) in northern China: Implication for beneficial branch architecture to produce Stemflow. Journal of Hydrology, 539, pp.577–588.

Zabret, K. and Šraj, M. (2021). How Characteristics of a Rainfall Event and the Meteorological Conditions Determine the Development of Stemflow: A Case Study of a Birch Tree. Frontiers in Forests and Global Change 4, p.663100.

Zhang, H., Fu, C., Liao, A., Zhang, C., Liu, J., Wang, N. and He, B. (2021). Exploring the stemflow dynamics and driving factors at both inter- and intra-event scales in a typical subtropical deciduous forest. Hydrological Processes 35(3), p.e14091.

Zhao, L., Fang, Q., Yang, Y., Yang, H., Yang, T. and Zheng, H. (2020). stemflow contributions to soil erosion around the stem base under simulated maize-planted and rainfall conditions. Agricultural and Forest Meteorology 281, p.107814.

Zhuang, H. (1999). Size distributions of particulate sulfate, nitrate, and ammonium at a coastal site in Hong Kong. Atmospheric Environment, 33(6), pp.843–853.

Zimmermann, F., Lux, H., Maenhaut, W., Matschullat, J., Plessow, K., Reuter, F. and Wienhaus, O. (2003). A review of air pollution and atmospheric deposition dynamics in southern Saxony, Germany, Central Europe. Atmospheric Environment, 37(5), pp.671–691.

Zotz, G. and Hietz, P. (2001). The physiological ecology of vascular epiphytes: current knowledge, open questions. Journal of Experimental Botany, 52(364), pp.2067–2078.

Zwieback, S., Qianyu C., Marsh P., Berg A., (2019). Shrub tundra ecohydrology: rainfall interception is a major component of the water balance. Environmental Research Letters 14(5), p. 055005.

1. Appendices

1. Guttering: https://www.plastics-express.co.uk/black-twinwall-duct-40mm-x-50m-coil-p-pm398

2. Containers: https://www.inoxia.co.uk/products/laboratory/bags-bottles/wide-mouth-bottles

3. Sealant: https://uk.gorillaglue.com/gorilla-all-conditions-sealant-white/

4. Sealant Safety sheet: https://uk.gorillaglue.com/wp-content/uploads/sites/18/2019/04/eu-gorilla-glue-sealant-white-1-1.pdf

5. Nails: https://www.amazon.co.uk/gp/product/B01FV5P2RE/ref=ppx_yo_dt_b_asin_title_o03_s00?ie=UTF8&psc=1

6. Frame Counter: Tour Tempo Frame Counter Golf, available on the IOS app store.

7. Synoptic Maps: https://www.willandweather.org.uk/mycharts.php

8. Geology viewer: https://www.bgs.ac.uk/map-viewers/geology-of-britain-viewer/

Appendix 9: The potential combinations of the ions

	Fluoride	Chloride	Nitrite	Bromide	Nitrate	Phosphate	Sulphate	Sodium	Ammonium	Potassium	Calcium	Magnesium
Fluoride		ClF - Chlorine Monofluoride	FNO2 - Nitryl Fluoride: Atmospheric pollutant	BrF3 - Bromine Trifluoride: Not naturally occuring	FNO3 - Fluorine Nitrate: Produced when flourine gas is bubbled through nitric acid	F-PO4 - Fluoride Phosphate: A family of double salts	SO4-F - Sulfate Fluoride: A family of Double salts	Fna - Sodium Fluoride: Used to fluorinate water supplies	NH4F - Ammonium fluoride: Used as an antiseptic in breweries	KF - Potassium Fluoride: Occurs naturally as the mineral carobbiite	CaF2 - Calcium Fluoride: Known as fluorspar	MgF2 - Magnesium Fluoride: Occurs naturally as the mineral Sellaite
Chloride			ClNO2 - Chlorine nitrite/ Nitryl chloride: Atmospheric pollutant	BrCl - Bromine Monochloride: Does not occur naturally	ClNO3 - Chlorine Nitrate: Stratopheric atmospheric gas	PoCl3 - Phosphoryl chloride: Doesn't occur naturally	HSO3Cl - Chlorosulfuric acid: Does not occur naturally	NaCl - 90% of sea salt	NH4Cl - Ammonium Chloride: Rare naturally, can be found around volcanic vents	KCl - Potassium Chloride: occurs naturally as a sea salt	CaCl2: Calcium Chloride: Occurs as evaporite minrals	MgCl2 - 3.7% of Sea Salt
Nitrite				Br-NO2: Bromide Nitrite: Does not exist	NO3-NO2: Does not exist	NO2-PO4 - Phosphurus nitrite: Does not exist	NOHSO4 - Nitrosylsulfuric acid: Occurs only though synthesis	NaNO2 - Sodium Nitrite: Common poison	NH4NO2 - Ammonium Nitrite: Forms freely in the Atmosphere	KNO2 - Potassium Nitrite: Present at very low levels in soil and natural water	Ca(NO2)2 - Calcium Nitrite: Can only be synthesised, has use as antifreeze	MgN2O4 - Magnesium Nitrite: Unstable compound
Bromide					BrNO3 - Bromine Nitrate: Produced only through sysnthesis	PBr - Phosphorus Bromide: Exists as PBr2, PBr5, and PBr7	SBr2 - Sulphur Dibromide: A toxic gas	NaBr - Sodium Bromide: Found in salt deposits	NH4Br - Ammonium Bromide: Occurs easily in water. Yellow colour	KBr - Potassium Bromide: Ocuurs through synthesis	CaBr2(H20)x - Calcium Bromide: Can only be synthesised	MgBr2 - Magnesium Bromide: Present as a sea salt
Nitrate						PO4-NO3 - Phosphate Nitrate: Does not exist	Sulfate Nitrates: A family of double salts	NaNO3 - Sodium Nitrate: Found in Chilean and Peruvian salt deposits	NH4NO3 - Ammonium Nitrate: Found naturally as gwihabaite. Most commonly synthesised	KNO3 - Potassium Nitrate: found mainly in cave deposits from excrement	Ca(NO3)2(H2O)x - Calcium Nitrate: Inorganic compound	Mg(NO3)2(H2O)x - Magnesium Nitrate: Occurs in cave systems as nitromagnesite
Phosphate							O8PS-5 - Phosphate sulphate: Does not exist	NaPO34-: Sodium Phosphates: Applied in food and water treatement	(NH4)PO4 - Ammonium Phosphate: used as a fertilizer	KH2PO4 - Monopotassium Phosphate: Used in greenhouse and indoor farming	CaHPO4 - Dicalcium Phosphate: Found as a food additive and in toothpaste	(Mg(H2PO4)2)xH20 - Monomagnesium Phosphate: Known as the E number E343
Sulphate								Na2SO4: Sodium Sulfate: occurs rarely in nature as Thernardite	NH4SO4 - Ammonium Sulphate - Occurs naturally as Mascagnite	K2SO4 - Potassium Sulphate: Occurs as the mineral Arcanite	CaSO4 - Calcium Sulfate: Known as the mineral gypsum	MgSO4 - Magnesium sulfate/Epsom Salt: Second most common sea salt
Sodium									H3NNa - Sodium Ammonia: Does not occur naturally	Sodium-Potassium pump: Important role in cell physiology	Sodium-Calcium exchanger: Single calcium ion is exported for the import of three sodium ions	MgNa3 - Magnesium Sodium: Does not occur naturally
Ammonium										KNH4 - Potassium Ammonium: Does not exist	Can be further combined with nitrate to form Calcium ammonium nitrate: A common fertilizer	Can be further combined with phosphate to create struvite
Potassium											CaK - Calcium Potassium: Does not exist	KMg - Potassium Magnesium: Does not ooccur naturally
Calcium												CaMg - Calcium Magnesium: Does not occur naturally
Magnesium												

Appendix 10: The potential of stemflow production in March 2021.